LIÈGE université Library

https://lib.uliege.be

https://matheo.uliege.be

Development of a test bench for assessing cyclists' aerodynamics in dynamic conditions

Auteur : Foguenne, Léonore
Promoteur(s) : Schwartz, Cédric; Andrianne, Thomas
Faculté : Faculté des Sciences appliquées
Diplôme : Master en ingénieur civil biomédical, à finalité spécialisée
Année académique : 2022-2023
URI/URL : http://hdl.handle.net/2268.2/17755

Avertissement à l'attention des usagers :

Tous les documents placés en accès ouvert sur le site le site MatheO sont protégés par le droit d'auteur. Conformément aux principes énoncés par la "Budapest Open Access Initiative"(BOAI, 2002), l'utilisateur du site peut lire, télécharger, copier, transmettre, imprimer, chercher ou faire un lien vers le texte intégral de ces documents, les disséquer pour les indexer, s'en servir de données pour un logiciel, ou s'en servir à toute autre fin légale (ou prévue par la réglementation relative au droit d'auteur). Toute utilisation du document à des fins commerciales est strictement interdite.

Par ailleurs, l'utilisateur s'engage à respecter les droits moraux de l'auteur, principalement le droit à l'intégrité de l'oeuvre et le droit de paternité et ce dans toute utilisation que l'utilisateur entreprend. Ainsi, à titre d'exemple, lorsqu'il reproduira un document par extrait ou dans son intégralité, l'utilisateur citera de manière complète les sources telles que mentionnées ci-dessus. Toute utilisation non explicitement autorisée ci-avant (telle que par exemple, la modification du document ou son résumé) nécessite l'autorisation préalable et expresse des auteurs ou de leurs ayants droit.

University of Liège - Faculty of Applied Sciences

Development of a test bench for assessing cyclists' aerodynamics in dynamic conditions

Final work carried out with the aim of obtaining the degree of Master "Biomedical Engineering" by

Léonore FOGUENNE

Supervisors :

Prof. Thomas ANDRIANNE & Prof. Cédric SCHWARTZ

Academic year 2022-2023

Acknowledgement

I would like to express my sincere gratitude to all those who have directly or indirectly contributed to the realisation of this work. Your support has been invaluable, and I am deeply appreciative of your assistance.

I am particularly grateful to my supervisors Pr. Andrianne and Pr. Schwartz for their invaluable guidance and generous allocation of time. They have consistently provided me with valuable advice, answered my many questions, and offered insightful ideas to further develop my work.

I would also like to thank the BinGoal team, with special mention to Mr. Wiggins. Working with this team and studying their remarkable equipment has been an incredible opportunity. Their collaboration and resources have significantly contributed to the success of this work.

Additionally, I wish to express my appreciation to all my friends who willingly participated in the numerous measurements I conducted throughout this work. Their enthusiastic involvement, even when faced with last-minute requests, has been truly appreciated. Moreover, I am grateful for their support and their willingness to address my questions on a daily basis.

Finally, I want to acknowledge and thank my family for their support throughout this journey. Your encouragement and belief in my abilities have been a constant source of motivation.

To each and every individual mentioned above, as well as those who have offered assistance in various other ways, I would like to express my gratitude. Your contributions have played an important role in the realisation of this work, and I am forever grateful for your support.

Abstract

This study aims to address the gaps in the field of cyclist aerodynamics by focusing on the evaluation of aerodynamics in dynamic conditions that closely resemble real-life situations. To achieve this, several key aspects are investigated.

Firstly, the study examines the order of magnitude of equipment, specifically helmets, to assess their impact on aerodynamics. By analysing these variations, the study provides insights into the influence of helmets on aerodynamic performance.

Next, the variations in cyclist replacement without feedback are evaluated, along with their corresponding impact on aerodynamics. The results reveal that the drag error resulting from these variations is significant, making it challenging to accurately assess the isolated impact of helmets on aerodynamics.

To mitigate these variations, a motion tracking algorithm is developed to provide feedback to cyclists regarding their positions. Although the algorithm does not yield precise cyclist positions, it assists in achieving replacements with a reasonable margin of error. However, the margin of error achieved with the feedback algorithm is not significantly smaller than when cyclists perform replacements without feedback.

Finally, all the preceding analyses are combined to develop a dynamic evaluation of cyclist aerodynamics, utilising the motion tracking algorithm. From this comprehensive evaluation, it is concluded that evaluating cyclists in dynamic conditions is of primary importance. Furthermore, the study finds that body position and shape have the most significant influence on aerodynamics, followed by equipment and yaw angle. These parameters can still be evaluated, even if the motion tracking algorithm failed to assess positions for various reasons. Those algorithm's weaknesses highlight several areas of improvement.

Contents

List of Figures

Introduction

Time trial cycling, a discipline renowned for its precision and individual performance, has gained immense popularity in the world of competitive cycling. With its focus on speed, efficiency, and aerodynamics, time trial events have become a crucial component in cycling competitions, including stage races, individual time trials, and even triathlons. In these races, cyclists strive to cover a specified distance in the shortest possible time, pushing the boundaries of human performance.

Given the significance of time trial events and the pursuit of marginal gains, extensive research has been conducted to enhance the aerodynamic efficiency of time trial cyclists. Studies have explored various aspects, including equipment optimisation, body position adjustments, and the impact of external factors such as wind. The primary goal has been to identify factors that contribute to reduced air resistance and improved performance, ultimately enabling cyclists to achieve their maximum potential.

The quest for improved aerodynamics in time trial cycling is driven by the understanding that even marginal improvements can have a substantial impact on overall performance. By minimising aerodynamic drag, cyclists can maintain higher speeds while expending less energy, leading to faster race times and improved chances of success. Consequently, the field of time trial cycling has witnessed a lot of research efforts dedicated to unravelling the complexities of aerodynamics and its interaction with cyclist position, equipment choices, and external influences.

However, while significant strides have been made in understanding time trial cyclists' aerodynamics, there are still crucial gaps that need to be addressed. One notable aspect is the need for dynamic evaluations that better simulate real-world conditions, accounting for the dynamic nature of a cyclist's position during a race. Additionally, there is a pressing requirement for accurate motion tracking techniques that facilitate the replication of a cyclist's position in controlled settings, such as wind tunnels, for reliable aerodynamic assessments.

In light of these research gaps, the primary aim of this work is to develop a comprehensive and dynamic evaluation framework for time trial cyclists' aerodynamics within a wind tunnel setup. By integrating motion tracking algorithms, the research seeks to provide a solution that allows for precise replication of a cyclist's position, enabling more accurate and repeatable aerodynamic measurements. Through this, the study aims to enhance the understanding of the intricate relationship between a cyclist's position, aerodynamic performance, and equipment

choices, thereby facilitating advancements in time trial cycling.

To achieve this objective, the methodology encompasses several key components.

First, in Chapter 1, this paper begins with an in-depth exploration of the aerodynamics and biomechanics of cyclists, setting the foundation for understanding the technicalities of their performance. A comprehensive review of the existing literature on the aerodynamics of cyclists is also presented, encompassing the significant body of work that has contributed to the current understanding of this field.

Then, in Chapter 2, an evaluation of the aerodynamic impact of the equipment, with a focus on time trial helmets, quantifies the variations in aerodynamic parameters resulting from different helmet designs. These findings contribute to understanding the impact of equipment choices on overall aerodynamic performance.

Next, in Chapter 3, the influence of position variability on aerodynamic measurements is investigated. Cyclists often struggle to maintain consistent positions, posing challenges in assessing the true impact of positional changes on aerodynamics. To address this, the study quantifies the magnitude of repositioning variations without feedback. This quantification allows for a comparison between the effect of positional errors and the impact of equipment on aerodynamics. By evaluating whether the error in aerodynamics due to incorrect repositioning is too significant, the study aims to determine if it is feasible to investigate the effect of equipment on aerodynamics.

In Chapter 4, a feedback system based on motion tracking algorithms is developed to address positional variations. It aims to provide real-time information and assistance to cyclists, facilitating accurate position replication during wind tunnel testing.

Finally, in Chapter 5, the comprehensive analyses conducted in this study are combined to perform a final evaluation of the cyclist's aerodynamics in a dynamic configuration within the wind tunnel. This final measure takes into account the individual contributions of different factors, such as helmet design, cyclist positioning, yaw angle, and their interaction with the airflow. By considering the dynamic nature of cycling and replicating real-world conditions as closely as possible, the evaluation provides valuable insights into the aerodynamic efficiency of the cyclist in a time trial scenario.

Chapter 1

State of the art

This Chapter presents an examination of the aerodynamics and biomechanics of cyclists, establishing a fundamental understanding of their performance intricacies. Furthermore, it provides a comprehensive review of existing literature on the aerodynamics of cyclists, encompassing a substantial body of work that has significantly contributed to the current knowledge in this domain. It commences by providing an overview of the cyclist's aerodynamics, delving into the factors that influence their airflow and drag characteristics. Subsequently, it explores the biomechanics of cyclists, focusing on the mechanical aspects of their movement and positioning. The evaluation of cyclist power and the various methodologies employed in power analysis are then discussed, along with an examination of previous research conducted on cyclist positions. Lastly, the Chapter addresses the existing gaps in the field of cycling aerodynamics and outlines the specific objectives of this study.

1.1 Aerodynamics of cyclists

A cyclist is subject to 6 direct aerodynamic actions (Figure 1.1) :

1. The drag force (F_D) that is the projection of the aerodynamic force along the direction of the relative wind. If the bike is aligned with the wind, it acts in the opposite direction of the cyclist's motion and is parallel to the ground.

2. The side force (F_S) that is perpendicular to the drag force and also parallel to the ground.

3. The lift (F_L) that is perpendicular to the ground.

4. The rolling moment (M_R) around the axis of the drag force.

5. the pitching moment (M_P) around the axis of the side force.

6. The yaw moment (M_Y) around the vertical axis (axis of the lift).

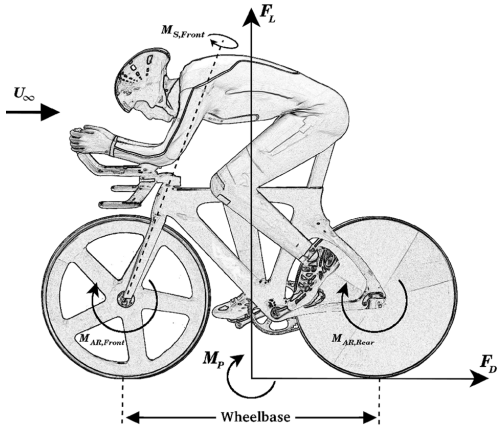

(a) *Side view*

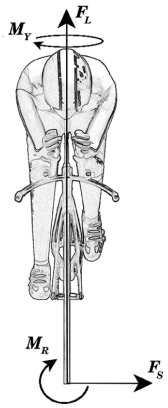

(b) *Frontal view*

Figure 1.1: *Cyclist and bicycle aerodynamic forces (F_L, F_D, F_S) and moments (M_P, M_R, M_Y) [1].*

If only the axis in the cyclist direction is considered, the drag force is the only one remaining. In this direction, the second Newton's law can be used in order to have the force balance :

$$F = ma_x + F_R + C + F_D, \tag{1.1}$$

where F is the total force produced by the cyclist, ma_x is the inertia force, F_R is the rolling resistance, C is the transmission losses that can be neglected and F_D is the drag force [1, 2, 3]. The rolling resistance can be decomposed as :

$$F_R = mg(C_{rr1} + C_{rr2}V), \tag{1.2}$$

where mg is the weight of the rider and the bike, C_{rr1} is the static rolling resistance coefficient, C_{rr2} is the dynamic rolling resistance coefficient (including wheel bearing losses and dynamic tire losses) and V is the speed of the cyclist [4].
The drag force, for its part, can be decomposed as :

$$F_D = \frac{1}{2}\rho A C_D W^2, \tag{1.3}$$

where ρ is the air density $[kg/m^3]$, A is the projected frontal area $[m^2]$, C_D is the drag coefficient [-] and W is the relative wind speed $[m/s]$. The relative wind speed has to be considered when there is a wind blowing at a speed U [m/s] and the cyclist have a speed V [m/s]. Then, the relative wind is evaluated as :

$$W = U - V. \tag{1.4}$$

In the following, it will be considered that there is no external wind. Subsequently, the speed of the wind perceived by the cyclist will be equal in value to his own speed but in opposite direction: $|W| = |V|$ [1, 3, 4, 5, 6].
Often, the drag coefficient and the projected frontal area are considered together in a variable called the drag area ($C_D A$), which is the product of the latter. The drag area represents the

position of the cyclist on the bicycle and the aerodynamics of the cyclist-bicycle system in this position. This variable provides a way to avoid the uncertainty introduced by the measure of the frontal area [1, 5, 6].

From Equations 1.2 and 1.3, it can be seen that the rolling resistance only depends linearly on the relative speed, while the drag force is proportional to the speed squared. This means that at high speed, the aerodynamic drag becomes the major resistive force. Indeed, at a speed equal or greater than 14 m/s ($\approx$50 km/h), 14 m/s being a normal speed for time trial, the drag force accounts for more than 90% of the total resistance. This is why this work will only focus on the drag force and the rolling resistance will be neglected. However, it is important to note that for professional cyclists, every force is important in order to minimise the resistance so as to be able to deliver the best performance even if they will not be considered here [1, 2, 3, 4, 5, 6, 7, 8, 9].

The aerodynamic drag of a body is generated by the interaction of this body with the flow. The drag force is composed of two forms of drag : the pressure and the skin-friction drag. The pressure drag represents the variation in air pressure that exists between the front and the rear of a moving body. It results from the boundary layer due to the fluid pressure on the body, and it leads to backward turbulence. The skin-friction drag is the resistance generated by the friction of fluid molecules directly on the surface of the body in motion. It increases with the size and roughness of the body surface [2, 5, 8].

On the aerodynamic point of view, the system composed of the biker and the bike can be considered as a bluff body because it exhibits large regions of separation. A bluff body has sharp edges or a much more dramatic reduction in body width toward the trailing surface. This type of body leads to large adverse pressure gradients on the boundary layer, those gradients are too important to keep the flow attached. As a result, bluff body flows are characterised by large regions of separated flow that may or may not reattach to the surface (Figure 1.2). For bluff bodies, the pressure drag is more important than the skin-friction drag. So in a general point of view, it is more important to reduce the frontal area than to reduce the wet area [1, 2, 4, 10].

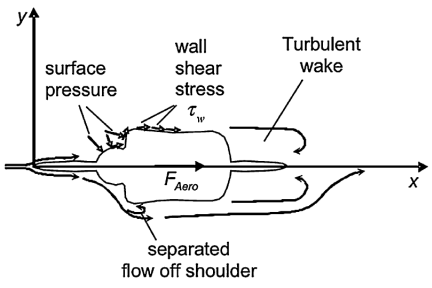

Figure 1.2: *Diagram of the flow field around a cyclist [1].*

The system studied here is composed of the cyclist, the bike and other components such as the helmet, the clothes, and the shoes. As the bike frontal area is much smaller than the cyclist one, the aerodynamic drag acts mostly on the cyclist's body. Indeed, it has been shown that the cyclist's drag is worth $\approx 70\%$ of the total drag, the remaining being the bike and the other components [2, 3, 4, 5, 6, 11, 12].
The main point to work on to reduce the cycling resistance are thus the rider position first, followed by the bike geometry and equipment and finally the rolling resistance. The best ways to improve aerodynamic efficiency are in order : lowering the frontal area, streamlining the geometry and lowering the surface roughness. Indeed, even if skin-friction is less important, for extreme competitions a few percent drag reduction can make a big difference. It is thus important to consider using specialised suits and shoes and use an aero-helmet [1, 6, 7].
In order to reduce the frontal area, the trunk must be close to parallel to the ground, the angle between the trunk and the horizontal must be closed to $0°$. The placement of the arms can also modify the frontal area. Place them under the torso or place them forward using aero-handlebars can also decrease the frontal area. However, the position of the cyclist is constrained by the bike geometry and also has to satisfy the Union Cycliste International (UCI) rules. Moreover, improving the position in an aerodynamic point of view does not always lead to an optimal position in terms of force production. It is thus important to find a compromise between power output and aerodynamics [3, 5, 6, 8].

The main way to study the cycling aerodynamics is in a wind tunnel. Indeed, wind tunnel testing is preferable to field-testing because it provides controlled environmental conditions that are repeatable and documentable. The most common measure is the time-averaged aerodynamic force measurement. In order to record those data, force plates are usually placed on the ground to quantify the ground reaction forces. The bike is placed on the force plates and can be fixed using a home trainer to allow pedalling. The whole setup is optimally placed on turn plates in order to induce a yaw angle to measure the effect of cross-winds. However, the wind tunnel testing does not represent exactly the real conditions and shows some limitations. First, there is a modification of the air flow around the bicycle if there is no movement of the bike and cyclist. Second, if the wheels are stationary, the effect of the surrounding wind is not measured. Finally, in real conditions, the cyclist presents some slight lateral movements that are not necessarily there in the wind tunnel. His position is thus not exactly the same as in real conditions. It is possible to overcome the second and third issue if the bike is placed on a home trainer or a treadmill, and it is in motion. But this new configuration induces two other issues : the pedalling induces noise in the measurement as the force varies within each pedal revolution and the slight lateral movements are dependent on the intensity of pedalling [1, 4, 5].

1.2 Biomechanics of cyclists

The biomechanical power can be measured as the output power at the crank using a power meter. The crank power can be computed as the force applied at the pedal [N] multiplied by the velocity of the pedal [m/s], or equivalently by the product of the crank's torque [N.m] and its angular velocity [rad/s], where the crank's torque is the product of the tangential force at the crank and the crank's length.
Thus, only the forces that are applied orthogonally to the crank can produce power. They are called the effective forces, while forces in other directions are ineffective but have a metabolic cost (Figure 1.3). It is however impossible to maximise the power output without producing ineffective forces.
Moreover, the effective forces can be in the direction of the movement, i.e. positive and thus increasing the power output, or in the opposite direction, i.e. negative and decreasing the power output.

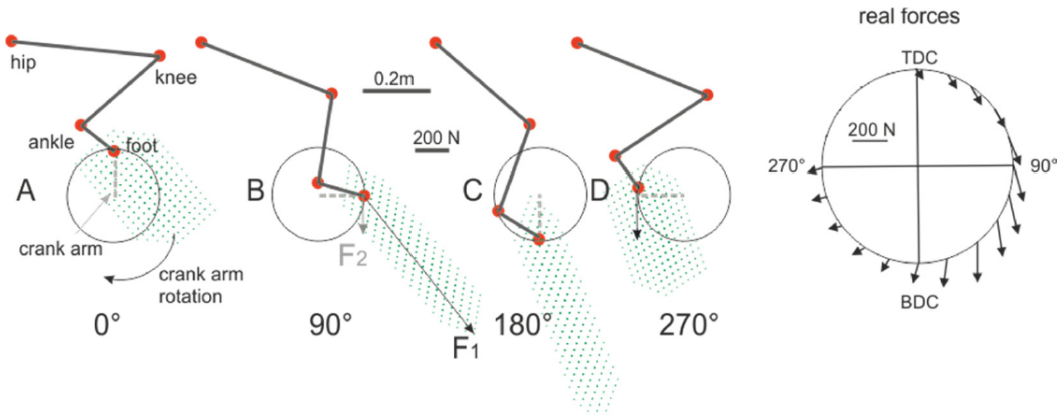

Figure 1.3: *Set of feasible forces at different joint configurations and illustration of real forces vectors over a revolution of the crank [13].*

The crank power is the association of all the joints power. The joint power is the scalar product of the joint torque [N.m], estimated using inverse dynamic, and the joint angular velocity [rad/s], that is the derivative of the position of the segments estimated with a motion tracking device. The contribution of the different joints to the joint power is approximately 40%, 40%, 15% and 5% for the hip, the knee, the ankle, and the trunk respectively. The upper limbs do not produce a lot of power, but they contribute mainly to provide stability to the cyclist.
The joint torque is the association of all the muscles efforts at a joint as well as passive tissues such as ligaments. The relationship between joint torque and crank power is not direct, and a maximised joint torque does not particularly lead to a maximised output power. Indeed, the torque produced does not necessarily produce forces in the right direction in order to be effective and some external factors such as gravity, inertial effects and pedalling frequency have to be considered.

Even if the joint torque is not directly related to power output, it is useful as it is related to muscle force. It can thus be used to compute a cost function to measure the global effort [14, 15].

It is important to note that biomechanical power is limited, as it has a limited efficiency (η) due to muscle's efficiency, as well as the cardio-respiratory capacity and mental aspect. The total efficiency is the generated mechanical energy, i.e. the work, divided by the supplied chemical energy. For trained cyclists, the efficiency can go up to 25% to 30%. The efficiency is also influenced by the pedal rate [4].

1.3 Power of cyclists

In order to combine the aerodynamic and the biomechanical powers, the concept of surplus power can be used. The surplus power is the power available for acceleration or gradient climbing :

$$P_{surplus} = P_{biomechanical} - P_{aerodynamic}. \tag{1.5}$$

The surplus power is useful as it combines the aerodynamic and the biomechanical aspects of the cyclist to find the optimal tradeoff between them and thus the best position.
The surplus power is composed of two terms. First there is the biomechanical power. As explained in the Section 1.2, it is the scalar product of the forces applied at the crank and the velocity. It is limited, as the power that can be produced by the cyclist is limited by the muscle's efficiency, as well as the cardio-respiratory capacity and mental aspects. Then, there is the aerodynamic power. It can be calculated as :

$$\begin{aligned} P_{aerodynamic} &= P_{drag} + P_{rolling} \\ &= F_D V + F_R V \\ &= \frac{1}{2}\rho A C_D V^3 + mg(C_{rr1} + C_{rr2}V)V. \end{aligned} \tag{1.6}$$

The power needed to overcome the air resistance increases with the third power of the speed, and the power to overcome rolling resistance increases with the speed squared.
The goal is then to maximise the biomechanical power while minimising the aerodynamic power in order to increase the power surplus as much as possible. This highlights the importance of reducing the drag force by finding the best position, as it is the term that has the biggest impact. It is even more important given that the biomechanical power is limited. Even a small change on the position can have a big impact on the power [4, 5, 6, 11, 16].

1.4 Research on position

As mentioned before, the main way to reduce drag is to reduce the frontal area. In order to do so, the cyclist has to adopt the most streamlined position as possible.
The position of the cyclist has already been the subject of a large number of studies, and some of those studies have resulted in the invention of exotic positions such as the Obree's or Superman positions. As a result of those inventions, the UCI had to intervene and define constraints on the bike geometry to prevent too exotic positions [1, 4, 17].

There are currently four main positions used in cycling : the traditional position with the hands on the brake hoods or the stem, the dropped position with the hands on the drops and the arm straight, the crouched dropped position with the hands on the drops and the arm bent and the time trial position (Figure 1.4).

(a) *Brake hoods and stem*

(b) *Dropped with straight arms*

(c) *Dropped with arms bent*

(d) *Time trial*

Figure 1.4: *Four main cycling positions [4].*

It has been shown that the time trial position is the most efficient, as it has the lowest drag, followed by the dropped position with the arms bent, then the dropped position with arms straight and finally the traditional position is the least efficient. The reduction in drag can be as high as 15% to 20% between the brake hoods and stem position and the dropped position with arms bent. The drag reduction can even go up to 30% to 35% for the time trial position.

The drag area is mainly affected by the trunk angle. An angle close to 0° gives a smaller frontal area and thus less drag. However, a low trunk angle leads to worse physiological variables such as an increase in oxygen consumption, breathing frequency and minute ventilation.

This has for consequence to reduce the performance. An improved position does not always lead to improved performances, it is important to find a trade-off between drag reduction on one part, and decrease of metabolic cost and increase of power output on the other part.

This can in part be studied by looking at the power. The maximum power output was found to be at middle torso angle and low shoulder angle. However, the maximum power surplus, that takes into account both aerodynamic and biomechanical power, was found to be at low torso angle and middle shoulder angle [1, 2, 4, 7, 8, 18, 19].

1.5 Gap in the field

Despite the extensive research conducted on cyclists' aerodynamics, there are some significant limitations that are consistently present in these studies. Two key areas that require attention are the representation of real-world cycling conditions and the challenge of maintaining repeatability in measurements.

Many aerodynamic studies in cycling utilise wind tunnels and employ models of cyclists to achieve greater repeatability. While this approach offers advantages in terms of controlling variables and ensuring consistency, it fails to fully capture the complexity of a real cyclist, particularly the dynamic nature of pedalling. Pedalling significantly impacts the aerodynamics of a cyclist, making it crucial to study them under realistic pedalling conditions that better represent actual cycling scenarios [1, 5, 7].

However, employing real cyclists for aerodynamic testing introduces challenges in terms of repeatability. It is inherently difficult for a cyclist to consistently replicate the exact same position for every test. Additionally, maintaining a fixed position over an extended period can be challenging, further compromising the repeatability of measurements. These variations in position directly influence the aerodynamics of the cyclist, making it challenging to isolate the effects of specific parameters being evaluated [1, 2, 10].

The two identified gaps in the field of cycling aerodynamics are closely linked. There is a need to evaluate the aerodynamics of real cyclists in motion, as this better reflects the dynamic nature of cycling. Additionally, it is essential to develop methods to accurately assess and monitor the position of cyclists throughout the measurement process. Addressing these gaps will enhance the understanding of how different factors affect aerodynamics and enable more accurate and meaningful analysis of the measured parameters.

1.6 Objectives

Given the existing gaps in the field of cyclists' aerodynamics, the primary objective of this work is to develop a dynamic measurement approach for evaluating the aerodynamics of cyclists in a wind tunnel. To achieve this, the study will be divided into several parts, each addressing a specific aspect of the measurement process.

The first part will focus on assessing the magnitude of variations in aerodynamic parameters resulting from different equipment, primarily different helmet designs. By conducting tests with various helmets, the aim is to quantify and compare the differences between them, providing insights into the impact of equipment on aerodynamics.

The second part will involve evaluating the magnitude of repositioning variations in cyclists without any feedback. This step is crucial for establishing a baseline to compare the subsequent results. By quantifying the inherent variations in cyclist positioning, the study aims to understand the challenges posed by maintaining a consistent position during testing.

Then, the influence of small errors in cyclist positioning on aerodynamics will be assessed to determine if variations in repositioning pose challenges when evaluating the effects of parameters such as equipment. A comparison between the magnitudes of variations in aerodynamics parameters for materials and positioning will be conducted.

Furthermore, a feedback system for position control will be implemented to examine whether it can effectively reduce variations in positioning, thereby improving measurement accuracy.

Finally, all the findings and methodologies from the previous parts will be integrated to evaluate the aerodynamic parameters of real cyclists in dynamic conditions within the wind tunnel. This comprehensive analysis will provide valuable insights into the aerodynamic performance of cyclists under realistic scenarios, accounting for equipment variations, repositioning challenges, and the effectiveness of feedback systems.

By addressing these different aspects and combining them into a holistic approach, this study aims to enhance the understanding of cyclists' aerodynamics and pave the way for more accurate and representative measurements in wind tunnels. Ultimately, the findings will contribute to the development of optimised cycling equipment and improved cycling performance.

Chapter 2

Evaluation of the aerodynamic impact of the equipment

In this Chapter, an assessment of the aerodynamic influence of equipment, specifically focusing on helmets, will be realised. The aim is to measure and quantify the variations in aerodynamic parameters that arise from different helmet designs. These findings play a crucial role in enhancing the understanding of how equipment choices affect the overall aerodynamic performance. Firstly, a concise overview of the wind tunnel will be provided, as it serves as the primary method for assessing aerodynamic parameters. Then, the setup utilised in the study will be described, outlining the experimental configuration and procedures. And finally, the obtained results will be presented, offering insights into the findings and their implications.

2.1 Wind tunnel

Wind tunnel testing is the gold standard to measure the cyclists' aerodynamics because it provides a controlled environment. The following measures were performed in the wind tunnel of the University of Liège (Figure 2.1). It is a closed loop subsonic tunnel (Mach<0.15) but it can operate in an open loop configuration. It is composed of two sections : the aeronautic/automobile test section (TS1) and the wind engineering test section (TS2). Both sections are equipped with a rotating test table. The TS1 is of dimensions $2m \times 1.5m \times 5m$ (width×height×length). It can perform in a speed range of 2 m/s to 60 m/s in closed loop configuration. The TS2 is of dimension $2.5m \times 1.8m \times 2m$ and the speed range goes from 2 m/s to 40 m/s in closed loop configuration [20].

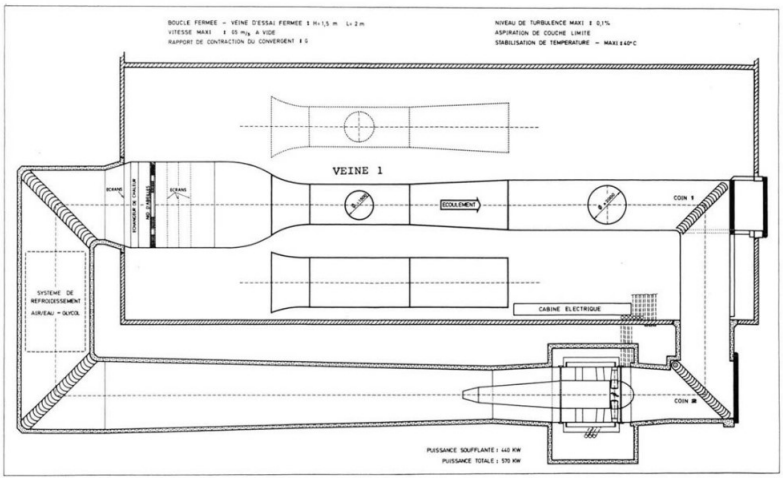

Figure 2.1: *Wind tunnel schematic view [20].*

2.2 Helmets analysis on a mannequin

The primary objective of this analysis is to examine the influence of helmets, as equipment, on the aerodynamics of cyclists. By quantifying and assessing the changes in aerodynamic performance caused by different helmet designs, the objective is to determine the extent of their impact on aerodynamic factors. Through measurements and analysis of relevant parameters such as drag, the study seeks to evaluate how different helmet types or designs affect the overall aerodynamic efficiency of cyclists.

2.2.1 Methodology

For this measure, the TS2 is used. A mannequin of a full body is placed in a position as representative as possible of the time trial position with the torso aligned with the wind, the head slightly turned up and, the legs and arms bent. The mannequin is attached, using a pole, to a force/torque sensor of resolution 0.25 N (*Omega 160*) (Figure 2.2). This sensor is able to measure the forces as well as the moments in all three directions.

Figure 2.2: *Helmets testing set up with the mannequin.*

In addition to the mannequin on itself, two helmets were studied : an aero-road helmet, helmet 1 (Figure 2.3a), and a time trial helmet, helmet 2 (Figure 2.3b). Each configuration was tested at five different speeds : 3.4, 7.3, 11.1, 15 and 18.9 m/s. Those speeds were chosen as they cover a large range of reachable speeds for cyclists.

(a) *Helmet 1*

(b) *Helmet 2*

Figure 2.3: *Different helmets tested.*

The protocol is the following :

1. The helmet is placed on the head of the mannequin.
2. A bias is applied in order to remove forces induced by the manipulation of the setup.
3. The first wind speed is applied.
4. The forces and the moments in the 3 directions are measured for 20 seconds.
5. The steps 3 and 4 are repeated for the 4 different wind speeds.

This protocol is reiterated for the two helmets and the mannequin without helmet.

The results of the measures can not be used as such, they first need to be calibrated. Indeed, when a moment is applied, it induces an undesired force. The values of the forces measured are thus not totally exact. There is a linear relationship between the moment and the force. It is therefore possible to find this relationship by applying weights on the setup and then measure the forces and moments induced. By performing this multiple times with different weights at different positions, different force values are found for different moments applied. Then the relationship between the forces and the moments can be found by interpolating (Figure 2.4).

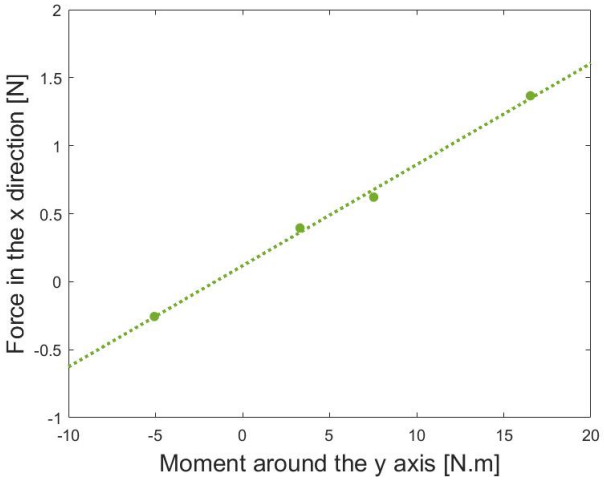

Figure 2.4: *Values of the moments and the forces for the calibration. The doted line represent the interpolation.*

2.2.2 Results

Unfortunately, the setup was not adapted to the measure. Effectively, the mannequin showed big variations in the position due to the wind. To assess the impact of wind on the mannequin's position, a visual analysis was conducted using image comparison techniques.

Images of the mannequin were captured for each helmet, including both a reference image of the mannequin without wind and images of the mannequin at each wind speed. Using the *Kinovea* software, these images were overlaid to visualise any differences in the mannequin's limb positions caused by the wind.

By aligning the images, the angles between the limbs of the mannequin at different wind speeds could be measured using reference points such as screws at the joints of the mannequin. These angles provide a quantitative representation of the changes in limb positions caused by the wind. The definition of the angles is demonstrated using the pictures of the mannequin for the helmet 2 at wind speeds of 0 m/s superposed with 25 m/s (Figure 2.5).

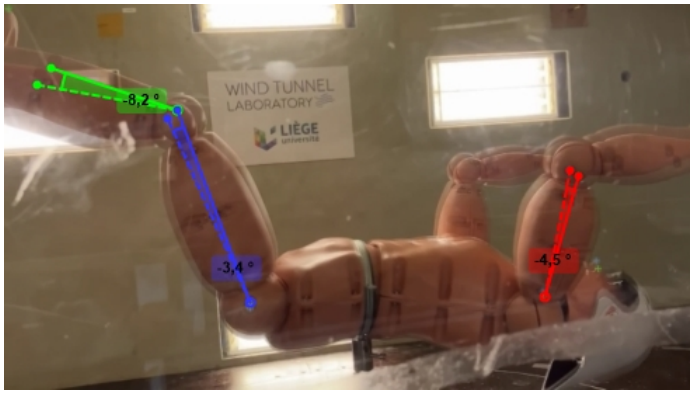

Figure 2.5: *Definition of the angle measures between the mannequin without wind and with different wind speeds (here 25 m/s). The calf angle is in green, the thigh angle is in blue and the arm angle is in red.*

The angles were measured for each helmet at each speed (Table 2.1). The overlay of the

different pictures can be found in Appendix A. The difference in angle can go up to 8.4°, which is considerable given that a variation in the inclination of the limbs leads to a variation of the frontal area and thus a non-negligible difference in the drag.

	Angle difference [°]			
	Helmet 1			
	7.3 m/s	11.1 m/s	15 m/s	18.9 ms
Thigh	/	-2	-3.4	-2.5
Calf	-1.5	-3.8	-8.4	-5.1
Arm	/	-1.7	-3.8	-2.7
	Helmet 2			
	7.3 m/s	11.1 m/s	15 m/s	18.9 ms
Thigh	/	-0.8	-2	-3.4
Calf	-1.4	-2.1	-4.1	-8.2
Arm	-1.1	-1.9	-4	-4.5

Table 2.1: *Difference in the position of the mannequin between the setup with no wind and with different wind speeds for both helmets. A "/" signifies that there was no noticeable difference in the position of the limbs.*

The observed variations in limb angles caused by the wind can introduce additional uncertainties and inaccuracies in the measurements of drag induced by different helmets. The changes in limb angles can contribute significantly to the overall drag experienced by the mannequin.

If the differences in drag induced by variations in limb angles are greater than the differences generated by the addition or change of helmets, it becomes challenging to isolate and accurately quantify the specific impact of the helmets on aerodynamics. The results of the measures can however be found in Appendix B).

2.3 Helmets analysis on a static head

2.3.1 Methodology

The previous limitations of the mannequin setup for evaluating helmet aerodynamics led to the development of a new setup focusing solely on the head of the mannequin. The revised setup involved removing the body of the mannequin and attaching only the head to the force and torque sensor. To accomplish this, a custom 3D printed piece was designed and created specifically to securely hold the mannequin head in place (Figure 2.6).

By isolating the head and directly connecting it to the force and torque sensor, this new setup allowed for a more controlled and reliable environment of the measurements of the aerodynamic effects of the helmets. The reduced complexity of the setup minimised potential confounding factors and improved the accuracy and repeatability of the measurements, specifically targeting the impact of the helmets on drag and other aerodynamic parameters.

(a) *Front view* (b) *Side view*

Figure 2.6: *Helmet's testing setup with the head of the mannequin.*

After implementing the new setup with the isolated mannequin head and confirming its stability during wind tests with the two previously evaluated helmets, the analysis was extended to nine new helmets (Figure 2.7).

(a) *Helmet A*

(b) *Helmet B*

(c) *Helmet C*

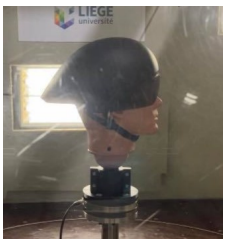

(d) *Helmet D*

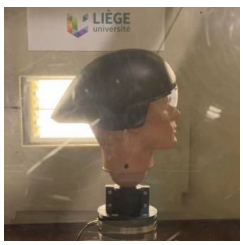

(e) *Helmet E*

(f) *Helmet F*

(g) *Helmet G*

(h) *Helmet H*

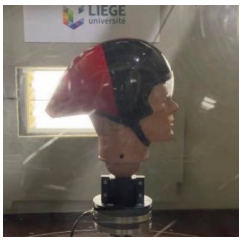

(i) *Helmet I*

Figure 2.7: *Different helmets tested.*

Helmets F and G are categorised as aero-road helmets, indicating that they are designed to optimise aerodynamics while still offering the necessary ventilation for road cycling conditions.

On the other hand, the remaining helmets (A, B, C, D, E, H and I) are classified as time

trial helmets. Time trial helmets are specifically designed to reduce aerodynamic drag and improve speed during time trial events where every second counts. These helmets are typically more streamlined and may sacrifice some ventilation for enhanced aerodynamic performance.

The helmets C, D, and E are prototypes that share the same shape, suggesting a consistent helmet design. However, each helmet incorporates a specific feature to distinguish them. Helmet C includes exhausts on the tail to help maintain the flow attached to the helmet and minimise turbulence. Helmet D features corrugation, which likely serves a similar purpose of promoting flow attachment and reducing turbulence. Helmet E, in contrast, has a smooth surface, which might aim to optimise aerodynamics by minimising surface disruptions.

It is worth noting that the presence of exhausts in helmets C and ventilation features in general, not only contribute to aerodynamic performance but also help in regulating the temperature inside the helmet. Adequate ventilation prevents the cyclist's head from overheating during intense efforts, contributing to overall comfort and performance.

Lastly, helmet I holds significance as it was used for the current one-hour world record. This indicates that it is a helmet recognised for its exceptional aerodynamic properties and has proven to be effective in achieving top-level performance.

Understanding the distinctions between these helmet models and their intended purposes provides valuable context for analysing the aerodynamic impact of each helmet on the cyclist's head and overall performance.

For those helmets, the protocol of Section 2.2.1 was slightly modified. First of all, only three speeds were tested : 11.4, 13.9 and 15.5 m/s. The other speeds were not analysed, as they are not likely to be used in race cycling. Secondly, the helmets were tested at two different pitch angles : 0° and 45° (Figure 2.8).

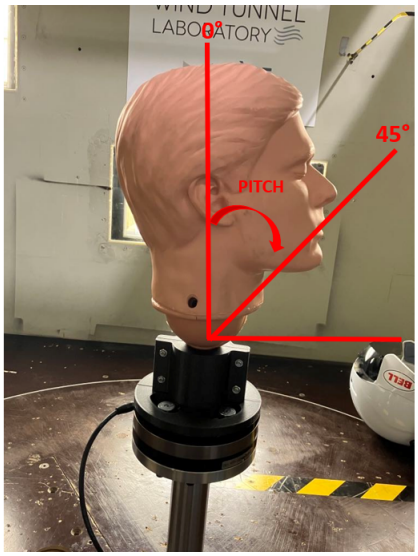

Figure 2.8: *Pitch angles of the head setup.*

Finally, four yaw angles were evaluated : 0°, 5°, 10° and 15°. The yaw angles were only examined for a 45° pitch angle as it is more common than the 90° pitch angle in racing and it better represents the reality. It was also only evaluated for the helmets A, C, D, E, H and I.

It is important to evaluate the yaw angle. Indeed, the evaluation of the yaw angle is crucial in assessing the aerodynamic performance of the helmets. In real-world cycling scenarios, it is common for a cyclist's head to experience slight oscillations and movements while pedalling. By considering the yaw angle, the analysis takes into account the realistic movements of the cyclist's head during a race. This provides a more comprehensive understanding of how the helmets perform under dynamic conditions, rather than assuming a static head position.

Evaluating the helmets' aerodynamic effects at different yaw angles helps to assess their ability to minimise drag and maintain airflow attachment even when the cyclist's head is not perfectly aligned. Helmets that effectively manage the airflow and reduce turbulence across a range of yaw angles are considered more aerodynamically efficient and beneficial for real-world cycling conditions.

By studying the helmets' performance at various yaw angles, the analysis can provide insights into their ability to optimise aerodynamics and minimise drag during dynamic situations, ultimately helping cyclists in their pursuit of improved performance and efficiency.

As the setup has changed, the calibration has to be performed once again. The same method was used in order to find the relation between the moments and the induced forces.

In the following, F_D will be considered as the force in the wind direction and F_S as the force in the direction perpendicular to the wind. F_X and, F_Y on the other hand, will represent the forces in the cyclist axes (Figure 2.9). When there is no yaw, the reference axes of the cyclist and of the wind are the same and $F_D = F_X$.

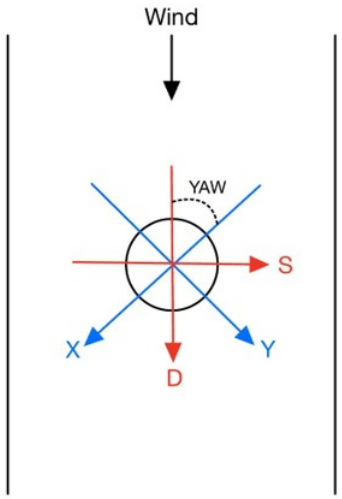

Figure 2.9: *Reference axes orientation.*

In addition to the force measurements, the wind velocity around two of the helmets has been assessed using the *ProCap* system. This allows to represent the streamlines around the helmets and study the airflow. This process is performed for the helmets C and I at wind speeds of 12.1, 14.4 and 15.9 m/s for a pitch angle of 45° and yaws angles of 0° and 15°. The helmets C and I were chosen in order to compare one of the prototypes to the helmet of the current one-hour world record.

Studying the streamlines around the helmets at different wind speeds, and pitch and yaw angles helps in understanding how the helmets interact with the surrounding airflow. It can reveal areas of separation, turbulence, or low-pressure regions, which are key factors in determining the aerodynamic efficiency and drag reduction of the helmets.

By combining the force measurements with the visual representation of the airflow patterns, a comprehensive understanding of the aerodynamic performance of the helmets can be obtained. This information is crucial in identifying the strengths and weaknesses of each helmet design and informing further improvements for enhanced aerodynamic efficiency and reduced drag.

2.3.2 Results

In order to evaluate the effect of the helmets on their own, each test was performed for the head alone. Then the results of the head were subtracted from the one of the helmets. The approach of evaluating the effect of the helmets by subtracting the results of the head alone allows for a direct comparison between different helmets and also enables comparison with existing literature, despite variations in the experimental setups. By isolating the contribution of the helmet, the focus is solely on the impact of the helmet design on the measured parameters.

The three parameters evaluated for each helmet configuration, namely the drag force (F_D), the drag area (C_DA), and the power (P), provide valuable insights into the aerodynamic performance of the helmets.

The power parameter reflects the extra power that a cyclist needs to generate to overcome the additional drag induced by the helmet. Minimising the power requirement is crucial for optimising cycling performance, as it directly affects the energy expenditure of the cyclist.

By considering these three parameters, the evaluation provides a comprehensive assessment of the aerodynamic efficiency and performance of the helmets. Lower values for the drag force, drag area, and power indicate superior helmet designs with reduced aerodynamic drag and improved energy efficiency.

Pitch angle = 0° and yaw angle = 0°

When analysing helmet forces for a pitch angle of 0° and a yaw angle of 0° (Figure 2.10), several important findings emerge. Firstly, the result of the helmet G at 11.4 m/s was removed as the value was irrelevant due to some drift in the measure, ensuring the reliability and accuracy of the results. Secondly, the study reveals that helmets F and G, which are specifically designed as aero-road helmets rather than time trial helmets, produce higher forces. This suggests that the aerodynamic features of these helmets contribute to increased force generation. Surprisingly, helmets A and B, despite being designed as time trial helmets, exhibit a surprisingly high drag. This unexpected result raises questions about the effectiveness of their design in reducing forces during time trial events. On the other hand, helmet I stands out as the best-performing helmet in terms of drag force, which could be expected as it is the helmet of the current one-hour world record. For their part, the helmets C, D, and E, which are still, prototypes also performs very well.

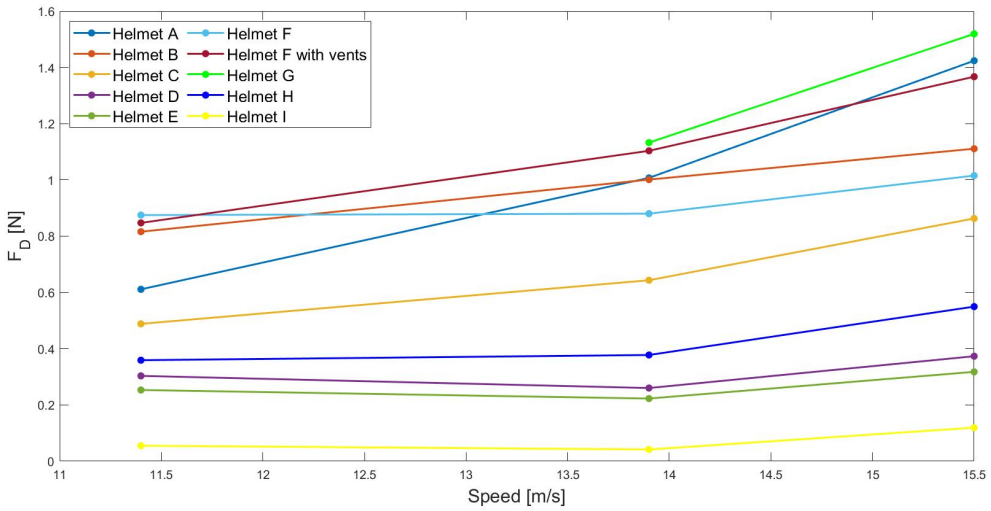

Figure 2.10: *Drag force [N] induced by the different helmets in the wind direction in function of the speed of the wind [m/s] for a pitch angle = 0° and yaw angle = 0°.*

It is observed that the drag area exhibits the same trends as the force because they are proportional one to another (Figure 2.11).
The nearly horizontal lines observed in the data indicate that the impact of Reynolds are small. Reynolds effects are a phenomenon that occurs in fluid flows, such as air, when the velocity and scale of the flow vary. This leads to changes in the flow characteristics, such as turbulence, vortex formation and flow separation. As the Reynolds number changes, the drag coefficient fluctuates, resulting in variations in the drag area. If the drag area is constant as a function of speed, this means that the resistance to the flow of helmets through a fluid remains the same, whatever the speed at which the object is moving. As a result, only one speed can be considered when comparing the different helmets. A speed of approximatively 14 m/s is the one that will be studied as it is the most representative of the time trial speed.

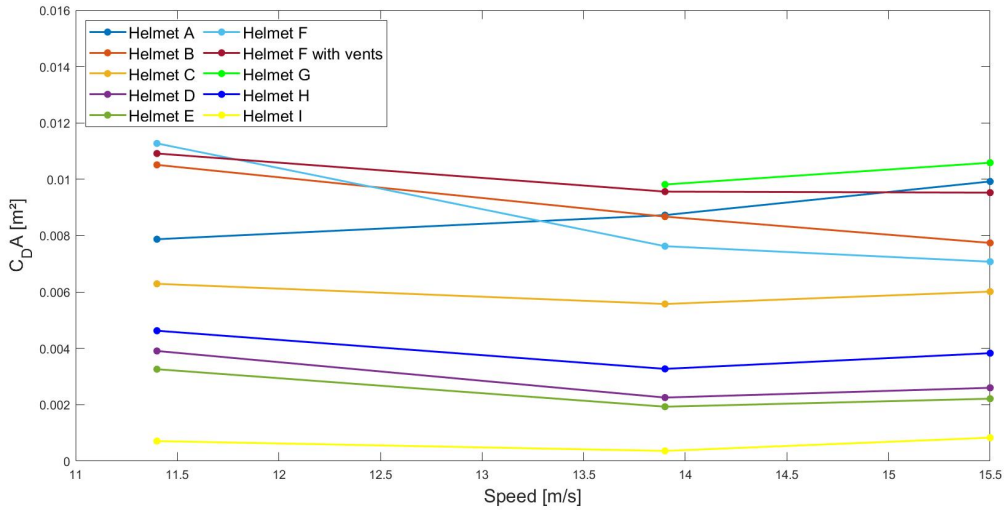

Figure 2.11: *Drag area [m^2] of the different helmets in the wind direction in function of the speed of the wind [m/s] for a pitch angle = 0° and yaw angle = 0°.*

The difference in power output between the various helmets is a significant factor to consider, as it directly impacts the additional power that cyclists must generate to overcome the added resistance caused by the helmet. Particularly for the poorest-performing helmets, this power difference with a better helmet can be substantial, ranging up to 20-25 W (Figure 2.12). Such figures should not be underestimated, given that the power output of a time trial cyclist typically hovers around 350 W [21]. Therefore, the power disparity resulting from helmet choice is non-negligible, and selecting a helmet that minimises the power penalty becomes crucial for time trial cyclists aiming to optimise their overall performance and energy efficiency.

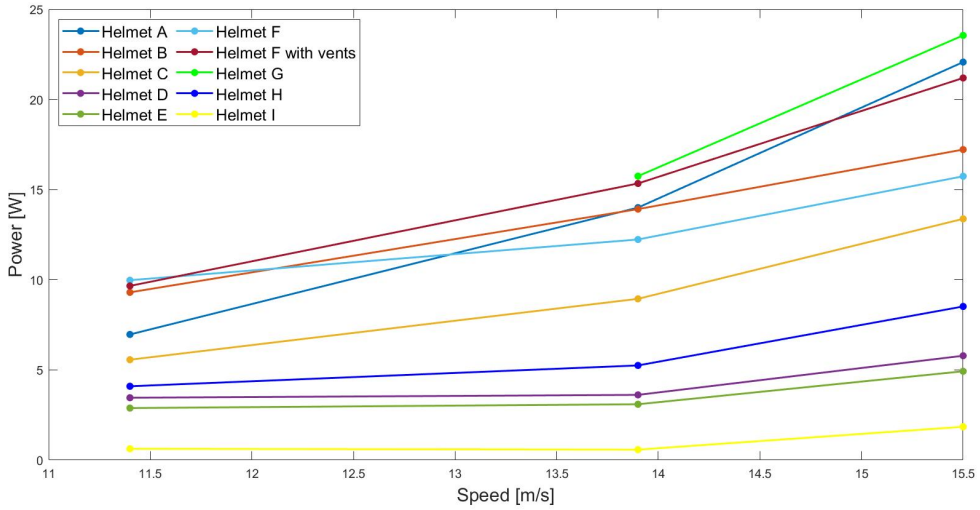

Figure 2.12: *Power [W] induced by the different helmets in function of the speed of the wind [m/s] for a pitch angle = 0° and yaw angle = 0°.*

Pitch angle = 45° and yaw angle = 0°

The pitch angle at 45° is more interesting compared to 0°, as it provides a better representation of reality. A pitch angle of 45° introduces a more realistic perspective, accounting for factors such as inclines, slopes, and changes in terrain that cyclists encounter during their rides, enabling a more accurate analysis.

In this particular case, it is notable that helmets F and G continue to exhibit inferior performance, while the prototype helmets demonstrate significant improvement compared to the other helmets (Figure 2.13). The force values of the different helmets show different trends, while the force of some helmets increases, the one of the other decreases. These changes can be attributed to the altered geometry and frontal area resulting from the 45° pitch angle. The modified angle likely affects the aerodynamic properties of the helmets, resulting in reduced or increased forces experienced by the cyclists. This observation emphasises the importance of considering realistic pitch angles when evaluating helmet performance, as it provides insights into the impact of design variations on aerodynamics and force reduction capabilities.

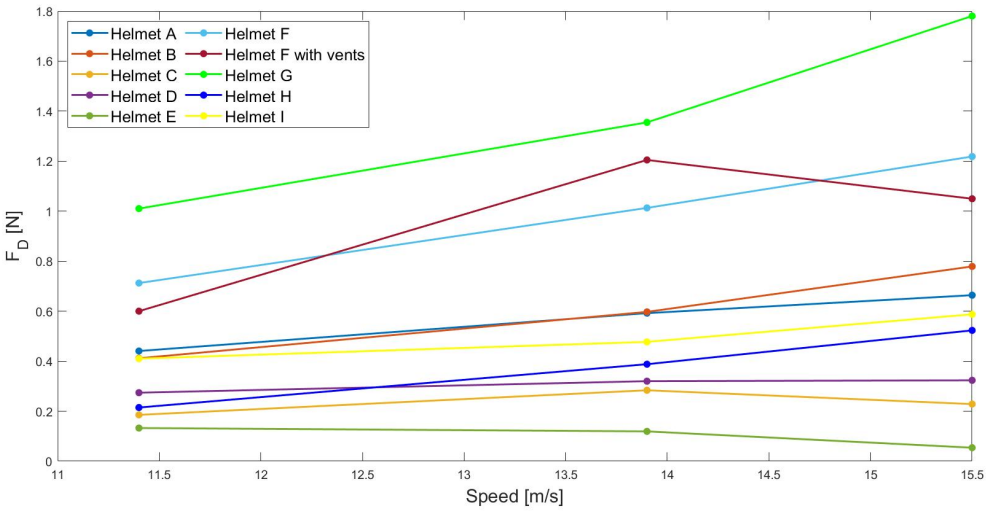

Figure 2.13: *Drag force [N] induced by the different helmets in the wind direction in function of the speed of the wind [m/s] for a pitch angle = 45° and yaw angle = 0°.*

Once again, the drag area results are almost horizontal lines, meaning that there are no significant Reynolds effects at a pitch of 45° (Figure 2.14). In terms of the superior and inferior performances, the drag area have the same trend as the force, with the prototype helmets having the lowest drag area and the aero-road helmets having the highest drag area.

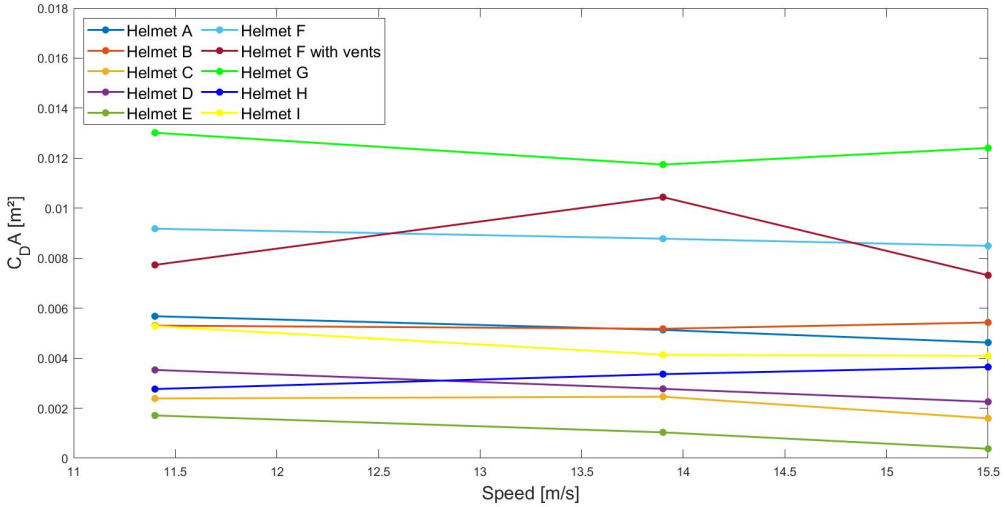

Figure 2.14: *Drag area of the different helmets in the wind direction [m^2] in function of the speed of the wind [m/s] for a pitch angle = 45° and yaw angle = 0°.*

The time trial helmets exhibit less variation in power between the different helmets than for the 0° pitch angle, while the aero-road helmets exhibit larger power (Figure 2.15). This confirms the fact that aero-road helmets are not manufactured in a way to be optimised aerodynamically.

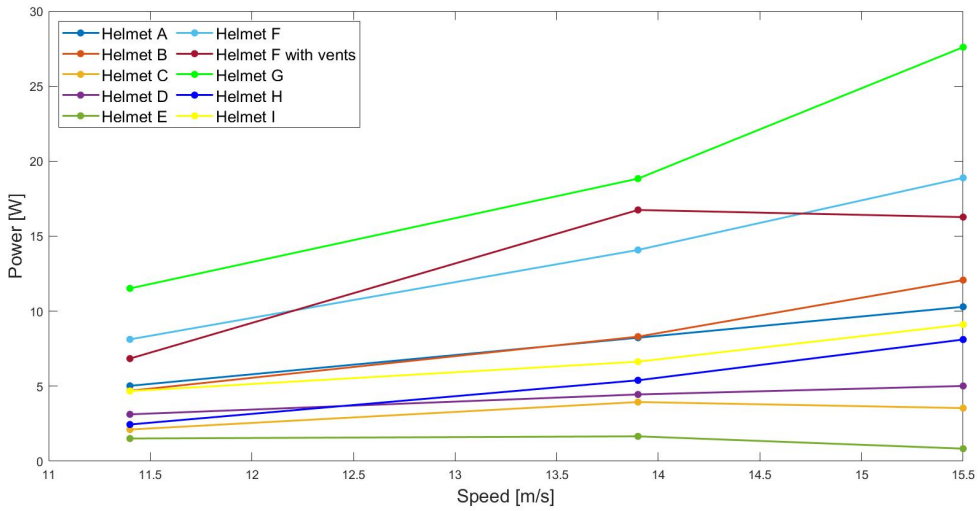

Figure 2.15: *Power [W] induced by the different helmets in function of the speed of the wind [m/s] for a pitch angle = 45° and yaw angle = 0°.*

The most important observations here are, firstly, the difference in the values of the results. The best helmets have a minor impact on the rider as the difference between the head without helmet and with helmet can be less than 1 W. But the disparity in drag force and drag area between the best and worst helmets can reach up to a factor 10 which is not negligible considering that it can lead to an addition up to 25 W that have to be overcome. In a time trial race, it is of major importance to reduce this power as much as possible, which emphasise the importance of the right helmet.
Secondly, the observation of the drag area has shown that there is no Reynold's effect and thus that only one speed can be studied when looking at the drag area as it is representative of the other speeds. In this case, a speed of approximatively 14 m/s will be chosen, as it represents a typical velocity for time trial events. By utilising a standardised speed, the performance of various helmets can be assessed and compared consistently. This approach provides a fair basis for evaluating the effectiveness of different helmet designs in the context of time trial cycling.

Effect of the yaw angle

Evaluating the effect of yaw is really important, as riders cannot maintain a perfectly straight head position throughout an entire race. Understanding how helmet performance varies with yaw angles enables a comprehensive assessment of its aerodynamic capabilities in real-world racing scenarios. Additionally, the yaw angle enables to account for crosswinds. Crosswinds can significantly influence the aerodynamic forces experienced by cyclists, and by analysing the helmet's response to varying yaw angles, valuable insights can be gained to optimise aerodynamic efficiency under different environmental conditions. The forces generated in the y-axis due to the yaw angle may not directly affect the performance of cyclists, but they still hold significance as they influence the stability of the cyclist. These forces can cause deviations from the intended trajectory, requiring the cyclist to exert effort and expend energy to stay on track.

While their impact on performance may be indirect, they play a crucial role in maintaining stability during cycling.

For this analysis, the aero-road helmets were not considered as well as the helmet B as it was performing less well. The tests were conducted at 13.9 m/s with a 45° pitch angle in order to be representative of the time trial situation.

The values of the forces in the direction perpendicular to the cyclist axis (y-axis) show the importance of the yaw angle study. The forces experienced in the y direction cannot be disregarded, as they reach values comparable to the forces experienced in the x direction (Figure 2.16). Moreover, it is notable that the forces along the x-axis show less variation with yaw compared to the forces along the y-axis. This suggests that changes in yaw angle have a greater influence on the forces experienced in the y direction. The differential performance between the x and y directions underscores the importance of considering multi-directional forces when evaluating helmet effectiveness and optimising aerodynamic performance.

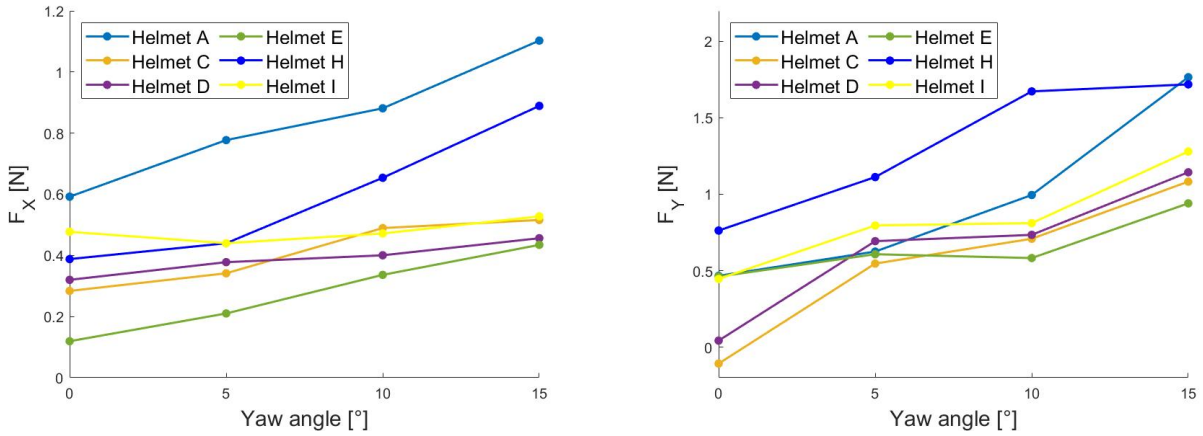

(a) *Drag force [N] in the cyclist axis in function of the yaw angle [°] for a pitch angle = 45° and a wind speed = 13.9 m/s.*

(b) *Drag force [N] in the direction perpendicular to the cyclist axis in function of the yaw angle [°] for a pitch angle = 45° and a wind speed = 13.9 m/s.*

Figure 2.16: *Forces in the cyclist reference axes.*

Overall the prototypes helmets perform the best with helmet E being the best one. It is surprising that it achieves better results as this helmet is smooth. Indeed, a smooth surface does not prevent the air flow from detaching from the surface, which can create bigger forces, but is does not seem to be the case here. However, the corrugation and exhausts seem to work at smaller speed, as the y forces are much smaller for the helmets C and D compared to the others.

Frontal area

The area of the helmets were evaluated with the head included using the method of weighing photographs (Figure 2.17). It can be observed that all the helmets exhibited similar values, with only minor variations between them. The changes in frontal area from one helmet to another were not large. However, a notable distinction is observed when comparing the different pitch angles. This variation in frontal area can likely be attributed to differences in helmet geometry, as well as the potential visibility of the tail of the time trial helmet when positioned at a 45° pitch angle. The influence of these factors on the frontal area highlight the importance of considering the overall helmet design and its impact on aerodynamics when evaluating performance and optimising the efficiency of time trial helmets, and thus studying the drag area that combine the aerodynamics with the geometry. It is important to note that the drag force does not present higher values at a 45° pitch angle even if the frontal area is bigger. This emphasises the fact that the helmets have to be designed to perform better in real-world conditions.

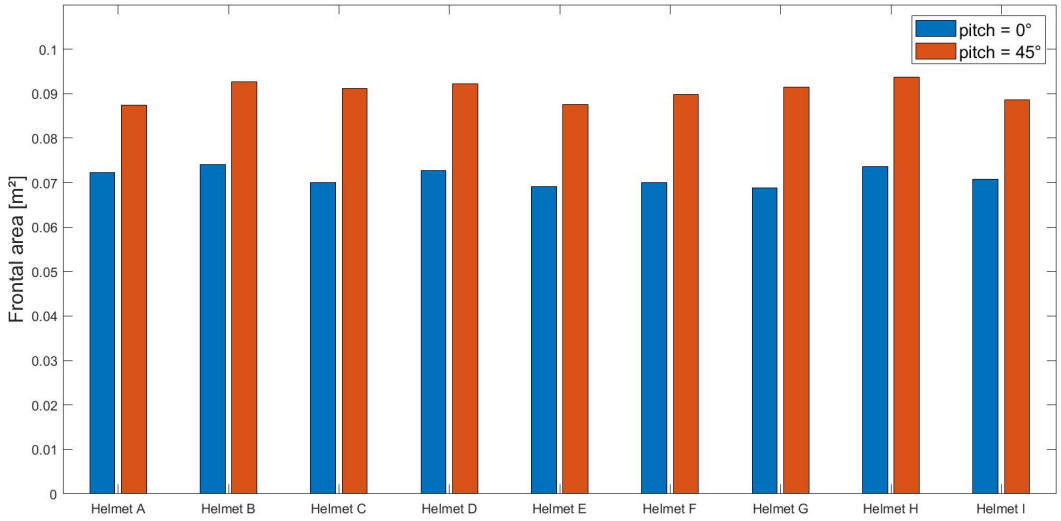

Figure 2.17: *Frontal area of the setup [m²] in function of the pitch angle [°].*

Comparison with the literature

The obtained values of the drag force and power closely resemble those reported in the literature, falling within the same range of values that is around -0.5 N to 1.8 N for the force and up to around 30 W for the power [22, 23]. When comparing the results obtained in this study with those of [2], it is evident that the drag force values align within the same magnitude (Figure 2.18).

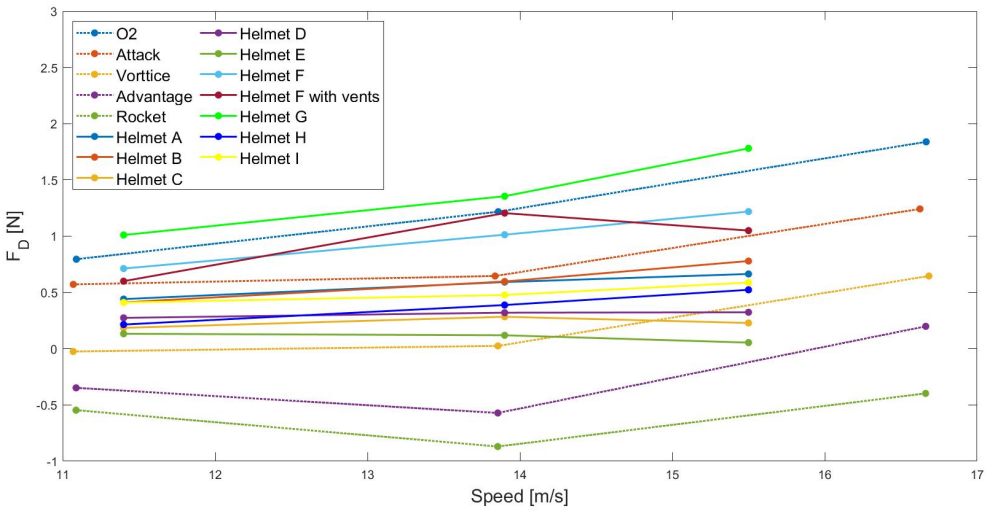

Figure 2.18: *Drag force [N] for a 45° pitch angle at 0° yaw angle for the helmets of the study as well as the helmets of [2].*

This consistency suggests that the experimental measurements align with existing knowledge and understanding of force and power output in similar setups.
The drag area may appear smaller in comparison to other papers. This difference is due to the fact that this analysis focuses on the difference between the different helmets without the head, whereas literature often provides the drag area for the entire setup. The values of the drag area vary around 0.2375 m^2 to 0.2425 m^2 for a helmet on a mannequin [24] and around 0.024 m^2 to 0.033 m^2 for a helmet on a mannequin's head [25]. By considering only the incremental change introduced by the helmet, the variation is up to 0.015 m^2, which coincides with the values obtained in this analysis.

The measured area values also align with those reported in the literature. Reported values for the helmets at 0° yaw and 0° pitch can range from 0.0686 m^2 to 0.0748 m^2 [23]. Similarly, in another paper, the values range from 0.0525 m^2 to 0.0565 m^2, with the higher values observed at a 50° pitch angle [25]. It correlates with the fact that the values obtained in this analysis at a 45° pitch angle are higher than for a 0° pitch angle. This consistency between the measured area values and the literature strengthens the reliability and comparability of the findings.

Wind velocity field evaluation

The Figures 2.19, 2.20, 2.21 and 2.22 depict the wind speed distribution around the helmet measured with the *Procap* system. Initially, a sagittal view illustrates the spatial distribution of the wind speed. This view provides a comprehensive understanding of the airflow patterns and the interaction of the wind with the helmet's surface. Additionally, streamlines are employed to visualise the flow trajectories, enabling us to identify any potential detachment of the airflow from the helmet. The sagittal view and the streamlines are also represented for both helmets with a 15° yaw angle (Figure 2.23).

The force exerted on an object tends to increase with the square of the speed, and this relationship is evident when looking in parallel at the figures depicting the speed distribution around the helmet and the values of the forces corresponding to different speeds. As the speed of the airflow increases, the force experienced by the object, in this case, the helmet, becomes progressively larger. This is in accordance with the fundamental principles of aerodynamics, where the force acting on an object is proportional to the dynamic pressure, which is determined by the square of the speed. By examining the figures depicting the speed distribution around the helmet, it becomes apparent that higher speeds result in a more significant impact on the airflow. Similarly, the values of the forces corresponding to different speeds clearly demonstrate that higher speeds indeed lead to higher forces.

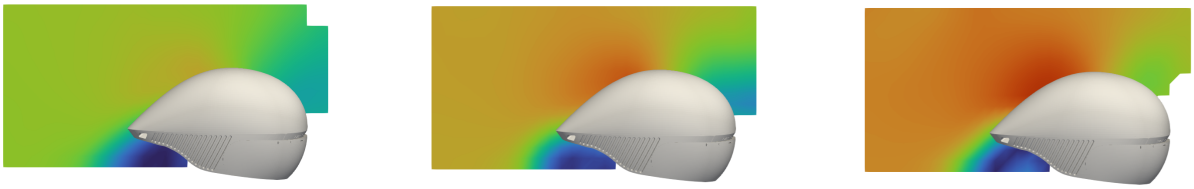

(a) *12.1 m/s* (b) *14.4 m/s* (c) *15.9 m/s*

Figure 2.19: *Sagittal view of the wind speed around the helmet C for different set wind speeds.*

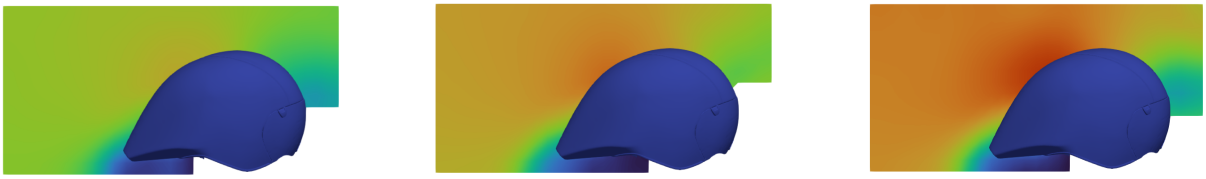

(a) *12.1 m/s* (b) *14.4 m/s* (c) *15.9 m/s*

Figure 2.20: *Sagittal view of the wind speed around the helmet I for different set wind speeds.*

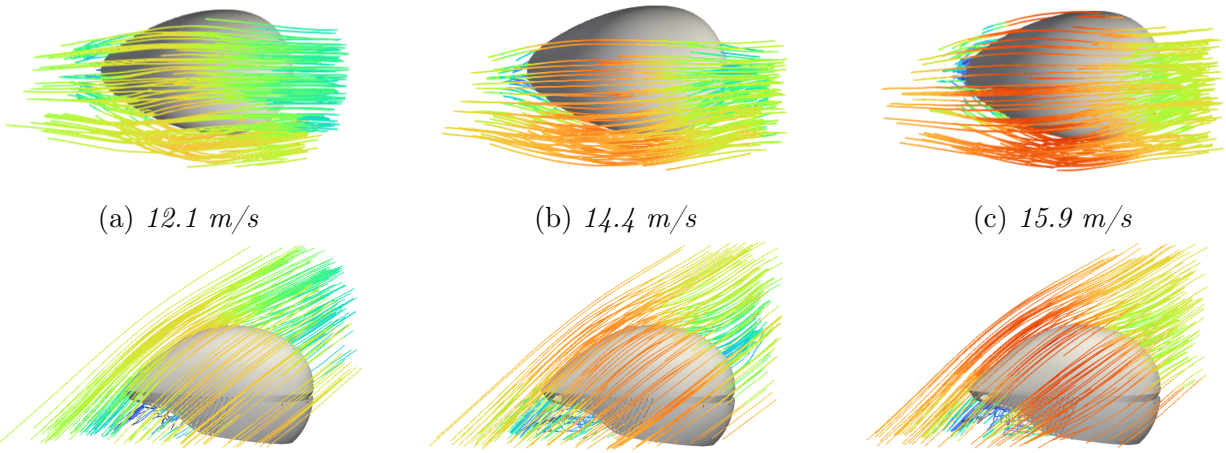

(a) *12.1 m/s* (b) *14.4 m/s* (c) *15.9 m/s*

(d) *12.1 m/s* (e) *14.4 m/s* (f) *15.9 m/s*

Figure 2.21: *Streamlines of the wind speed around the helmet C for different set wind speeds viewed from above and from the side.*

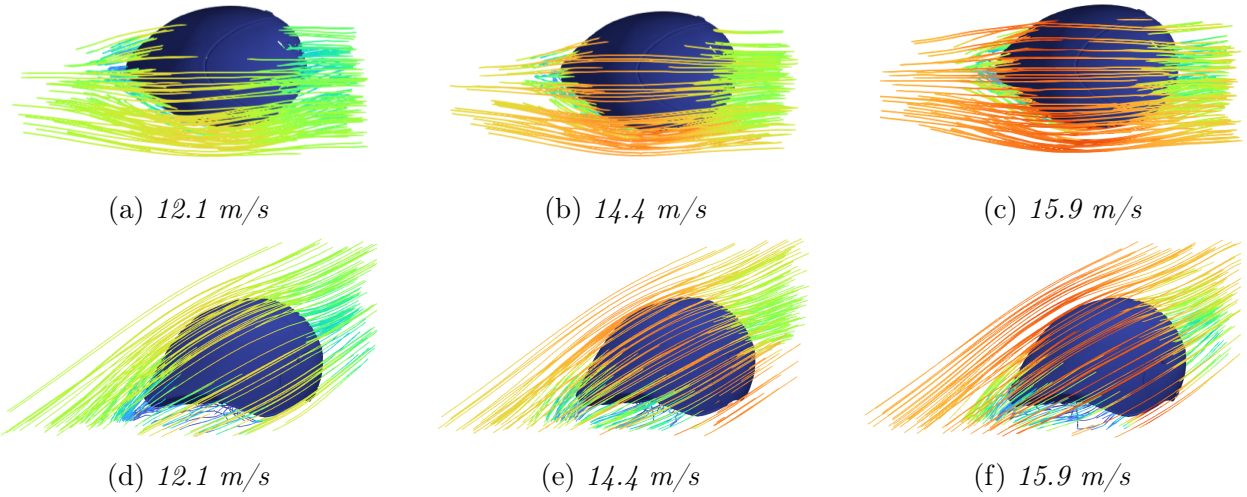

(a) *12.1 m/s* (b) *14.4 m/s* (c) *15.9 m/s*

(d) *12.1 m/s* (e) *14.4 m/s* (f) *15.9 m/s*

Figure 2.22: *Streamlines of the wind speed around the helmet I for different set wind speeds viewed from above and from the side.*

Upon observing the streamlines around the helmet at a yaw angle of 15° (Figure 2.23), it becomes apparent that the flow remains attached even for the helmet I that does not have corrugation or exhausts. This observation suggests that a yaw angle of 15° is relatively small, preventing airflow detachment from the helmet. Furthermore, the wind speed around the helmet with a yaw angle is higher compared to the helmets without any yaw angle, emphasising the significance of helmet geometry. The design of the helmet prioritises frontal wind conditions rather than crosswinds, which contributes to its improved aerodynamic performance. Additionally, the influence of forces in the y direction becomes notably evident when examining the flow behaviour, highlighting their importance in understanding the overall aerodynamic characteristics of the helmet.

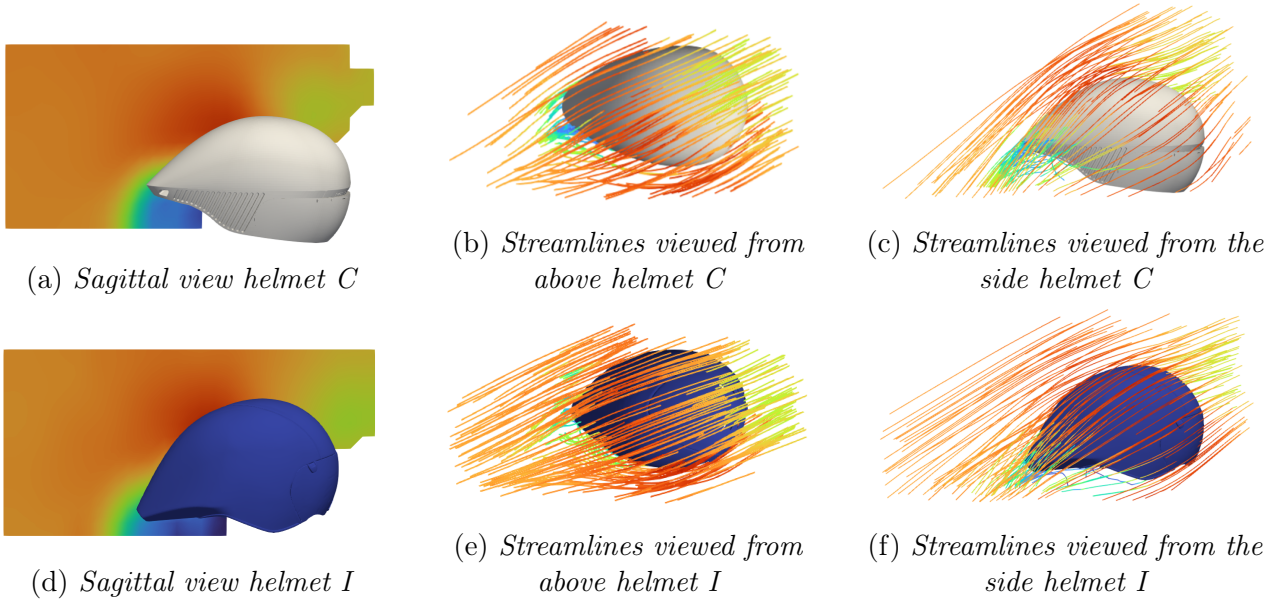

(a) *Sagittal view helmet C* (b) *Streamlines viewed from above helmet C* (c) *Streamlines viewed from the side helmet C*

(d) *Sagittal view helmet I* (e) *Streamlines viewed from above helmet I* (f) *Streamlines viewed from the side helmet I*

Figure 2.23: *Sagittal view of the wind speed and streamlines viewed from above and from the side for the helmets C and I at 15.9 m/s with a yaw angle of 15°.*

It is important to highlight the fact that the setup consisted of a standalone head with a helmet, which does not perfectly represent the reality since, in reality, the helmet works in conjunction with the shoulders to prevent detachment or turbulence. Therefore, the helmet would not achieve precisely the same results in real-life scenarios. Here, turbulence are observed beneath the tail of the helmets, but those may not be present if the helmets were positioned on a person, taking into account the combined effect of the helmet and shoulders. It is essential to acknowledge that this isolated setup provides valuable insights into the helmet's aerodynamic behaviour, but may not fully capture the complex interactions that occur when an individual wears the helmet.

2.4 Conclusion

In conclusion, this analysis examined a range of helmet models with distinct design features and purposes: aero-road helmets (such as F and G) designed for optimal aerodynamics and ventilation in road cycling conditions, and time trial helmets specifically engineered to minimise aerodynamic drag and enhance speed in time trial events.

The evaluation of the helmets encompassed testing at various speeds, pitch angles, and yaw angles, taking into account realistic head movements during a race. This comprehensive approach provided insights into how the helmets performed under different conditions, considering factors like airflow attachment, turbulence, and drag reduction.

The results of the evaluation focused on three key parameters: drag force, drag area, and power, which were consistent with previous literature findings. Notably, the analysis revealed significant variations in the results. The best helmets demonstrated minimal impact on the rider, with a difference of less than 1 W between riding without a helmet and wearing one. However, the disparity between the best and worst helmets could reach a factor of 10 for the drag force and the drag area, resulting in an additional power requirement of up to 25 W. This emphasises the importance of selecting the right helmet to minimise power penalties, particularly in time trial races.

Additionally, the analysis highlighted the absence of the Reynolds effect, indicating that a single speed ($\approx$14 m/s) could be chosen to represent the drag area across different speeds. This standardised approach allowed for fair and consistent evaluation of helmet performance in the context of time trial cycling. Furthermore, the study underscored the significance of studying forces in the y-axis (perpendicular to the cyclist's axis), as they exhibited values comparable to those experienced in the x-axis.

It is crucial to acknowledge that the setup involved a standalone head with a helmet, which does not precisely replicate real-life conditions where the helmet interacts with the shoulders to prevent detachment or turbulence. Therefore, the observed turbulence beneath the helmets' tail may not be present when helmets are worn by individuals, considering the combined effect of the helmet and shoulders. While this isolated setup provided valuable insights into helmet aerodynamics, it may not fully capture the complex interactions that occur in the real-world.

Chapter 3

Influence of position variability on aerodynamics

Now, the analysis focuses on exploring the impact of position variability on aerodynamic measurements. Maintaining a consistent position can be challenging for cyclists, making it difficult to accurately assess how positional changes affect aerodynamics. To overcome this challenge, the study measures the extent of repositioning variations without any feedback. This measurement enables a comparison between the influence of positional errors and the impact of equipment on aerodynamics. By determining the significance of the aerodynamic error caused by incorrect repositioning, the study aims to assess the feasibility of investigating the isolated effect of equipment on aerodynamics.

To do this, the study first examines the variation in angles during self-repositioning. Then, the study evaluates the impact of those angle variations on aerodynamics. This evaluation aims to compare the effect of angle variations on aerodynamics with the results obtained in Chapter 2, in order to determine whether the error surpasses the values of the aerodynamic parameters of the helmets.

3.1 Self repositioning of the cyclist

One of the main challenges for cyclists is maintaining a consistent position over multiple repetitions and extended periods of time. Lack of repeatability in positioning pose significant drawbacks when testing aerodynamics on real cyclists. This is particularly important because the cyclist's position has a substantial impact on aerodynamics, making it a crucial factor to consider.

3.1.1 Methodology

To evaluate the error in repositioning of the cyclist, a test was conducted using 3D cameras and markers placed at specific anatomical landmarks. These markers were positioned at the front of the foot, the 5th metatarsus, the calcaneum, the malleolus, the lateral epicondyle, the

great trochanter, the left, and right anterior iliac crest, the left, and right posterior iliac crest, the acromion, the elbow, and the wrist. The test was performed using the following procedure:

1. The participant positioned themselves on the bike with specific constraints : the right crank had to be vertical with the pedal at the bottom and the hands had to be on the drops of the bike.

2. Once the participant felt comfortable, they stopped moving and paid close attention to their position, trying to memorise it.

3. The participant's position was recorded for a duration of 5 seconds and saved as the reference position.

4. The participant dismounted from the bike.

5. The participant then attempted to reposition themselves on the bike, aiming to replicate the reference position they had memorised. This repositioned position was recorded for 5 seconds.

6. Steps 4 and 5 were repeated five times, allowing for multiple attempts at repositioning.

The aim of this test was to evaluate how accurately the participant could reposition themselves on the bike and replicate the reference position. The repeated measurements provided insights into the consistency and precision of the participant's repositioning abilities. This analysis helps quantify the potential error and variability associated with the repositioning process, highlighting the challenges faced in maintaining a consistent position for aerodynamic testing.

3.1.2 Results

In the evaluation of the repositioning accuracy, only the elbow angle, shoulder angle, and the angle between the torso and the horizontal plane are taken into consideration as they are the primary angles that constrain the cyclist's position. The knee and ankle angles are not studied because they are in constant motion in pedalling conditions.

To quantify the error in repositioning, the root mean square error (RMSE) can be computed between the angles of the reference position and the ones of the five repetitions performed by each participant. The mean RMSE is then calculated over the five repetitions to assess the overall repositioning accuracy (Table 3.1). The results reveal variations between participants, indicating that some individuals are better able to replicate their position compared to others.

	Root mean square error [°]		
	Elbow	Shoulder	Hip
Participant 1	9.14	2.72	1.41
Participant 2	1.26	4.13	1.68
Participant 3	3.23	2.55	0.76

Table 3.1: *Mean root mean square error (RMSE) between the reference position and the 5 repetitions for each participant and each joint angle.*

Additionally, the standard deviation of the RMSE values across the different repetitions is found to be 1.31°. This indicates a significant amount of variability and inconsistency in the repositioning process. The standard deviation being of the same order of magnitude as the error itself highlights the considerable variations observed.

Overall, these findings emphasise the challenges and limitations in achieving consistent and precise repositioning of the cyclist. The results suggest that there is a notable amount of variability and uncertainty in replicating the reference position, further underscoring the difficulties faced in maintaining a stable and repeatable position for aerodynamic testing.

3.2 Effect of the angle error on the drag

3.2.1 Methodology

To assess the influence of the material on its own, it is crucial to examine the impact of minor changes in the cyclist's position on the drag. This is particularly important considering the practical challenges faced by cyclists in replicating their exact position consistently. It is difficult for cyclists to maintain the same position over time and to precisely replicate their body orientation during each ride. As observed in Section 3.1, there are indeed variations in the repositioning accuracy both within different repetitions and among different individuals. Therefore, by evaluating the effects of slight variations in position on drag, it is possible to gain insights into the relative importance of material properties independent of other factors. This analysis enables a more comprehensive understanding of how subtle changes in position can affect the overall aerodynamic performance of the cyclist and their equipment.

In order to evaluate the impact of position, the same setup as the one for the helmet tests (Section 2.3.1) was employed. The head was tested without helmet at pitch angles of 40°, 45°, and 50°, while exposed to wind speeds of 11.5 m/s, 13.9 m/s, and 14.4 m/s. The primary focus was to evaluate the resulting drag under these conditions.

3.2.2 Results

The drag force was evaluated at the three speeds for the three pitch angles (Figure 3.1).

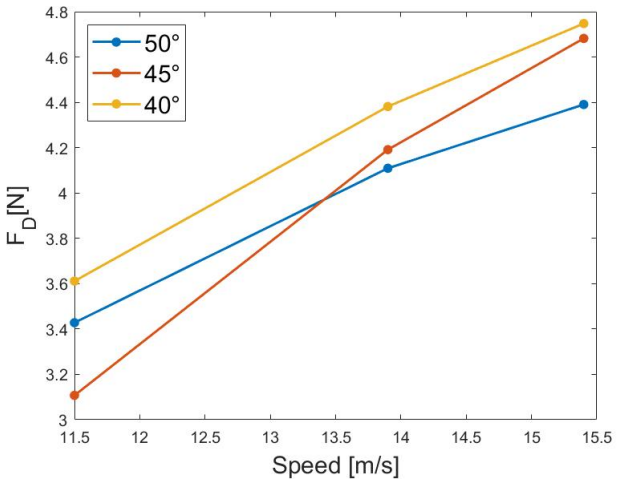

Figure 3.1: *Drag force [N] of the head in function of the speed of the wind for pitch angles of 40°, 45° and 50°.*

The absolute value of the difference between the drag force measures at a 45° and at both other pitch angle can be computed to see the impact on the drag force of a slight change in the angle (Table 3.2). This analysis allows us to quantify and evaluate the influence of even small variations in the angle on the resulting drag force.

	Absolute value of the difference in drag force [N]		
	11.5 m/s	13.9 m/s	14.4 m/s
45°- 40°	0.320	0.0820	0.291
45°- 50°	0.504	0.190	0.065

Table 3.2: *Absolute value of the difference between the drag force measures at a 45° pitch angle and the drag force measures at a 40° and 50° pitch angle for three speeds.*

The impact of a slight angle change on the drag force is significant and should not be overlooked. The variations in drag force between different helmets range from approximately 0.1 N to 1.8 N, highlighting the substantial effect of even minor angle adjustments, as a small difference of 5° in position can result in drag force changes of up to 0.5 N, which is of comparable magnitude as the variations in drag force induces by the different helmets. These findings emphasise the sensitivity of the drag force to small alterations in angle and accentuate the importance of precisely controlling and optimising the positioning of the cyclists in order to minimise drag and enhance overall performance.

Establishing a connection between the cyclist's position and the aerodynamics holds significant potential. This objective is pursued in the paper [26], where researchers aim to identify

a correlation between the angles of the joints and the frontal area. By investigating the relationship between joint angles and the resulting frontal area, the study seeks to shed light on how the cyclist's body position influences aerodynamics. Such insights can be instrumental in developing strategies to optimise performance and minimise drag by understanding the impact of specific joint angles on the overall frontal area. The research contributes to advancing the understanding of the intricate interplay between cyclist position, joint angles, and aerodynamic efficiency. The paper defined the relation between the frontal area and the joint angles as follows :

$$\text{frontal area} = 0.4(\pm 0.07)\text{elbow} + 0.13(\pm 0.02)\text{spine} + 0.11(\pm 0.02)\text{head} + 0.03, \tag{3.1}$$

where frontal area is the relative frontal area and elbow, spine and head are the relative angle of the joints. The angles were measured based on photos and IMUs (Figure 3.2).

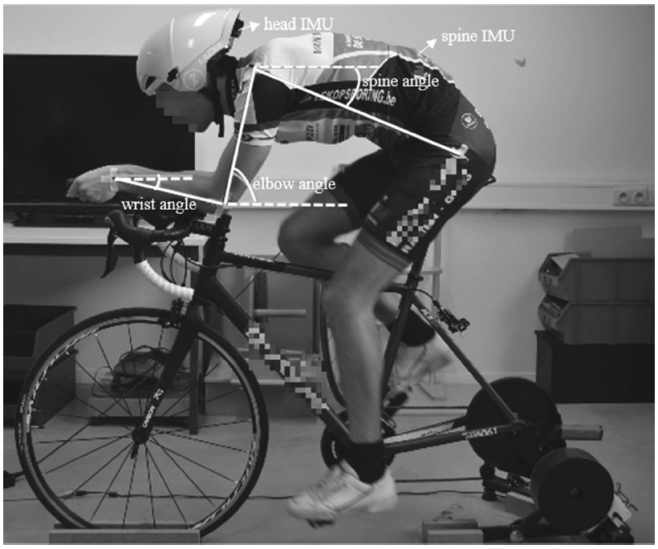

Figure 3.2: *Definition of the joint angles for the evaluation of the link between the joint angles and the frontal area [26].*

The elbow angle has the highest coefficient in Equation 3.1, indicating that it has the greatest impact on the frontal area. By keeping the spine and head angles fixed, it is possible to examine how variations in the relative elbow angle affect the frontal area (Figure 3.3). Even a small difference in angle can result in a significant change in the frontal area, potentially amounting to several square centimetres, which can already make a big difference in the aerodynamics.

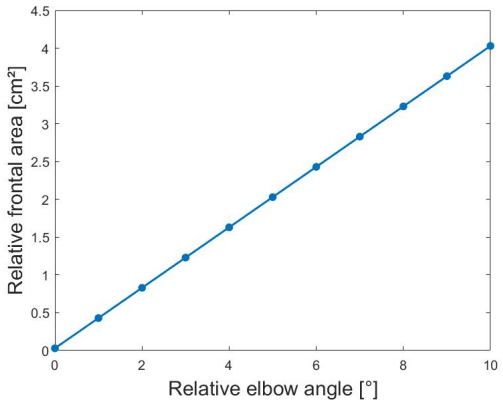

Figure 3.3: *Relative frontal area [cm²] in function of the relative elbow angle [°].*

Employing the Equation 3.1 to establish a link between aerodynamics and position appears highly intriguing. However, it is important to note that the variation in frontal area alone does not provide sufficient information to fully assess the effects on aerodynamics, specifically drag. Nevertheless, this equation does offer valuable insights, such as identifying the significant impact of the elbow angle, as indicated by its larger coefficient. While further analysis and considerations are necessary to comprehensively evaluate the overall aerodynamic effects, the formula serves as a valuable starting point for understanding the influence of joint angles on the aerodynamics of the cyclist's body position.

By analysing the collected data, it is feasible to attempt the development of an equation that establishes a relationship between the head angle and the corresponding drag area :

$$D_X A = 0.000019\text{head}^2 - 0.0015\text{head} + 0.0642, \tag{3.2}$$

where head represents the angle of the head with respect to the horizontal plane in degrees. This equation exhibits an excellent fit with the observed data points (Figure 3.4).

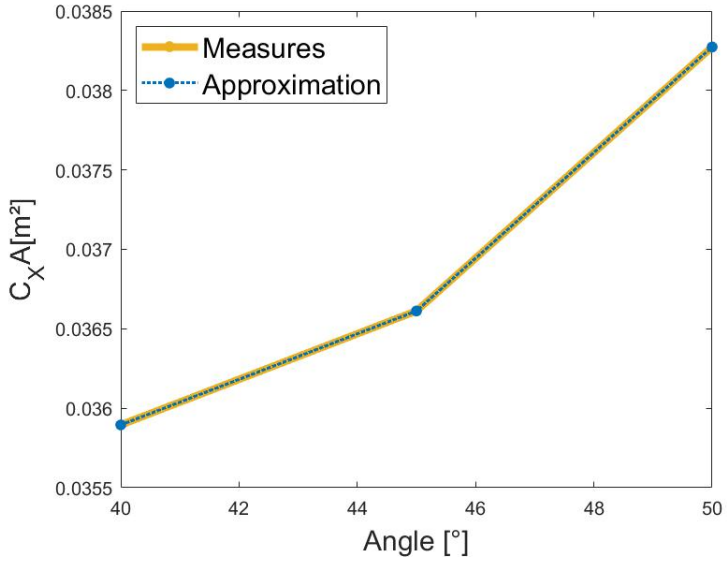

Figure 3.4: *Real values and approximation of the drag area [m²] in function of the head angle [°] at 13.9 m/s.*

It is important to note, however, that this equation is derived from a single measurement conducted at a particular speed within the defined experimental setup. Consequently, its applicability may be limited to the specific conditions of this study and may not directly translate to other experiments or real-world scenarios.

3.3 Conclusion

It is crucial not to underestimate the impact of slight angle changes on drag force. The analysis reveals significant variations in drag force among slight angle changes. For instance, a mere 5° difference in position can lead to drag force change of up to 0.5 N, which is comparable to the variations induced by different helmets ranging from approximately 0.1 N to 1.8 N. This indicates that even minor adjustments in angle can have a substantial effect. These findings underscore the sensitivity of drag force to small angle alterations and underscore the importance of precise control and optimisation of cyclist positioning, as the variations in position prevent the possibility to study the isolated impact of the equipment. Such measures are essential for minimising drag and enhancing overall performance.

Chapter 4

Motion tracking

In this Chapter, a motion tracking algorithm-based feedback system is developed to overcome positional variations. This system aims to offer real-time information and support to cyclists, enabling them to replicate their positions accurately during wind tunnel testing.
The Chapter begins by providing a comprehensive explanation of the motion tracking system algorithm. Various aspects of the code are then examined, starting with the definition of joint angles and followed by an investigation into the comparison between 2D and 3D coordinates. Additionally, the evaluation of different marker placements is discussed, and finally, the repeatability of the motion tracking algorithm is estimated. Various techniques for code improvement were also explored, including the implementation of real-time filters. However, due to inconclusive results, these techniques are not further discussed in this Chapter.

One of the primary challenges in studying cyclists is the inherent difficulty in achieving consistent and repeatable positions. The variations in rider position can have a significant impact on the aerodynamics of the cyclist and ultimately affect the validity of laboratory measurements. To address this challenge, it becomes essential to assess and analyse the cyclist's position in order to enhance repeatability in laboratory testing and to identify optimal positions that can be maintained outside the lab.

Human motion analysis methods, facilitated by 3D camera systems such as *Vicon* or *Optitrack*, offer a solution for tracking and analysing motion. However, these systems are typically bulky and expensive, making them impractical for use outside the laboratory setting. Even within the lab, integrating such systems within wind tunnels poses challenges, as they require significant space and may disrupt the airflow within the tunnel.

Therefore, alternative approaches are sought to overcome these limitations. One such approach is the utilisation of computer vision algorithm, which can provide position estimation using 2D cameras. While these methods may not offer the same level of accuracy and precision as 3D camera systems, they offer a more accessible and portable solution for assessing cyclist positions. The use of computer vision deep learning algorithm could allow for increased repeatability of laboratory measurements and provides an opportunity to explore optimised positions for cyclists.

Furthermore, the analysis of cyclist positions can extend beyond the laboratory setting. By evaluating and monitoring positions outside the lab, cyclists can strive to maintain the most aerodynamically efficient positions during real-world cycling activities. This can lead to improved performance and better understanding of the impact of position on aerodynamics.

Overall, while traditional 3D camera systems have their merits, the use of computer vision deep learning algorithms could offer more practical and accessible means to assess cyclist positions, enhance repeatability in laboratory testing, and explore optimised positions for real-world cycling activities.

4.1 Mediapipe Pose algorithm

The problem of human pose estimation is defined as the localisation of human joints in images and videos. It involves estimating the configuration of the different body parts in input data, such as images. In return, it gives geometric and motion information of the human body [27]. The advantage of using deep learning-based algorithms to perform human pose estimation is their ability to learn complex patterns and features from a large amount of labelled training data. This allows them to generalise well to unseen data and accurately estimate the human pose in various real-world scenarios.

Nowadays, many human pose estimation algorithms based on deep learning exist. For this work, Mediapipe's Pose solution was chosen. Mediapipe, as a framework, provides a convenient and efficient pipeline for implementing and deploying machine learning models, including pose estimation, on different platforms. It offers pre-built solutions and a set of tools and libraries for building and customising machine learning pipelines for time series data. This makes it easier for developers to integrate pose estimation capabilities into their applications without having to start from scratch. This algorithm was chosen among other mainly due to those advantages :

- It is open source;
- It offers pre-built solutions that are easily installed and implemented;
- It is customisable;
- It is lightweight and does not require high performances of the graphic card;
- It accelerates the process, allowing near real-time processing of the videos.

However, Mediapipe Pose also presents some drawbacks :

- It does not allow the detection of more than one person, but this is not a problem for the analysis of a cyclist as only one rider at the time will be present in the wind tunnel;
- The depth analysis is not on point, but this will be developed later on in the Section 4.3;
- As the algorithm is quite new, there is a lack of documentation on it [27, 28, 29, 30, 31].

In human pose estimation, three models are mainly used :

- The kinematic model (Figure 4.1a). It uses a set of joints and segments to connect those joints in order to represent the body structure and limbs orientations. It can represent the body in two and three dimensions.
- The planar model (Figure 4.1b). It is used to represent the body shape, often using rectangles. It can only represent the body in two dimensions.
- The volumetric model (Figure 4.1c). It allows representing the body's soft tissues. It can only represent the body in three dimensions.

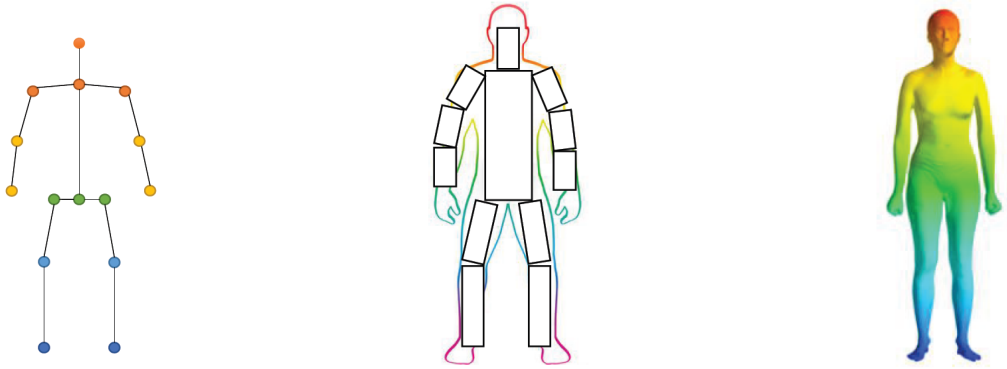

(a) *Kinematic model* (b) *Planar model* (c) *Volumetric model*

Figure 4.1: *Mainly used models in human pose estimation [32].*

Mediapipe Pose is a kinematic model that is able to detect 33 landmarks (Figure 4.2). It identifies more key points than the *COCO topology* that is usually used in other algorithms. Indeed, it combines the *COCO topology*, that have 17 landmarks across the torso, the arms, the legs, and the face, with the BlazeFace and BlazePalm topologies, that are developed by *Google*. Each landmark has three degrees of freedom : the x, y and z. The visibility is also given as output[31, 33, 34].

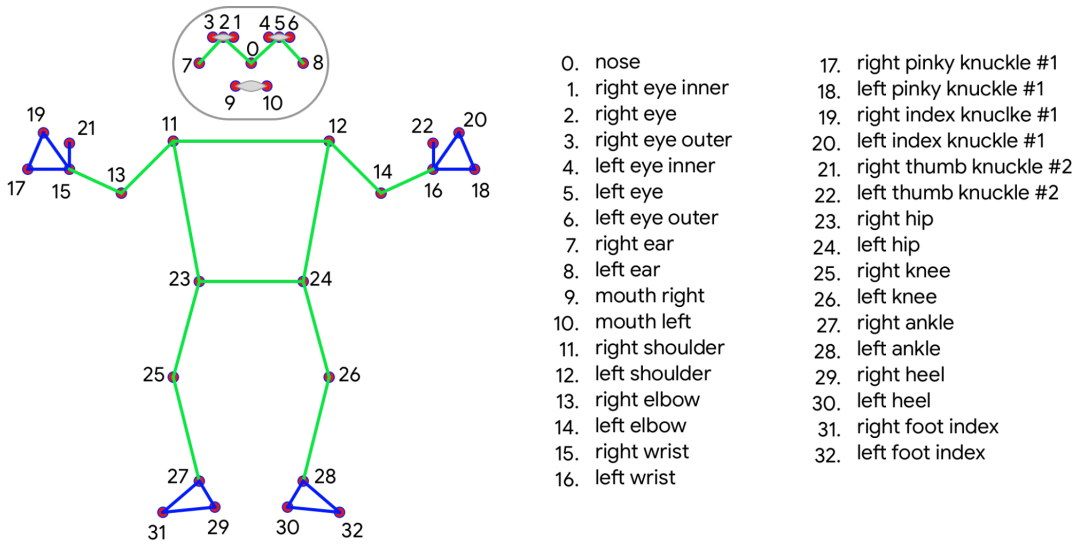

Figure 4.2: *33 landmarks, COCO topology in green and BlazeFace and BlazePalm in blue [33].*

In order to effectuate the pose tracking, Mediapipe Pose works in a two steps machine learning pipeline, that consists in a detector and in a tracker (Figure 4.3) :

1. The detector first scans the frame in order to find region of interests (ROI) where the pose could be located.

2. Then, based on the ROI, the tracker predicts the position of the 33 landmarks.

It is worth noting that in the case of videos, the Mediapipe Pose detector operates primarily on the first frame. Once the initial detection is performed, subsequent frames utilise a tracking mechanism that relies on the key points identified in the previous frame (Figure 4.3). This approach, known as tracking by detection, allows the algorithm to optimise its efficiency and achieve near real-time pose detection.

The tracking mechanism works by estimating the ROI in subsequent frames based on the key points' positions in the previous frame. This means that instead of performing a full detection process on each frame, the algorithm tracks the movement and changes in body pose using the established key points.

However, there are situations where the tracking mechanism may fail to identify the body in the previous frame, such as when a person moves out of the camera's field of view. In such cases, the detector is reactivated to perform a full detection on the current frame and establish new key points for tracking in subsequent frames.

This clever combination of detection and tracking techniques allows the algorithm to maintain close to real-time performance while still providing accurate pose estimation. By utilising tracking after the initial detection, the algorithm can leverage temporal information and reduce the computational overhead associated with repeated detections in every frame [33, 34, 35, 36].

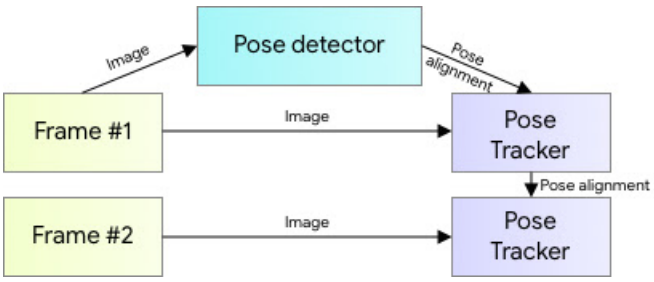

Figure 4.3: *Mediapipe Pose pipeline [33].*

During the development of Mediapipe Pose, the primary objective was to achieve fast and efficient performance without relying on specialised hardware like a dedicated graphics card. While the initial implementation using the detector already yielded promising results, further enhancements were made to improve efficiency.

An interesting observation made during the development process was that the face provides the strongest signal in the neural network, which can be leveraged to detect other body parts. This approach relies on the assumption that the face is always within the camera's field of view. By detecting the face, two virtual key points are created : the midpoint of the hips and the midpoint of the shoulders.

Using these two virtual key points, it becomes possible to infer the position and orientation of the entire body. Inspired by Leonardo da Vinci's Vitruvian Man, the midpoint between the hips and the midpoint between the shoulders are critical for estimating the radius of the circle that encompasses the person's body and the inclination of the line that connects the midpoint of the hip to the midpoint of the shoulder, which represents the person's overall posture (Figure 4.4).

By utilising the face as a reliable anchor point and making use of these derived virtual key points, Mediapipe Pose can accurately estimate the pose and configuration of the entire body. This approach not only improves the speed and efficiency of the algorithm, but also allows for robust pose estimation even without the need for specialised hardware [33].

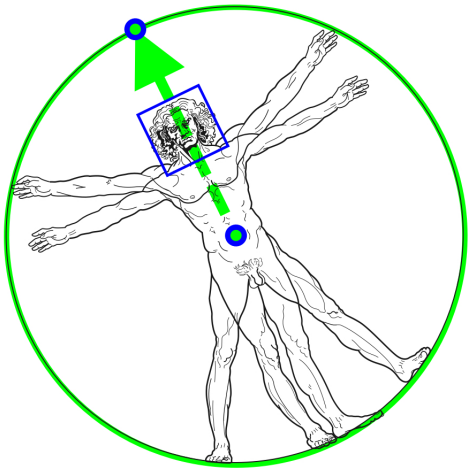

Figure 4.4: *Vitruvian man and virtual key points [33].*

As said before, Mediapipe Pose is a single person detector. For algorithms using deep learning, there are two categories of single person detector pipelines :

- The regression methods. In order to learn a mapping from the input image to body joints or properties of human body models, regression methods utilise an end-to-end framework;
- The heat map-based methods. The goal of heat map-based human pose detector techniques is to teach a body part detector to anticipate the locations of body joints [32].

MediaPipe Pose uses the regression method, but it is in addition supervised by a heat map combined to an offset prediction of all key points (Figure 4.5). During training, the heat maps are first used to train the rest of the network, then the heat maps are removed, and the regression encoder is trained with only the supervision of the heat maps (Figure 4.5). The training database consists of manually annotated images [33].

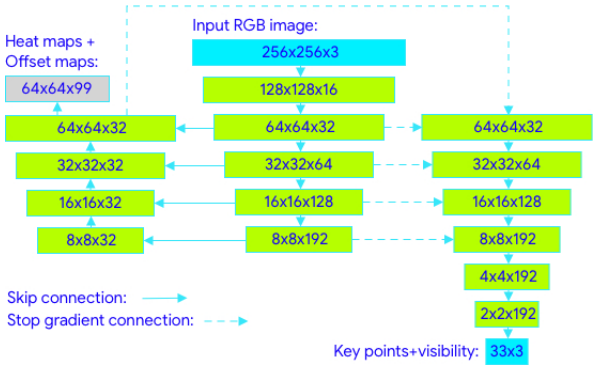

Figure 4.5: *Regression pipeline with heat map supervision [33].*

Mediapipe Pose takes as input an image, a video or a live video. In return, it gives three possible outputs :

- The pose landmarks in coordinates normalised by the image. The coordinate x is the abscissa, and it is normalised by the width of the image in order to have a value between zero and one and; the y coordinate is the ordinate, and it is normalised by the height of the image in order to have a value between zero and one also. The origin of the x- and y-axis is in the bottom left corner of the image. The z coordinate indicate the depth of the image, it has the same scale as the x-axis, its origin is the point between the hips of the person, and its value decreases as it comes closer to the camera. There is a fourth term to the output, which is the visibility of the landmark between zero and one.
- The pose landmarks in the world coordinates. The axis origin is in the centre of the hips and the scale is in meter as in the real world. There is also a visibility term. However, Mediapipe never specifies how it converts the coordinates in meters.
- A segmentation mask. It is a matrix the size of the input image filled with values between zero and one, where zero indicates a high certainty of background and one indicate a high certainty of human.

The pose landmarks in normalised coordinates are used for this study because the final aim is to compute angles, making the conversion in metre not necessary [33].

4.2 Angles definitions

Based on the pose landmarks normalised coordinates estimated by Mediapipe Pose, the angle values of the different joints can be computed for each frame. The angle between two segments, defined by four points, is calculated as follows :

$$\begin{aligned} u_1 &= \frac{a-b}{norm(a-b)}; \\ u_2 &= \frac{d-c}{norm(d-c)}; \\ angle &= 2\arctan\left(\frac{norm(u_1-u_2)}{norm(u_1+u_2)}\right), \end{aligned} \tag{4.1}$$

where a and b are the starting and ending points of the first segment, and c and d are the ones of the second segment. The joint angles of interest in the analysis of the position of a cyclist were firstly defined based on the Mediapipe Pose landmarks (Figure 4.2) as follows :

- The elbow angle : wrist → elbow, elbow→ shoulder;
- The shoulder angle : elbow → shoulder, shoulder → hip;
- The neck angle : hip → shoulder, shoulder → nose;
- The hip angle : shoulder → hip, hip → knee;
- The knee angle : hip → knee, knee → ankle;
- The ankle angle : knee → ankle, heel → front of the foot.

In the case of 3D cameras, markers are typically placed on anatomical landmarks to define the angles for an analysis in order to reduce the soft tissues artefacts that are introduced by the relative motion of the soft tissues with respect to the bones. However, different markers can be used to define the same angle. It is important to compare these different definitions to determine which one is the most representative and resemble the most to the Mediapipe Pose landmarks for accurate analysis.

Since the cyclist's body is symmetrical, it is sufficient to analyse the angles on one side of the cyclist. This simplifies the analysis by focusing on the angles of one side, which can still provide valuable insights into the cyclist's body position and movement.

4.2.1 Methodology

1. Goal : Evaluate which angle definition based on the markers of the 3D cameras is closer to the angles defined in Mediapipe Pose.

2. Parameters :

   - The angles of the elbow, the shoulder, the hip, the knee, and the ankle are measured.
   - Only the left side of the participant is studied.
   - The angles are measured in two static positions and in a dynamic configuration.

3. Population : 1 participant as it is a test measure

4. Material used :

   - 3-dimensional cameras to measure a reference position
   - 12 individual markers to be placed at specific anatomical landmarks
   - A computer with Mediapipe Pose and a camera

5. Protocol to follow :

   (a) Placement of the camera facing the participant such that the whole body of the participant is in the field of view.

   (b) Installation of the markers on the participant (the participant should wear clothes that stick to the skin) :

   - Arm : 1 on the elbow and 1 on the wrist
   - Shoulder : 1 on the acromion
   - Pelvis : 2 on the right and left sides of the anterior superior iliac spine (RASIS and LASIS) and 2 on the right and left sides of the posterior superior iliac spine (RPSIS and LPSIS)
   - Knee : 1 on the lateral epicondyle
   - Foot : 1 on the lateral malleolus, 1 on the calcaneum, 2 on the 1^{st} and 5^{th} metatarsus (meta 1 and meta 5)

   (c) Make sure that all the markers are detected by the 3D cameras by performing a short static pose acquisition. The position should be recorded.

   (d) Analysis :

   - Static analysis : Place the participant in a T-pose (arms and legs at 180°), facing the camera (position 1, Figure 4.6a). Turn on Mediapipe Pose and the 3D cameras. Perform a static analysis during 10 seconds, and turn off Mediapipe Pose and the 3D cameras. Repeat 3 times. The participant should keep the same position during all the acquisitions. Perform the same analysis but in a position

where the participant is seated with the arms bent (arms and legs at 90°) and is turned at 90° with respect to the camera (position 2, Figure 4.6b).

(a) *Position 1*

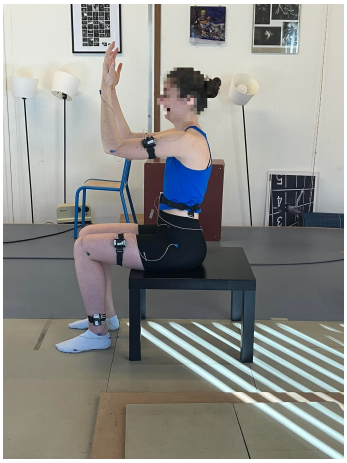

(b) *Position 2*

Figure 4.6: *Positions of the static analysis*

- Dynamic analysis : The participant starts in the second position (Figure 4.7a). Turn on Mediapipe Pose and the 3D cameras. The participant stands up and straighten his arms (Figure 4.7b). Stop Mediapipe Pose and the 3D cameras. Repeat 3 times.

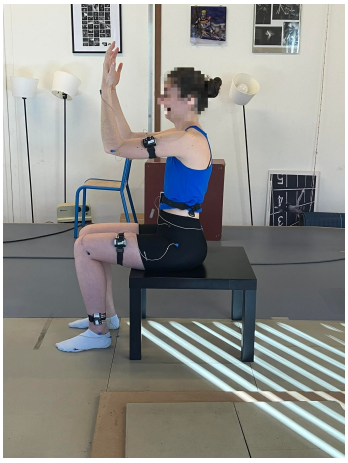

(a) *Start*

(b) *End*

Figure 4.7: *Starting and ending positions of the dynamic acquisition*

6. Processing the data : From the data collected with the 3D cameras, extract the two sets of angles based on the 2D coordinates obtained :

   (a) First set of angles :

   - Elbow angle : wrist - elbow, elbow - acromion
   - Shoulder angle : elbow - acromion, acromion - LASIS
   - Hip angle : acromion - LASIS, LASIS - lateral epicondyle

- Knee angle : LASIS - lateral epicondyle, lateral epicondyle - lateral malleolus
- Ankle angle : lateral epicondyle - lateral malleolus, lateral malleolus - meta 5

(b) Second set of angle :

- Elbow angle : wrist - elbow, elbow - acromion
- Shoulder angle : elbow - acromion, acromion - trochanter
- Hip angle : acromion - trochanter, trochanter - lateral epicondyle
- Knee angle : trochanter - lateral epicondyle, lateral epicondyle - lateral malleolus
- Ankle angle : lateral epicondyle - calcaneum- meta 5

7. Comparison :

- See which of the angles definition gives results closer to Mediapipe Pose.

4.2.2 Results

The comparison between Figure 4.8a and Figure 4.8b with Figure 4.9 reveals noticeable differences in the calculated angles. The second definition of angles appears to be closer to the angles computed by Mediapipe Pose.

Among the angles evaluated, significant changes can be observed in the shoulder, hip, knee, and ankle angles. However, the most substantial difference is observed in the hip angle, which shows a significant reduction with the second definition.

This comparison suggests that the second definition of angles provides a closer approximation to the angles obtained from Mediapipe Pose.

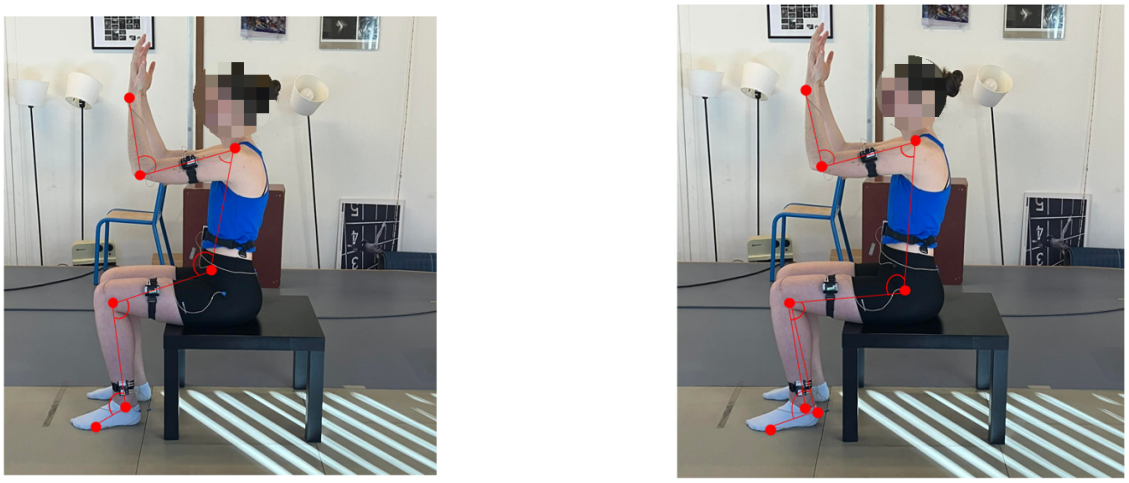

(a) *First definition of angles* (b) *Second definition of angles*

Figure 4.8: *Comparison of the two definitions of angles*

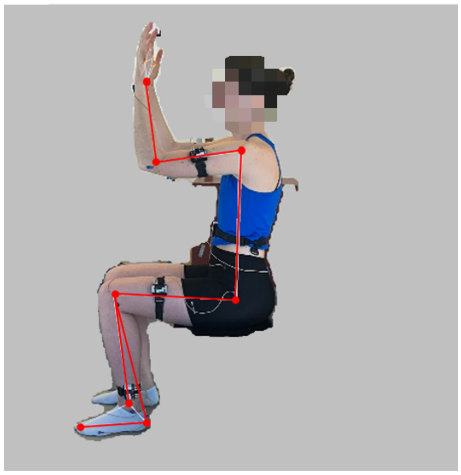

Figure 4.9: *Angles defined based on the landmarks detected by Mediapipe Pose*

The mean root mean square error (RMSE) between the angles based on the 3D cameras and the angles based on Mediapipe Pose can be computed for each angle definition. This evaluation provides a quantitative measure of the difference between the two methods.

To compute the RMSE, the angles obtained from Mediapipe Pose and the 3D cameras are compared at each moment for the 3 repetitions and the 2 positions. The RMSE is then calculated for each joint angle. The mean RMSE is then averaged over time, followed by averaging over the 3 repetitions and the 2 positions (Table 4.1).

The RMSE values provide insights into the accuracy of the angle estimation using the two methods. Lower RMSE values indicate a smaller discrepancy between the angles obtained from Mediapipe Pose and the 3D cameras, suggesting a higher level of agreement.

	Mean root mean square error [°]				
	Elbow	Shoulder	Hip	Knee	Ankle
Def. 1	11.42	16.77	17.23	10.92	22.44
Def. 2	10.58	17.43	8.5	5.95	16.93

Table 4.1: *The mean root mean square error (RMSE) between the angles based on the 3D cameras and the angles based on Mediapipe Pose for the two definitions of the angles.*

The RMSE analysis reveals that the second definition of angles provides a considerable reduction in RMSE compared to the first definition. The hip angle, in particular, shows the largest variation between the two definitions. The only value that does not change much is the RMSE of the elbow, as the definition of this angle is the same in both situations. This aligns with the visual comparison of Figures 4.8a, 4.8b, and 4.9, which clearly demonstrate that the second definition is closer to the angles calculated by Mediapipe Pose.

Despite the improvement, there still exists a significant RMSE between the measurement methods, indicating a difference between Mediapipe Pose and the 3D cameras. To further minimise this disparity, adjustments can be made to the marker placement. For instance, the shoulder marker could be repositioned towards the middle of the shoulder instead of the top extremity. Similarly, for the foot index marker, placing new markers in a location closer to the

middle front of the foot, as used by Mediapipe Pose, could help reduce the RMSE instead of the meta 5 and meta 1 markers used for the 3D cameras that are placed further back on the side of the foot. The effectiveness of this marker placement adjustment is investigated in Section 4.4.

4.3 3D coordinates issues

In order to learn how to estimate the poses, the deep learning algorithm use a database. In 2D, the database consists of annotated images. However, creating 3D human pose databases is a more complex task compared to 2D pose annotation. The depth variable cannot be directly annotated using a single monocular camera, requiring multiple viewpoints to accurately define 3D poses. Setting up a laboratory with specialised cameras and equipment is necessary to acquire such data. Another approach is to build synthetic databases, but this approach limits the diversity of environments and poses that can be encountered.

To address this challenge, Mediapipe Pose is integrated with a statistical 3D human body model called *GHUM*. *GHUM* leverages a database of complete 3D scans of humans in various poses to provide trainable generic human models. By fitting the *GHUM* model to the 2D data, a third key point is obtained to estimate 3D real-world coordinates. Additionally, the data set is enhanced by incorporating the depth order of landmarks, saying which landmark is closer to the camera compared to the others. This depth order is crucial because different poses can have the same 2D projection if the relative depth of landmarks is not known.

Despite the combination of Mediapipe Pose with the *GHUM* model and the inclusion of depth order information, the accuracy of the z coordinate (depth) is reported to be only 32.43%. However, the accuracy of the x and y coordinates (horizontal and vertical axes) is higher at 71.76%. Therefore, it is recommended to utilise the 2D projection of landmarks rather than relying on the 3D real-world coordinates due to the limited accuracy in the depth estimation [28, 37].

To assess the differences between 2D and 3D coordinates and confirm the limitations of 3D accuracy, a comparison can be made between the two coordinate systems and the 3D cameras. By examining the disparities between the 2D projections and the corresponding 3D coordinates, and the exact 3D coordinates measured by the 3D cameras, insights can be gained into the accuracy of the 3D estimation.

4.3.1 Methodology

The measurements for comparing the results obtained with 2D and 3D coordinates can be conducted following a protocol similar to the one described in Section 4.2.1. However, in this case, the focus is on comparing the results obtained using Mediapipe Pose in 2D and 3D.

The protocol involves executing the measurement procedure twice. First, the Mediapipe Pose code is utilised to obtain 2D coordinates of the landmarks. Then, the measurement procedure is repeated using the same code, but this time with the 3D coordinates.

To compare the results, the angles extracted from the 3D cameras, using the second definition of angles, are considered as the reference. The results from the 3D cameras are imported twice: once as 3D coordinates, and once as 2D coordinates projected on the x-z plane.

It is important to note that for this analysis, the new marker placement, mentioned earlier, is not used. The comparison between 2D and 3D coordinates was performed concurrently with the comparison between the two definitions of angles, and any improvements resulting from the marker adjustments were not yet implemented.

By comparing the measurements obtained from the 2D and 3D coordinates, it is possible to assess the differences and discrepancies between the two coordinate systems, shedding light on the accuracy and limitations of 3D estimation in relation to 2D projections.

4.3.2 Results

The mean RMSE is calculated between the angles in 2D obtained from Mediapipe Pose and the 2D angles measured by the 3D cameras, as well as between the 3D angles obtained from both methods for each position and each repetition (Table 4.2). This analysis provides insight into the level of agreement and discrepancy between the angle measurements in 2D and 3D from Mediapipe Pose and the 2D and 3D angles captured by the 3D cameras.

By comparing the mean RMSE values, it is possible to assess the level of similarity and accuracy between the two methods in terms of angle estimation in both 2D and 3D.

	Mean root mean square error [°]				
	Elbow	Shoulder	Hip	Knee	Ankle
2D	10.58	17.43	8.5	5.95	16.93
3D	28.66	27.18	16.99	17.20	16.20

Table 4.2: *The mean root mean square error (RMSE) between the angles based on the 3D cameras and the angles based on Mediapipe Pose for the 2D and 3D coordinates.*

The results presented support the conclusion that the 2D angles obtained from Mediapipe Pose are closer to the actual angles compared to the 3D results. This indicates that despite the improvements made in Mediapipe Pose, the depth estimation component still faces challenges in accurately capturing the depth information from the images. This highlights the limitations and inherent complexities associated with depth estimation in human pose estimation tasks.

For the remainder of this study, the focus will be on using the 2D coordinates obtained from the Mediapipe Pose algorithm. Given that the 2D coordinates are a projection of the landmarks onto the camera's screen, it is important to ensure that the camera is positioned at a 90° angle (side view) from the cyclist. This specific angle ensures that the projection on the screen accurately represents the 3D coordinates, minimising differences between the 2D and 3D measurements.

Additionally, it is worth investigating the effect of small camera displacements on the measurements. This analysis will help determine whether the camera needs to be strictly fixed, or if minor variations in its position do not have an impact on the results. Two camera positions are being studied: position 1, which serves as the reference position with the camera positioned 90° from the cyclist, and position 2, where the camera is shifted 10 cm to the left.

The results indicate that even a relatively small displacement of 10 cm can lead to variations of several degrees in the estimated angles (Table 4.3). This highlights the significance of accurately placing the camera and ensuring its stability throughout the duration of the evaluation. Any movement or displacement of the camera can introduce errors and affect the reliability of the angle measurements.

Therefore, it is crucial to carefully position and secure the camera at the optimal angle to obtain accurate and consistent results. This will ensure the reliability of subsequent analyses and minimise the potential for errors introduced by camera movement or misalignment.

	Angle [°]				
	Elbow	Shoulder	Hip	Knee	Ankle
Position 1	164.45	57.29	107.45	124.32	115.64
Position 2	162.50	58.93	103.48	120.14	127.88

Table 4.3: *Angle values of the different joints for two positions of the camera.*

However, even with 2D coordinates, the values of the root mean square error (RMSE) between Mediapipe Pose and the 3D cameras still remain high. This indicates a significant difference between the measurements obtained from the two methods.

4.4 Comparison of marker placement

One possible explanation for the differences observed between the results obtained from Mediapipe Pose and the 3D cameras is the variation in the definition of angles used by the two methods, as the landmarks are not placed exactly in the same place. To address this, an interesting approach is to modify the markers used by the 3D cameras to closely resemble the landmarks detected by Mediapipe Pose.

Specifically, the markers on the shoulder and the foot can be adjusted to better align with the corresponding landmarks detected by Mediapipe Pose. By making these modifications, the angles measured by the 3D cameras can be more directly comparable to the angles estimated by Mediapipe Pose.

This adjustment in marker placement aims to establish a closer alignment between the two methods, allowing for a more accurate comparison of the results. By ensuring that the markers resemble the landmarks detected by Mediapipe Pose, it becomes possible to evaluate the position with greater consistency and reduce differences between the two measurement techniques.

4.4.1 Methodology

1. Goal : Compare two marker placements to the results of Mediapipe Pose.
2. Parameters :
   - The angles of the elbow, the shoulder, the hip, the knee, and the ankle are measured.
   - Only the left side of the participant is studied.
   - The angles are measured in 3 static positions.
3. Population : 1 participant as it is a test measure
4. Material used :
   - 3-dimensional cameras to measure a reference position
   - 13 individual markers
   - A computer with Mediapipe and a camera
5. Protocol to follow :
   (a) Placement of the camera facing the participant such that the whole body of the participant is in the field of view.
   (b) Installation of the markers on the participant (the participant should wear clothes that stick to the skin) (Figure 4.10) :
      - Arm : 1 on the elbow and 1 on the wrist
      - Shoulder : 1 on the acromion and 1 in the middle of the shoulder
      - Pelvis : 2 on the right and left sides of the anterior superior iliac spine (RASIS and LASIS) and 2 on the right and left sides of the posterior superior iliac spine (RPSIS and LPSIS)
      - Knee : 1 on the lateral epicondyle
      - Foot : 1 on the lateral malleolus, 1 on the 5^{th} metatarsus (meta 5), one on the middle front of the foot (front foot), 1 just under the calcaneum at the same height as the front foot marker

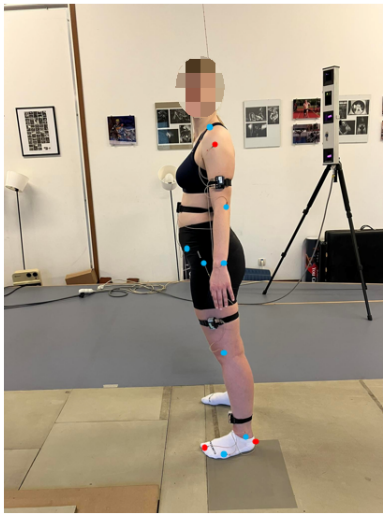

Figure 4.10: *Placement of the markers. The new markers are represented in red, while the markers that were already used are represented in blue.*

(c) Make sure that all the markers are detected by the 3D cameras by performing a short static pose acquisition. The position should be recorded.

(d) Analysis : 3 positions are studied. Place the participant in position 1 (Figure 4.11a), then perform an acquisition of 10 seconds with the 3D cameras and Mediapipe Pose. Repeat 3 times. Repeat with the positions 2 and 3 (Figures 4.11b and 4.11c).

(a) *Position 1*

(b) *Position 2*

(c) *Position 3*

Figure 4.11: *Positions of the static analysis*

6. Processing the data : From the data collected with the 3D cameras, extract the set of angles based on the 2D coordinates obtained with the new markers :
    - Elbow angle : wrist - elbow, elbow - middle shoulder
    - Shoulder angle : elbow - middle shoulder, middle shoulder - trochanter
    - Hip angle : middle shoulder - trochanter, trochanter - lateral epicondyle
    - Knee angle : trochanter - lateral epicondyle, lateral epicondyle - lateral malleolus
    - Ankle angle : lateral epicondyle - lateral malleolus, calcaneum - front foot
7. Comparison :
    - See if the angles obtained with the new markers gives results closer to Mediapipe Pose than the previous ones.

4.4.2 Results

The root mean square error (RMSE) is computed between the angles obtained with the 3D cameras, with the new marker placement, and Mediapipe Pose for each moment of each repetition of the three positions, then it is averaged over time (Table 4.4). The analysis of the RMSE between the angles obtained from the 3D cameras with the new marker placement and Mediapipe Pose confirms that the new marker placement leads to improved results compared to the former placement. The overall RMSE values are significantly smaller, indicating a closer alignment between the detected landmarks by Mediapipe Pose and the 3D cameras.

However, it is important to note that despite the improvements, the RMSE values are still relatively high. This suggests that there are substantial differences between the angles obtained from Mediapipe Pose and the 3D cameras, with variations of up to 20° for certain joint angles. Even though the majority of RMSE values are below 10°, these differences are not negligible, especially in the context of studying a cyclist's position where even a small change in angles can have significant effects on aerodynamics and drag.

Additionally, it is worth mentioning that the RMSE values vary across different joint angles and positions. This indicates that there is no consistent offset between Mediapipe Pose and the 3D cameras that can be corrected by adding a constant value. The differences between the two methods are not uniform and cannot be easily addressed by a simple adjustment.

Therefore, it can be concluded that the angles detected by Mediapipe Pose do not precisely represent the exact position of the participant. While the new marker placement improves the alignment between the two methods, there are still inherent limitations and differences between them that need to be considered when analysing and interpreting the results.

	Root mean square error [°]				
	Former marker placement				
	Elbow	Shoulder	Hip	Knee	Ankle
Mean	10.58	17.43	8.5	5.95	16.93
	Position 1				
	Elbow	Shoulder	Hip	Knee	Ankle
Repetition 1	18.24	12.06	11.16	1.08	21.9
Repetition 2	19.23	12.43	12.41	1.32	22.23
Repetition 3	20.63	13.06	11.9	1.01	19.59
	Position 2				
	Elbow	Shoulder	Hip	Knee	Ankle
Repetition 1	10.02	1.33	3.55	9.74	8.71
Repetition 2	10.83	2.75	4.67	10.52	9.26
Repetition 3	11.39	0.98	3.24	9.85	8.70
	Position 3				
	Elbow	Shoulder	Hip	Knee	Ankle
Repetition 1	7.04	7.66	1.65	7.05	4.01
Repetition 2	6.15	8.94	2.67	4.98	6.72
Repetition 3	5.26	9.90	3.85	6.92	1.57

Table 4.4: *The root mean square error (RMSE) between the angles based on the 3D cameras and the angles based on Mediapipe Pose for each repetition of the three positions.*

Although, while the RMSE values may vary between positions and joint angles, it is worth highlighting the consistency observed within the repetitions of a particular position. This consistency suggests that, despite the differences between Mediapipe Pose and the 3D cameras, the results obtained from Mediapipe Pose are relatively stable within the same position.

For instance, when examining the joint angles of position 1 (Figure 4.12), even though there is a notable disparity between the angle measurements of Mediapipe Pose and the 3D cameras, the angles detected by Mediapipe Pose tend to fall within a similar range of values across the repetitions.

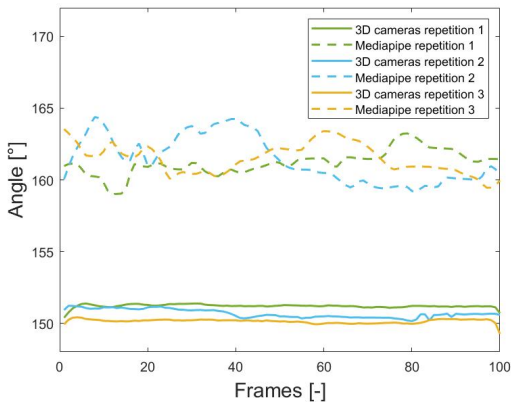

(a) *Elbow*

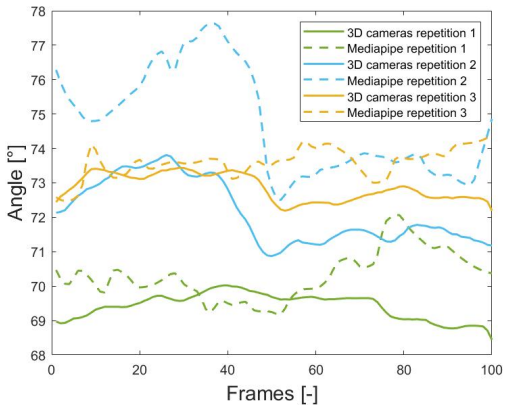

(b) *Shoulder*

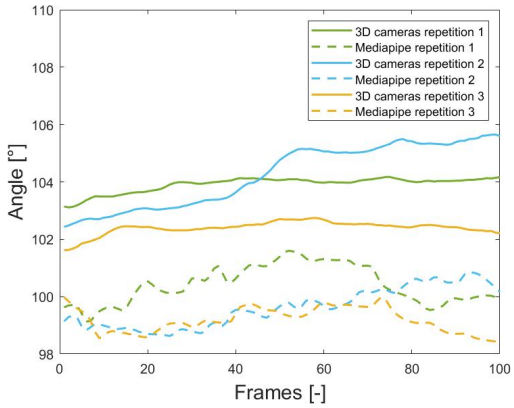

(c) *Hip*

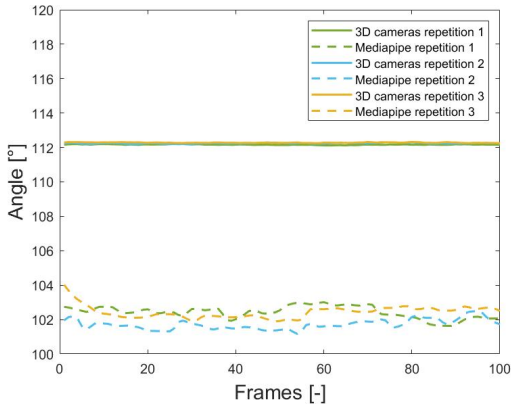

(d) *Knee*

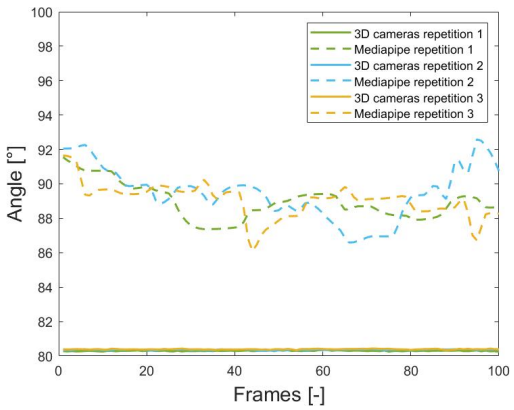

(e) *Ankle*

Figure 4.12: *Joint angles [°] detected by Mediapipe Pose and the 3D cameras in function of the frame number [-] for each repetition of the position 1.*

The low RMSE values between the first repetition and the other two repetitions within each position provide further evidence of the consistency of Mediapipe Pose in detecting angles (Table 4.5). The fact that the RMSE values remain under 5° for most measurements indicates that Mediapipe Pose consistently captures angles within a small margin of error across repetitions.

This level of consistency suggests that Mediapipe Pose could be potentially useful in scenarios where the goal is to replace someone in a similar pose within a tolerance of approximately 5°. It implies that if a person's pose is captured using Mediapipe Pose, it would be feasible to

reproduce a similar pose within a reasonable degree of accuracy.

However, it is worth noting that the higher RMSE values observed in certain cases may be attributed to specific data processing issues. It is crucial to carefully examine and address these cases to ensure the reliability and accuracy of the results.

	Root mean square error [°]				
	Position 1				
	Elbow	Shoulder	Hip	Knee	Ankle
Repetition 2	2.58	3.20	0.75	1.40	1.66
Repetition 3	2.27	2.60	0.53	1.01	1.46
	Position 2				
	Elbow	Shoulder	Hip	Knee	Ankle
Repetition 2	2.31	4.82	1.24	0.88	1.52
Repetition 3	1.47	3.38	1.34	0.52	1.14
	Position 3				
	Elbow	Shoulder	Hip	Knee	Ankle
Repetition 2	6.12	1.78	0.77	2.65	7.29
Repetition 3	1.87	2.31	2.54	3.02	3.10

Table 4.5: *The root mean square error (RMSE) between the angles of the first repetition of Mediapipe Pose and the two other repetitions for the three positions.*

Based on this analysis, it can be concluded that the new marker placement improves the alignment of the detected landmarks with Mediapipe Pose, resulting in a reduction in the RMSE between the angles measured by the two methods. This suggests that the new marker placement provides a better representation of the landmarks detected by Mediapipe Pose.

However, it is important to note that Mediapipe Pose does not provide exact angles, as evidenced by the elevated RMSE between the values obtained with Mediapipe Pose and the 3D cameras. Despite this, Mediapipe Pose consistently returns similar results for each repetition, indicating its potential utility in replacing someone in the same position. This aspect holds particular significance in the context of studying cyclists, as the primary goal is to replicate the cyclist's position accurately across multiple repetitions. While exact position evaluation may be less important, ensuring consistent and repeatable positioning becomes predominant in achieving reliable and comparable results. Therefore, despite the lack of exact results provided by Mediapipe Pose, the focus can still be placed on studying the repeatability, which is the most crucial aspect of interest.

Nevertheless, it is essential to consider an error margin of approximately 5° when using Mediapipe Pose, as there is still a small discrepancy between the different repetitions. Careful consideration should be given to this margin of error when utilising the results obtained from Mediapipe Pose.

4.5 Estimation of Mediapipe Pose repeatability

Two codes have been implemented to provide feedback to the cyclist and assist in replacing themselves in the same position. Those codes can be found in Appendix C. The first code, `starting_position.py`, utilises Mediapipe Pose in 2D without any filtering. The cyclists are required to position themselves in a specific pose, which is recorded by the code. The position during the few last seconds is averaged, and then saved as the reference position.

The second code, `2D_mediapipe_pose_detection.py`, also uses Mediapipe Pose in 2D without any filtering. It detects the current position of the cyclist and provides feedback to help them adjust their pose. The code calculates the difference between the reference position and the current position and then displays the live video of the cyclist with specific segments of interest highlighted in different colours based on the magnitude of the difference.

This colour-coded feedback allows the cyclist to visually observe the areas where their current pose differs from the reference pose, enabling them to make the necessary adjustments to align themselves correctly :

- Green : : good position-5° < current position < good position+5°
- Yellow : good position-10° < current position < good position-5°
- Orange : good position+5° < current position < good position+10°
- Red : current position < good position-10° & good position+10° < current position

An error margin of ±5° was chosen based on the analysis conducted in the Section 4.4.2, where it was observed that the range of angle differences between two repetitions remained under 5°. Therefore, a 5° margin around the reference position was considered as an acceptable error.

In addition, the feedback provided by the code indicates, for each joint, whether the cyclist needs to increase or decrease the angle to align with the reference position (Figure 4.13). The code specifically focuses on the elbow, shoulder, neck, and hip joints, as the knee and ankle joints are in constant motion during cycling and attempting to precisely reposition them would be impractical.

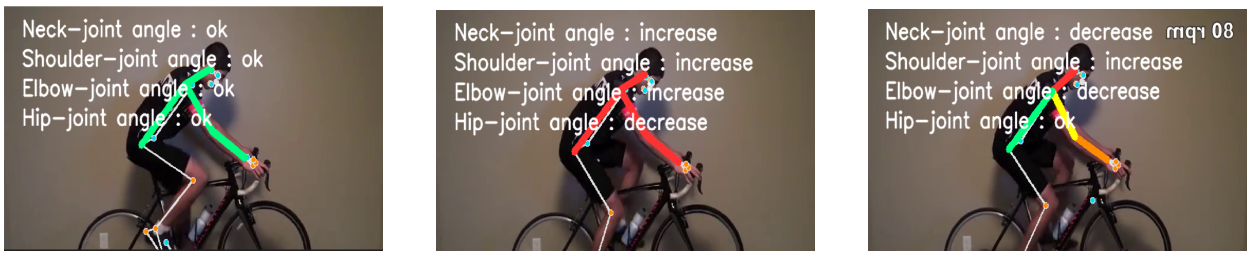

(a) *Good position* (b) *Wrong position* (c) *Different feedbacks*

Figure 4.13: *Visual feedback with colours and indications.*

After conducting several tests, it was observed that the initial definition of the angles was not optimal for the intended purpose. Two specific issues were identified.

Firstly, the hip angle was found to vary constantly during cycling, as it was measured with respect to the thigh, making it unreliable for estimating the torso position when it remains stationary. Therefore, it was not suitable for studying the angle of the hip independently.

Secondly, the movement of the torso caused changes in the neck angle, making it impossible to isolate and study the angle of the neck alone.

To address these issues, a new approach was adopted. Instead of measuring the angles between segments, the angles were measured between each segment and the horizontal plane. This revised approach provided a more reliable and meaningful representation of the joint angles, allowing for more accurate feedback and analysis of the cyclist's position.

This led to a new definition of the joint's angles :

- The elbow angle : wrist - elbow, elbow - shoulder
- The shoulder angle : elbow - shoulder, shoulder - hip
- The neck angle : shoulder - nose, horizontal plane
- The hip angle : shoulder - hip, horizontal plane
- The knee angle : hip - knee, knee - ankle
- The ankle angle : knee - ankle, heel - foot index

In order to assess the repeatability of Mediapipe Pose, a series of measures were conducted. The joint angles were measured using both Mediapipe Pose and the 3D cameras, and the results were analysed for consistency.

The goal was to observe if there was low variation in the results obtained by Mediapipe Pose across multiple runs, as well as in the measurements obtained from the 3D cameras. A high level of repeatability would indicate consistent and reliable measurements.

The analysis of the results should provide insights into the stability and consistency of Mediapipe Pose, allowing for an assessment of its repeatability.

4.5.1 Methodology

1. Goal : Evaluate the repeatability of Mediapipe Pose.
2. Parameters :
    - The angles of the elbow, the shoulder, and the hip are measured.
    - Only the left side of the participant is studied.
3. Population : 10 participants in order to make statistics

4. Material used :

   - 3-dimensional cameras to measure a reference position
   - 12 individual markers
   - A computer with Mediapipe, a camera and a screen to see the results
   - A fixed bike

5. Protocol to follow :

   (a) Placement of the camera at 90° to the bike such that the whole body of the participant and the bike are in the field of view.

   (b) Placement of a screen connected to the computer displaying the feedback in front of the bike such that the participant can see it when he is placed on the bike.

   (c) Installation of the markers on the participant (the participant should wear clothes that stick to the skin) :

      - Arm : 1 on the elbow and 1 on the wrist
      - Shoulder : 1 in the middle of the shoulder
      - Pelvis : 2 on the right and left side of the anterior superior iliac spine (RASIS and LASIS) and 2 on the right and left side of the posterior superior iliac spine (RPSIS and LPSIS)
      - Knee : 1 on the lateral epicondyle
      - Foot : 1 on the lateral malleolus, 1 on the 5^{th} metatarsus (meta 5), one on the middle front of the foot (front foot), 1 just under the calcaneum at the same height as the front foot marker

   (d) Make sure that all the markers are detected by the 3D cameras by performing a short static pose acquisition. The position should be recorded.

   (e) Analysis :

      i. The participant places himself on the bike. The right pedal should be down with the crank vertical. The hands should be on the drops of the handlebar (Figure 4.14). The participant should be able to see the feedback screen (that is not turned on at the moment). Once the participant is comfortable, he should pay attention to his position and try to memorise it. The participant does not move

      ii. The code `starting_position.py` is run in order to save the position. The 3D cameras are also turned on in order to record this position during 5 seconds. The position is labelled as the good position.

      iii. The participant get off the bike.

      iv. The code `2D_mediapipe_pose_detection.py` is run. The feedback appears on the screen in front of the bike.

v. The participant have to reposition himself on the bike in order to have the good position (segments lighten in green).

vi. Once the participant is in the good position, he holds it for 5 seconds while the 3D cameras records it.

vii. The steps 3 to 6 are repeated 5 times.

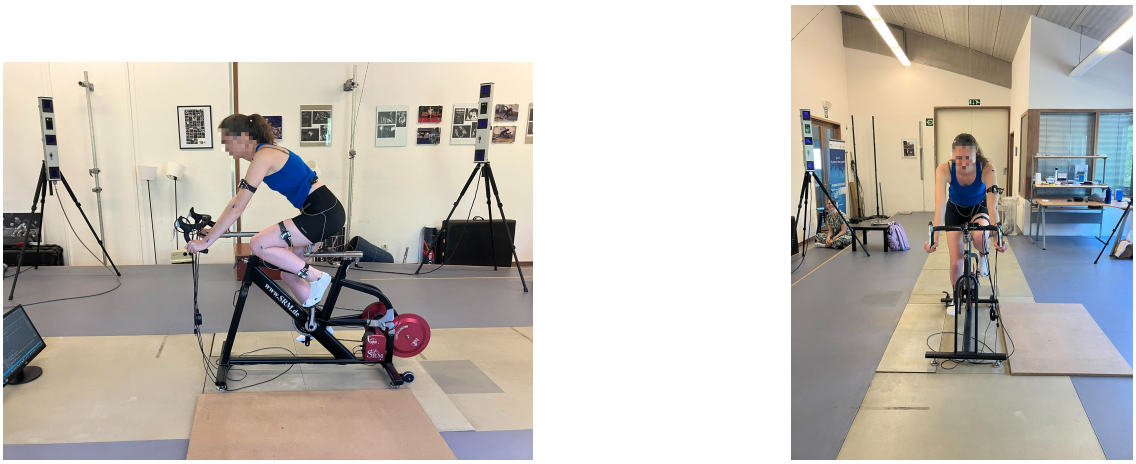

(a) *Side view* (b) *Front view*

Figure 4.14: *Repeatability measures setup*

6. Processing the data : From the data collected with the 3D cameras, extract the set of angles described in the Section 4.4.2 except for the hip and neck that are now measured with respect to the horizontal plane.

7. Comparison :

   - Evaluate the difference between the reference position and the different repetitions for Mediapipe Pose and for the 3D cameras in order to see if they detect the same angle at each repetition.

4.5.2 Results

In this analysis, only three joint angles are studied: the elbow, the shoulder, and the hip. The knee and ankle angles are not included in the analysis, as they are constantly in motion during cycling. The neck angle is also excluded from the analysis due to the absence of markers on the participants' heads, making it impossible to extract the neck angle from the 3D camera data. The analysis focuses on two key elements. Firstly, the variation between the reference position and the five repetitions measured by Mediapipe Pose should be low. This indicates that the code consistently detects the same angles across multiple runs. Secondly, the variation between the reference angle and the five repetitions measured by the 3D cameras should also be minimised. A low variation in this case suggests that Mediapipe Pose accurately captures the same angles in reality.

To evaluate the variations, the mean value of the RMSE between the reference position and the five repetitions is computed for each angle and each participant (Table 4.6). The RMSE values for Mediapipe Pose exhibit a mean of approximately 1.10° across all angles and participants. This low value indicates that Mediapipe Pose consistently detects the same angles in each repetition.

	Mean root mean square error [°]									
	P1	P2	P3	P4	P5	P6	P7	P8	P9	P10
Elbow	0.95	1.12	1.02	1.04	0.87	1.42	1.20	0.98	1.20	1.14
Shoulder	1.45	1.18	1.46	0.92	1.47	0.93	0.43	1.34	1.50	1.32
Hip	0.86	0.99	0.93	0.36	1.14	0.73	0.30	1.08	1.32	1.44

Table 4.6: *The mean value over all 5 repetitions of the root mean square error (RMSE) between the reference angle and the angles of all 5 repetitions measured by Mediapipe Pose for the 10 participants (P1 → 10).*

The RMSE values obtained from the 3D cameras indicate slightly higher variations compared to those obtained from Mediapipe Pose (Table 4.7). Although the majority of the RMSE values from the 3D cameras are low, there are some instances where higher values are observed, particularly for the elbow and shoulder angles. But the order of magnitude of the RMSE is the same for both methods.

However, it is important to consider that while individual RMSE values for the 3D cameras may occasionally be relatively high, the overall mean RMSE remains below the specified 5° error margin. The calculated overall mean RMSE for the 3D cameras is 2.47°. This suggests that, despite the presence of outliers or higher variations in some cases, the majority of the measurements obtained from the 3D cameras fall within an acceptable range of accuracy.

	Root mean square error [°]									
	P1	P2	P3	P4	P5	P6	P7	P8	P9	P10
Elbow	8.05	1.65	1.33	3.90	9.14	2.00	0.98	3.33	1.58	3.88
Shoulder	1.23	3.44	2.47	0.66	3.99	3.09	1.03	4.46	1.35	2.70
Hip	2.24	1.72	0.80	0.58	1.82	0.64	0.60	4.15	1.15	1.60

Table 4.7: *The mean value over all 5 repetitions of the root mean square error (RMSE) between the reference angle and the angles of all 5 repetitions measured by the 3D cameras for the 10 participants.*

Box plot figures are effective in illustrating the results (Figure 4.15). They provide a visual representation of data distribution and help identify variations within and between repetitions. The height of the box in the box plot represents the variations of the angles during the time of one repetition, as the participant can move slightly over time. A taller box indicates higher variability, while a shorter box suggests lower variability within that repetition. Furthermore, the differences in angles between the different boxes reflect the variations between repetitions.

If the boxes are noticeably at different ordinates from one another, it indicates significant variability between the repetitions. To provide a reference point, a solid line is used to indicate the reference value. This line serves as a benchmark against which the data can be compared. Additionally, the error margin of $\pm 5^\circ$ is denoted by the dotted lines. These lines help identify whether the data falls within an acceptable range or exceeds the allowed variation.

Based on the box plot figures, it is apparent that the elbow measurements from the 3D cameras exhibit higher variations. This observation is supported by the presence of boxes that lie outside the error margin, suggesting significant differences between the repetitions in that particular joint.

On the other hand, the box plots clearly demonstrate low variations in the repetitions overall, as indicated by the relatively consistent and compact boxes close to the reference position.

Moreover, the box plots also show that the values obtained from the 3D cameras differ from those generated by Mediapipe Pose. This discrepancy suggests that Mediapipe Pose does not fully represent the reality of the measured angles. However, it is worth noting that both methods yield plausible results, even though they are not identical. The observed discrepancies can be attributed to the variations in how angles are precisely defined in Mediapipe Pose and the 3D cameras.

Nevertheless, it is notable that the variations in the box ordinates generally remain within a low range, typically within the 5° error margin. This highlights the potential utility of Mediapipe in effectively replacing the cyclist across various analyses.

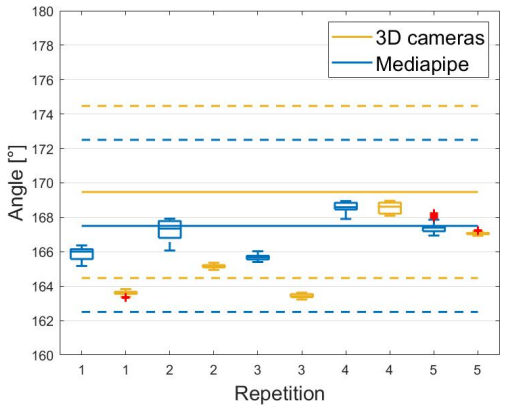

(a) *Elbow*

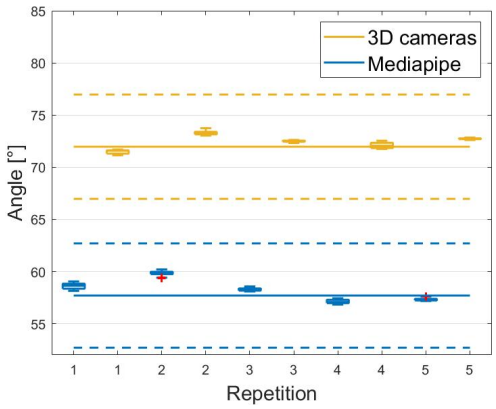

(b) *Shoulder*

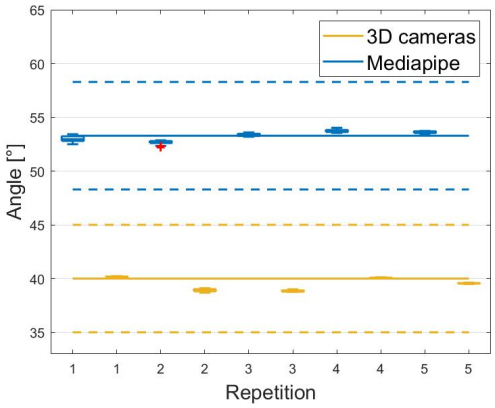

(c) *Hip*

Figure 4.15: *Box plot of the joint angles [°] detected by Mediapipe Pose and the 3D cameras. The x-axis represents the five repetitions of the participant 4. The solid line represents the reference positions and the doted lines represent the error margin of ±5°.*

One possible explanation for the observed variation in the elbow and shoulder values is the method used to compute those angles. The elbow and shoulder angles are calculated as a relative angle between the forearm and the upper arm, whereas other angles, such as the hip angle, are measured with respect to the horizontal plane.

When measuring an angle between two segments, there is a potential for error association between those segments. In the case of the elbow angle, any inaccuracies or variations in the measurement of the forearm and upper arm can contribute to the overall variability of the calculated elbow angle.

A similar issue may also apply to the shoulder angle, as it is computed as a relative angle between the upper arm and the torso.

To address this problem, one potential solution is to evaluate the elbow and shoulder angles with respect to the horizontal plane, similarly to how the hip or neck angles are measured. By referencing the angles to a common horizontal plane, the potential error association between the segments can be minimised. This approach provides a more consistent measurement framework.

It results from this analysis that Mediapipe Pose can be used in order to replace the cyclist in the same position with an error margin below 5°. Effectively, even if the values of the 3D

cameras and Mediapipe Pose show a large offset, the low values of the RMSE for Mediapipe indicate that the values of Mediapipe Pose do not vary much from one repetition to another and the values of the RMSE of the 3D cameras also stay quite low, even if it is slightly higher, which indicates that Mediapipe Pose actually detect the same angle from one repetition to another. So, Mediapipe can be considered as a repeatable way to replace the cyclist in the same position. However, the definition of the elbow and shoulder angle has to be changed in order to be evaluated with respect to the horizontal so that the error is reduced (Figure 4.16). This definition of angles is the one implemented in the final codes `starting_position.py` and `2D_mediapipe_pose_detection.py`.

Figure 4.16: *Final angle definition : the neck angle is in orange, the shoulder angle is in blue, the elbow angle is in green and the hip angle is in red.*

4.6 Conclusion

In conclusion, the results obtained from Mediapipe Pose provide an estimation of the position with a margin of error of $\pm 5°$. Unfortunately, this level of error is too significant to reliably evaluate the specific effects of materials, such as helmets, as a 5° variation in angle can result in drag variations of similar magnitude as the differences observed between the helmets (Section 3).

Based on the information provided in Section 3.1, where the self-repositioning of the cyclists was evaluated using 3D cameras, it appears that the accuracy of Mediapipe Pose is similar to the results obtained from self repositioning. Mediapipe Pose does not show smaller levels of error, as indicated by similar values for the root mean square error (RMSE) and standard deviation between different repetitions (1.14° for Mediapipe Pose and 1.31 for the self repositioning).

Therefore, in terms of repositioning accuracy, Mediapipe Pose does not appear to outperform the self repositioning evaluated using 3D cameras. The margin of error and variations in positioning are of a similar range for both approaches.

It is important to consider these limitations and uncertainties when using Mediapipe Pose

for evaluating cyclist position in aerodynamic studies. While this method can provide useful insights and general evaluations, it may not offer the level of precision required for detailed analysis or comparison of specific equipment effects on drag.

However, Mediapipe Pose can still be utilised in other valuable ways. It can be employed to assess the replacement of the cyclist in the same position for simulations or to assess if the cyclists naturally reposition themselves in the desired position. These applications allow for general evaluations or comparisons.

Indeed, one advantage of using Mediapipe Pose is that it provides feedback on the position of the cyclist with less bulky equipment compared to 3D cameras. The use of 3D cameras typically involves setting up a complex system of cameras and markers, which can be cumbersome and require a significant amount of space. In contrast, Mediapipe Pose relies on computer vision algorithms and can be implemented using a single camera or even a webcam, making it a more portable and accessible option.

By using Mediapipe Pose, cyclists can receive real-time feedback on their position without the need for extensive equipment setup. This can be particularly useful for on-the-field evaluations, training sessions, or quick assessments of position during simulations.

Therefore, while the accuracy of Mediapipe Pose may not be suitable for precise analysis of equipment effects on drag, it still has utility in broader assessments and positional evaluations within a reasonable margin of error.

Chapter 5

Dynamic evaluation of the cyclist's aerodynamics

The original objective of this study was to develop a dynamic analysis of the cyclist's aerodynamics. To achieve this, several factors were considered and evaluated in order of magnitude. Firstly, the influence of different materials was assessed to understand their impact on aerodynamics. Secondly, the significance of cyclist repositioning was evaluated, taking into account the associated errors and their effects on aerodynamics. However, it was found that the error introduced by repositioning was too high for accurate analysis of the specific effect of the equipment.

To address this challenge, a feedback algorithm was implemented. Although this algorithm helps mitigate the error caused by repositioning, it is not precise enough to isolate and evaluate the influence of materials independently. Nevertheless, it can still be utilised effectively for assessing cyclist repositioning.

Now, armed with the insights gained from evaluating material influence, repositioning errors, and the feedback algorithm, it is possible to combine all these aspects to conduct a comprehensive evaluation of cyclist aerodynamics. The study considers various characteristics such as body shape, positioning, helmet design, and yaw angle, allowing for a more holistic understanding of their impacts on aerodynamics.

By considering these factors together, valuable insights into the overall aerodynamic performance of the cyclist can be gained and the specific effects of different characteristics can be understood.

5.1 Methodology

The experimental setup utilised in this study involved several components. Firstly, two force plates were positioned inside the wind tunnel, with one placed in front of the other. These force plates were mounted on a turning plate.

A home trainer was then positioned on the force plates with the front wheel of the bike placed on the first force plate, while the rear wheel was positioned on the second force plate.

The home trainer was positioned so as to be aligned with the wind. To ensure repeatability, the exact placement of the home trainer was marked on the force plates, allowing for consistent positioning during each measurement.

A camera was placed outside the wind tunnel, positioned to capture the entire cyclist and bike within its field of view through the tunnel's window. This camera was connected to a computer that ran the Mediapipe Pose code, which processed the camera feed to estimate the poses and angles of the cyclist in real-time, then sent this feedback to the cyclist using a screen that was positioned flat on the ground in front of the force plates (Figure 5.1).

(a) *Front view*

(b) *Side view*

Figure 5.1: *Measures setup*

Three time trial pro athletes took part in the analysis. The different athletes have different body shape : Guillaume is tall and has a broader figure, Ludovic is also tall but has a slimmer figure and Julian is smaller with a slim figure. Each cyclist was tested in different configurations which would include variations in helmet, yaw angle and wind speed :

- First configuration : helmet H (time trial helmet of the team), yaw angle = 0° and wind speed = 12.6, 13.9 and 15.2 m/s.
- Second configuration : helmet H (time trial helmet of the team), yaw angle = 15° and wind speed = 12.7, 14 and 15.3 m/s.
- Third configuration : helmet I, yaw angle = 15° and wind speed = 12.7, 14 and 15.3 m/s.
- Fourth configuration : helmet D, yaw angle = 15° and wind speed = 12.7, 14 and 15.3 m/s.

In addition to those configurations, two other tests were performed :

1. A comparison of the old and new De Rosa bikes : the forces of both bikes were evaluated without rider at a 0° yaw angle and at wind speeds = 9.3, 11.5, 13, 14.3, 15.8 and 17.4 m/s.

2. A comparison of two positions : Ludovic performed the test in the first configuration twice, and the height of the handlebars was decreased by 2 cm for the second time. This led to a change in his position.

For each configuration, the cyclist was riding the new DeRosa bike and was wearing an aero suit. The cyclist was asked to ride at a constant power output of his choice. The measure was started at a 0 m/s wind speed in order to evaluate a reference position and to measure the offset of the force plates. Then the wind was started at the first speed.

For each configuration, the measurement process was conducted as follows :

1. The cyclist place himself in the right position.
2. The position is measured as a reference position using `starting_position.py`.
3. The position is measured, and the feedback is given using `2D_mediapipe_pose_detection.py` during the whole measure without interruption.
4. The measurement of the forces is launched, and the forces are measured during the whole measure without interruption.
5. The wind is set at the first speed.
6. The cyclist is asked not to pedal as the forces are measured in a static state.
7. The cyclist is asked to pedal at a constant power output of his choice as the forces are measured in a pedalling state.
8. The wind is set at the second and third speed, and the steps 6 and 7 are repeated.

5.2 Results

5.2.1 Aerodynamics

Comparison of different bikes

The new De Rosa design have a slightly smaller drag area, indicating improved aerodynamics compared to the old bike (Figure 5.2). This means that the new bike offers a reduced resistance to airflow, resulting in potential gains in speed and efficiency.

The difference in aerodynamic performance between the old and new bike becomes more noticeable at both lower and higher speeds. At lower speeds, the improved aerodynamics can contribute to easier acceleration and enhanced manoeuvrability. On the other hand, at higher speeds, the reduced drag area allows the cyclist to maintain greater velocity with less effort, potentially resulting in improved overall performance, as the cyclist can achieve the same level of performance with less effort due to the lower drag resistance.

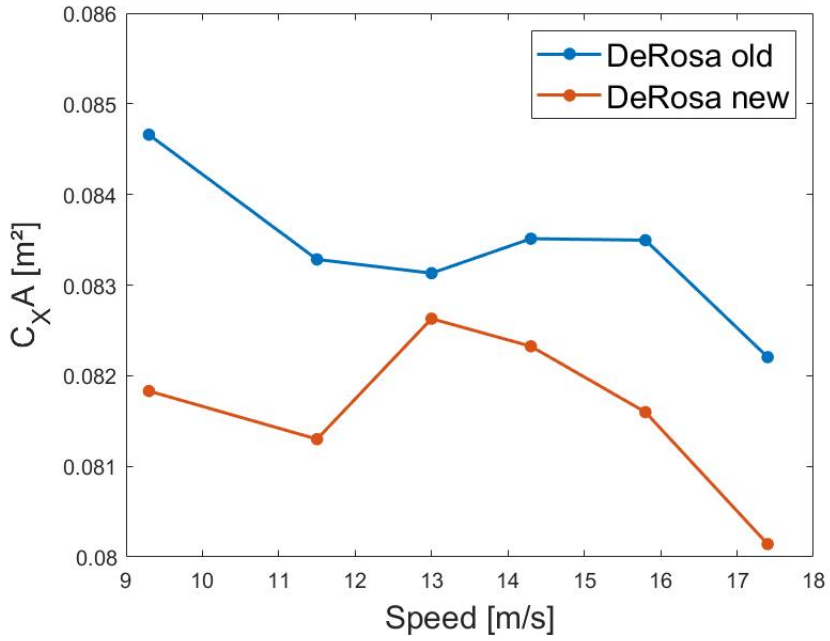

Figure 5.2: *Comparison of the drag areas of the old and new De Rosa bikes in function of the speed of the wind [m/s] in the x-axis for a yaw angle = 0°.*

Comparison of two positions

Optimising the position to achieve the smallest frontal area is the most effective approach to improving aerodynamics. In this study, two positions were compared: Position 1, which is a classic time trial position, and Position 2, which involved adopting a time trial position with the handlebars positioned 2 cm lower than in Position 1. The remarkable finding is that this relatively small adjustment in height has a significant impact on aerodynamics.

The reduction of 2 cm in handlebar height yields a substantial decrease in the drag area (Figure 5.3). Specifically, it results in a reduction of approximately 7.5% at lower speeds and 5.5% at higher speeds. This comparison highlights the fact that even a small modification in the cyclist's position can lead to a significant difference in aerodynamic performance.

By demonstrating the substantial impact of a 2 cm height reduction in handlebars, the study underscores the importance of fine-tuning body position to optimise aerodynamics. These findings emphasise that even minor adjustments to the cyclist's position can yield noticeable improvements in aerodynamic efficiency. Therefore, paying close attention to optimising position and minimising frontal area can have a profound impact on the overall aerodynamics of the cyclist.

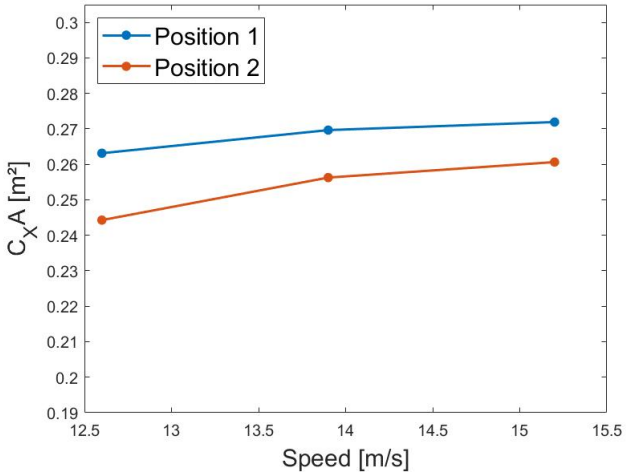

Figure 5.3: *Comparison of the drag areas of the positions 1 and 2 in function of the wind speed [m/s] in the x-axis for a yaw angle = 0°.*

Comparison of static and pedalling conditions

One of the primary focuses of this study was to investigate the aerodynamics of cyclists in a dynamic configuration. This approach was deemed important as it provides a more realistic representation of real-world conditions and their impact on aerodynamics. To assess this, the drag areas were analysed for the three cyclists wearing helmet H at yaw angles of 0° and 15° (Figure 5.4).

The results revealed that in pedalling conditions, the drag areas were found to be up to 10% higher compared to static conditions. This highlights the influence of dynamic factors, such as pedalling motion, on aerodynamics. Furthermore, the difference becomes even more pronounced when the yaw angle deviates from 0°, indicating the significance of considering different angles of wind flow.

These findings underscore the importance of studying aerodynamics in dynamic pedalling conditions rather than solely focusing on static scenarios in order to gain a more comprehensive understanding of how different variables impact cyclist aerodynamics.

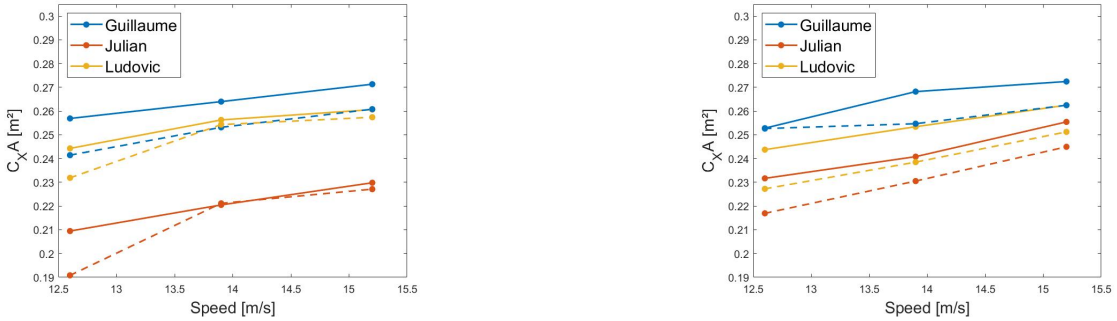

(a) *Yaw angle = 0°* (b) *Yaw angle = 15°*

Figure 5.4: *Comparison of the drag areas of static and pedalling conditions in function of the wind speed [m/s] in the x-axis for a yaw angle of 0° and 15°. The solid lines represent the drag areas in pedalling conditions, and the doted lines represent the drag areas in static condition.*

Comparison of different yaw angles

The inclusion of a yaw angle in the cyclist's configuration enables a more realistic representation of real-world conditions. Consistent with the Section 2.3.2, the drag areas along the x-axis exhibit minimal variation. However, significant variations are observed in the drag areas along the y-axis (Figure 5.5). Notably, at a yaw angle of 15°, the drag area in the y-axis becomes remarkably significant, even as high as twice the force experienced in the x-direction.

This notable difference in drag areas can be attributed to the aerodynamic forces generated by the bike itself, taking into account its geometry. Furthermore, the presence of a full rear wheel amplifies these forces. Consequently, the yaw angle has a substantial impact on the cyclist's aerodynamics. However, its primary effect is on the cyclist's trajectory, potentially leading to deviations, rather than directly affecting performance metrics.

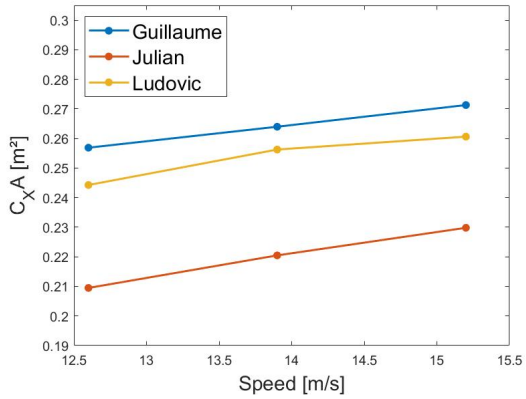

(a) *Drag areas in the x-axis at yaw angle = 0°*

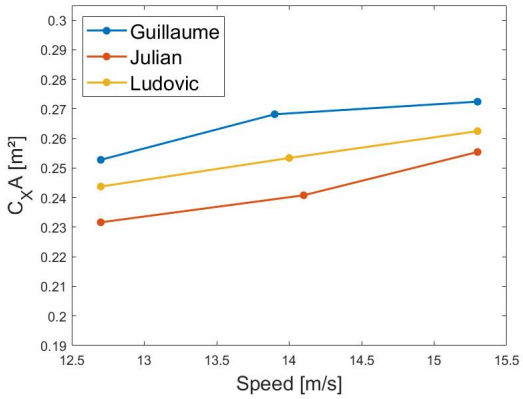

(b) *Drag areas in the x-axis at yaw angle = 15°*

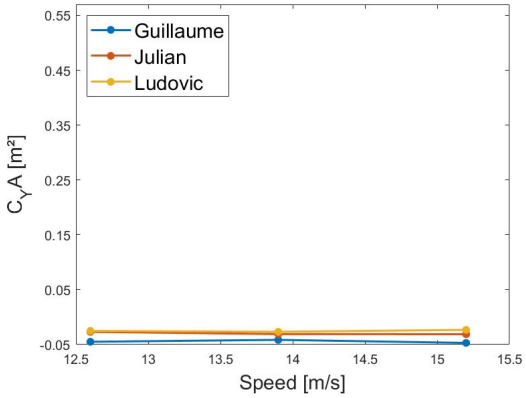

(c) *Drag areas in the y-axis at yaw angle = 0°*

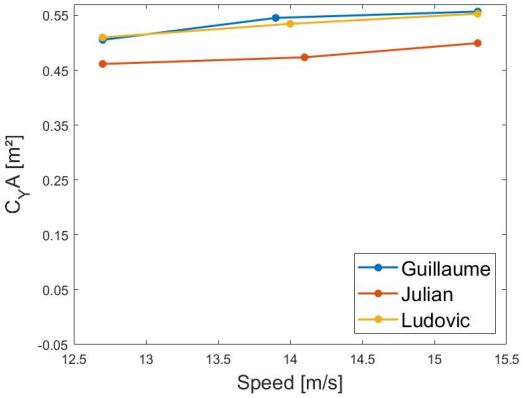

(d) *Drag areas in the y-axis at yaw angle = 15°*

Figure 5.5: *Comparison of the drag areas in function of the wind speed [m/s] at yaw angles of 0° and 15° in the x- and y-axes.*

Comparison of different helmets

In contrast to the Section 2.3.2, where the helmets exhibited variations in the drag areas, the current findings reveal similar drag areas and uniform behaviour for the different helmets (Figure 5.6). When looking closely, the helmet D presents a marginally smaller drag area in the y-direction. Although this difference does not directly impact performance, it can confer a small advantage to helmet D over the other helmets, considering the fact that the forces experienced in the y-axis are significant.

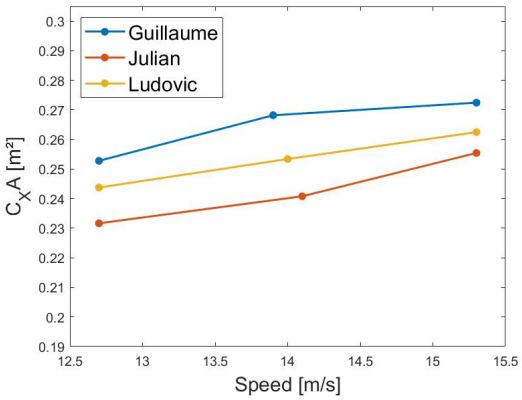

(a) *Helmet H in the x-direction*

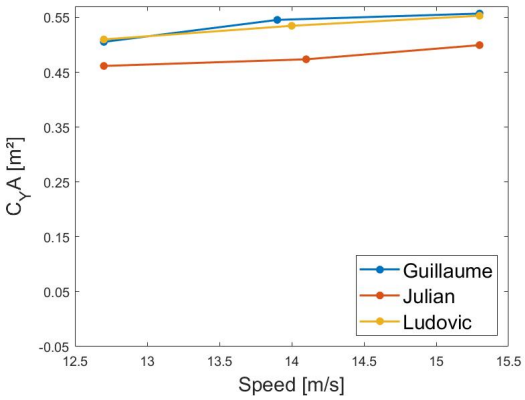

(b) *Helmet H in the y-direction*

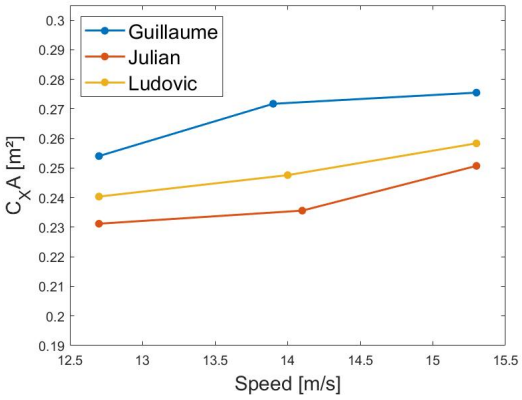

(c) *Helmet I in the x-direction°*

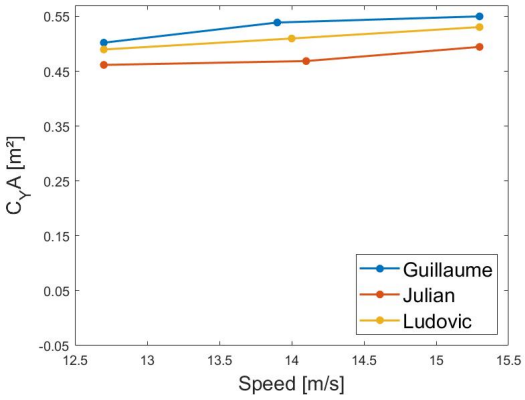

(d) *Helmet I in the y-direction*

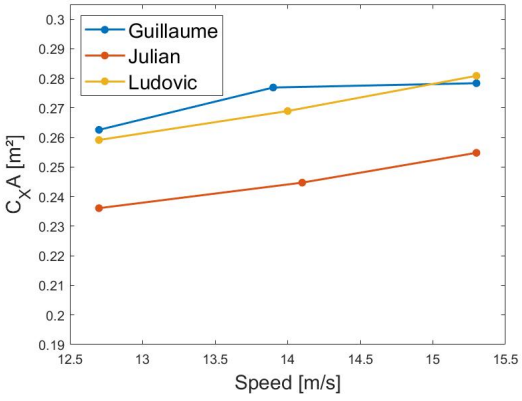

(e) *Helmet D in the x-direction*

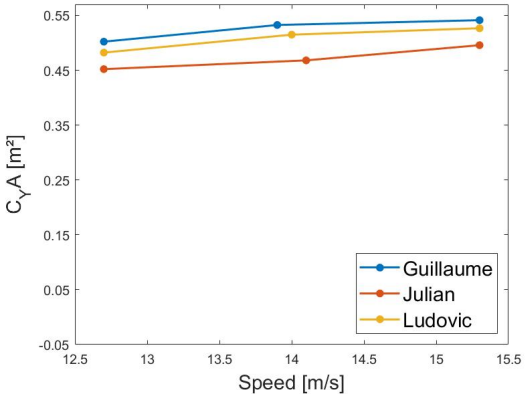

(f) *Helmet D in the y-direction*

Figure 5.6: *Comparison of the drag areas of the different helmets for each cyclist in function of the wind speed [m/s] in the x- and y-axes at a yaw angle of 15°.*

Analysing the drag areas of the helmets for each cyclist reveals different behaviour depending on the cyclist (Figure 5.7).

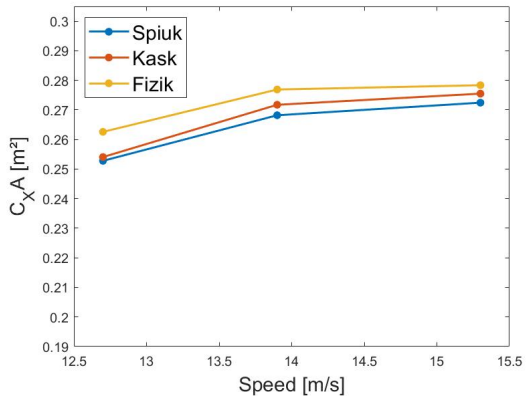

(a) *Guillaume in the x-direction*

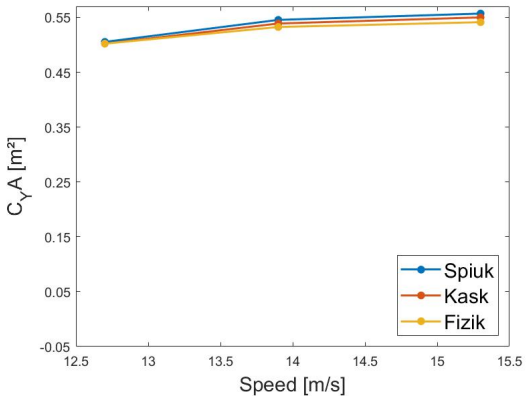

(b) *Guillaume in the y-direction*

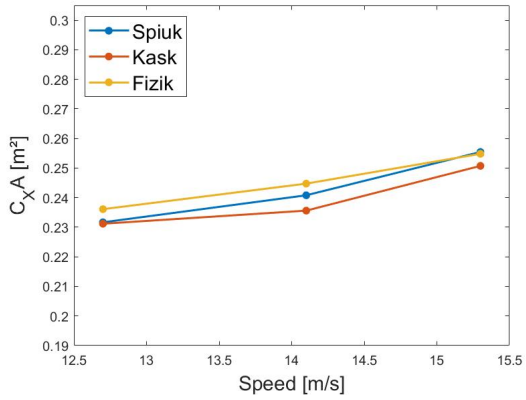

(c) *Julian in the x-direction*

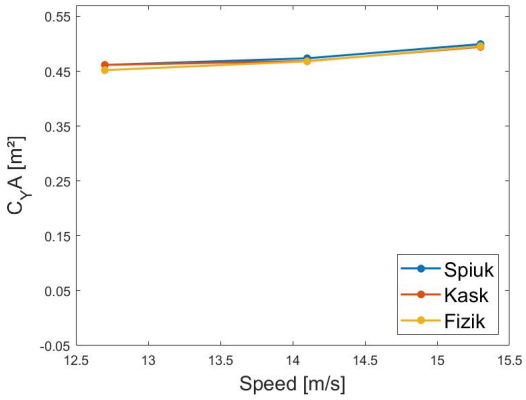

(d) *Julian in the y-direction*

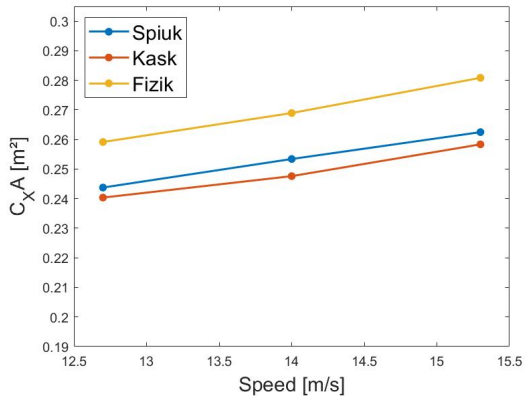

(e) *Ludovic in the x-direction*

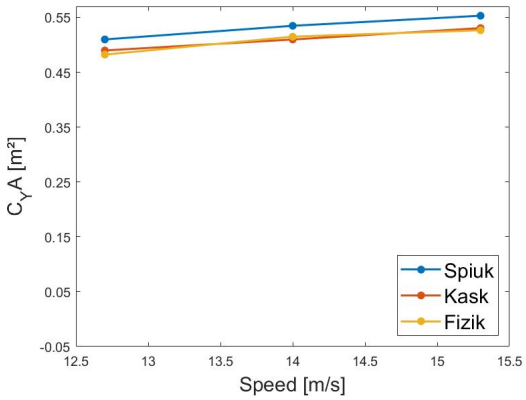

(f) *Ludovic in the y-direction*

Figure 5.7: *Comparison of the drag areas of the different helmets on each cyclist in function of the wind speed [m/s] in the x- and y-axes at a yaw angle of 15°.*

Indeed, the disparity between these results and the Section 2.3.2 arises from the fact that, here, the helmets were studied in conjunction with the full body. This interaction influences the airflow around the helmet's tail, as it combines with the cyclist's shoulders to mitigate turbulence.

Given the unique body shape of each cyclist, it becomes crucial to acknowledge that the effects and performance of helmets will vary depending on the individual. The interaction between a cyclist's body shape and the chosen helmet significantly influences its aerodynamic characteristics. Therefore, it is important to individually assess the impact of different helmet designs on each cyclist. By conducting these personalised evaluations, cyclists can gain a better understanding of how specific helmets interact with their unique body shape, ultimately influencing their overall aerodynamic performance. The helmet that best suits a particular cyclist differs for each individual. However, when examining the y-axis, helmet D appears to yield the smallest drag area for each cyclist, albeit the difference is minimal. This can be attributed to the presence of corrugations in helmet D, which are designed to prevent air detachment and the creation of turbulence that would otherwise increase forces on the head. The helmets H and I does not present those corrugations and have a smooth surface.

Comparison of different body shapes

The analysis considered three distinct body shapes represented by the riders: tall with broader shoulders, tall and slim, and small and slim. Examining the drag areas of these three cyclists reveals a clear pattern. The tallest and broader body shape consistently exhibits the highest drag area, while the smallest and slimmest body shape displays the smallest drag area. The difference is most significant at a 0° yaw angle, reaching up to 20%. However, at a yaw angle of 15°, the difference diminishes significantly.

Several factors contribute to these drastic variations. Firstly, the body shape directly impacts the frontal area. A smaller and slimmer figure naturally presents a smaller frontal area, resulting in a smaller drag area. Additionally, there are regulations of the *Union Cycliste Internationale* (UCI) dictating certain measurements for bikes. For instance, the distance between the saddle and handlebars must not exceed 85 cm [38]. Consequently, different body shapes are limited in their ability to achieve the same positions on the bike. A smaller figure may opt for a more elongated position with the arms positioned further forward, whereas a taller figure may have to adopt a more compact position with the arms tucked under the torso.

As seen in the Section 5.2.1, even a 2 cm adjustment in the handlebar position has a substantial impact on the drag area. This underscores the critical role of optimising the position to minimise drag area. Therefore, it becomes evident why significant differences emerge among the different riders in this study. The combination of body shape and positioning variations contribute to the pronounced disparities in drag areas.

Comparison with the literature

The close agreement between the drag area values obtained in this analysis and those reported in the literature is a positive indication of the reliability and accuracy of the experimental setup and measurements. The range of 0.2 to 0.3 m^2 for the drag area of a cyclist on a bike is commonly observed, and the results obtained in this study fall within this expected range [1, 4, 8]. When comparing the minimum and maximum drag area values from this study to those

of other studies conducted under pedalling conditions at a 0° yaw angle, it is evident that the values obtained in this study fall within the same range as the other studies (Figure 5.8). This suggests that the experimental setup and measurements are consistent with established knowledge in the field.

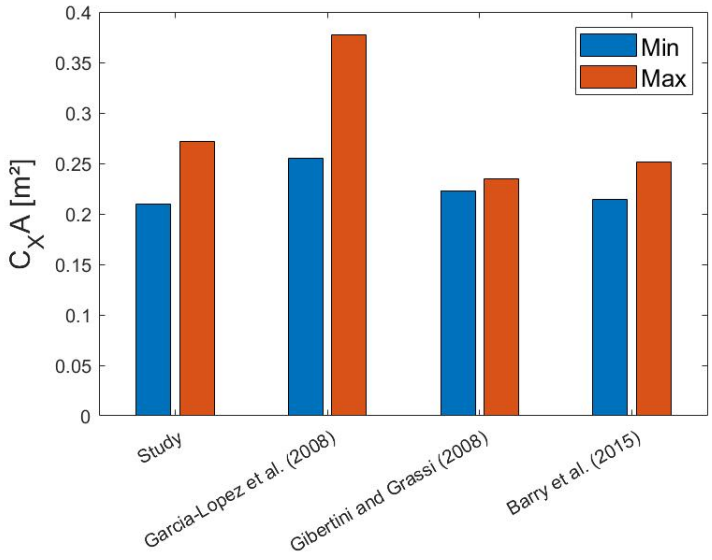

Figure 5.8: *Comparison of the minimal and maximal values of drag area of the values obtained in this study and the one found in the literature for a 0° yaw angle and pedalling conditions [4, 11, 39]*

The observed variations in the drag area resulting from changes in position are also in line with previous findings. Changes in position can lead to fluctuations in the drag area ranging from 5% to 20% [1, 2, 4, 7]. The variations reported in this study fall within this range, further confirming that the experimental setup and measurements are capturing realistic changes in aerodynamic performance.

Furthermore, the comparison between the drag of the cyclist and the bike together, at 0° yaw angle, and the drag of the bike alone reveals that the bike contributes just over 30% of the total drag. This aligns with the understanding that the bike itself is a significant contributor to the overall aerodynamic drag experienced by the cyclist, but the cyclist is the principal contributor to the drag [1, 2].

These findings provide valuable insights into the aerodynamic characteristics of the cyclist and the bike, demonstrating the accuracy and relevance of the experimental measurements and their agreement with established knowledge in the field of aerodynamics in cycling.

5.2.2 Evaluation of the position

The intended use of the Mediapipe Pose algorithm was to provide feedback to the cyclist regarding their position. However, several challenges arose that hindered the proper utilisation of the feedback and accurate measurement of the position. Firstly, in the initial configuration, the cyclist was positioned against the light source, which created difficulties for the Mediapipe Pose algorithm in detecting the cyclist. To address this issue, a spotlight was added to ensure equal exposure to light on both sides of the cyclist.

Secondly, the cyclist's suit featured bright colours and intricate patterns. This posed a challenge for the Mediapipe Pose algorithm in accurately detecting the various segments of the body. The complex patterns and colours disrupted the algorithm's ability to precisely identify and track the body segments. In contrast to the issues encountered with the upper body, a different problem arose with the detection of the cyclist's feet. Both the cyclist's shoes and the bike itself were black, leading to difficulties in visibility for the camera and the Mediapipe Pose algorithm. Consequently, when the cyclist's foot was positioned in front of the bike, it became challenging for the camera and algorithm to detect and track the foot accurately.

Additionally, the cyclists wore helmets that covered a significant portion of their heads. As explained in the Section 4.1, the Mediapipe Pose algorithm begins by detecting the head to locate the rest of the body. However, the helmets obstructed the face, making it difficult for the algorithm to identify the region of interest where the body is located.

Furthermore, when a yaw angle of 15° was introduced, the cyclist's body was rotated in a way that partially obstructed the head behind the shoulder. This further complicated the task for the Mediapipe Pose algorithm to accurately detect and track the head region.

Moreover, at the yaw angle of 15°, another issue arose as the camera was not adjusted and remained in its original position. Consequently, the camera was no longer perpendicular to the cyclist, causing a deviation from the optimal viewing angle. Since the coordinates of the joints were estimated based on their projection on the screen, this deviation resulted in incorrect evaluations of the angles. The misalignment between the camera and the cyclist's actual position introduced errors in the angle measurements. However, even if the angle values were wrong, this should not have impacted the repeatability.

Additionally, the `2D_mediapipe_pose_detection.py` code encountered difficulties in execution. The code relies on the detection of the cyclist's body to initiate the feedback process. However, given the challenges mentioned before, the code failed to detect the cyclist's body accurately. As a result, it became impossible to provide real-time feedback to the cyclist based on the Mediapipe Pose algorithm. These technical limitations prevented the intended use of the code and hindered the evaluation and improvement of the cyclist's position during the study.

These challenges collectively impeded the effective use of the Mediapipe Pose algorithm for providing feedback and accurately measuring the cyclist's position. Future improvements could involve exploring alternative approaches or adaptations of the algorithm to address these specific issues and enhance its performance in dynamic cycling scenarios.

In light of the challenges faced with the initial code, an alternative code utilising the Me-

diapipe Pose algorithm was employed for the study. This code functioned similarly to the `2D_mediapipe_pose_detection.py` code, but with the key difference that it solely focused on detecting the position without providing real-time feedback to the cyclist. This alternative code was chosen because it could initiate even without detecting the full body, allowing it to start tracking once the cyclist began moving, as it was easier for the code to detect the segments when they were moving.

However, despite the ability to initialise without complete body detection, the pose detection results from this code were not satisfactory. Several issues were encountered during the analysis, including inaccurate identification of the arms, unstable tracking of the leg joints, and misplaced shoulder joints (Figure 5.9). These limitations and inaccuracies in pose detection hindered the comprehensive evaluation of the cyclist's body position and movements.

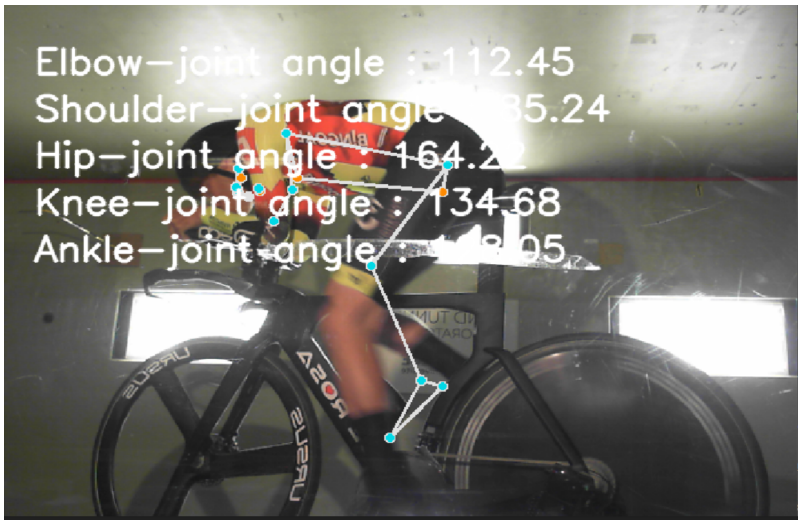

Figure 5.9: *Detection of the position of the cyclist using Mediapipe Pose algorithm for the cyclist in the wind tunnel.*

As anticipated, the results obtained from comparing the reference position with the positions during different measurements exhibited significant variations (Table 5.1). Notably, the RMSE values for the elbow and shoulder angles were considerably high since these joints could not be accurately detected by the code, rendering those results insignificant.

On the other hand, the hip angles displayed smaller values in comparison. This can be attributed to the fact that the code was able to detect the hip angle more reliably, making it closer to the actual measurement. However, upon examining the standard deviation in the results, it becomes apparent that the variation falls within the same order of magnitude as the measurements themselves. This highlights the uncertainty associated with the code and its inability to accurately detect and track the cyclist's body.

Overall, the limitations of the code and the inherent uncertainty in body detection and angle estimation underscore the need for further improvements and more precise methodologies to reliably assess and analyse the cyclist's joint angles during pedalling conditions.

	Root mean square error [°]		
	Guillaume		
	Elbow	Shoulder	Hip
Configuration 1	19.33	7.64	1.83
Configuration 2	25.30	39.52	82.58
Configuration 3	35.53	6.41	4.43
Configuration 4	27.59	16.01	11.96
Standard deviation	6.70	15.35	38.49
	Julian		
	Elbow	Shoulder	Hip
Configuration 1	10.51	8.42	1.76
Configuration 2	18.33	11.61	1.98
Configuration 3	15.13	13.32	5.68
Configuration 4	14.57	12.90	5.96
Standard deviation	3.21	2.12	2.28
	Ludovic		
	Elbow	Shoulder	Hip
Configuration 2	17.61	6.47	1.76
Configuration 3	16.01	7.22	1.50
Configuration 4	23.71	5.97	2.58
Standard deviation	4.06	0.63	0.56

Table 5.1: *The root mean square error (RMSE) between the angles of the reference position and the angles measured during the four configurations for the three cyclists, and standard deviation of the RMSE measures for the different joint angles of the different cyclists.*

Although the accurate evaluation of the cyclist's position was not possible due to the limitations of the code and the detection challenges, it can be reasonably concluded that the variations in position did not introduce significant fluctuations in the assessment of different aerodynamic parameters. This assertion is supported by the bike's geometry and the time trial position adopted by the cyclists.

Considering the fixed height of the saddle and the predetermined placement of the handlebars, the cyclist's position was inherently constrained. These design constraints limited the freedom for the cyclist to vary their position during the measurements. Consequently, the potential for unintended variations in the evaluation of aerodynamic parameters arising from positional changes was minimised.

Furthermore, it is worth noting that the participants in the study were professional cyclists. As such, they are used to maintaining a consistent and repeatable position. Therefore, the expected variations in position can be considered smaller compared to those discussed in Section 3.

It is important to acknowledge that although the variations in position were constrained by the bike's geometry and the fixed components, further investigations and refinements in position evaluation methodologies are warranted to provide a more comprehensive understanding of the cyclist's aerodynamics and the impact of position adjustments on performance.

5.3 Conclusion

In conclusion, the dynamic evaluation of the cyclist's aerodynamics was proved successful in assessing various aerodynamic parameters and studying their influences. However, the measure process encountered limitations in accurately evaluating the cyclist's position.

The study encompassed an extensive range of aerodynamic parameters, including the comparison of different bikes, positions, static and pedalling conditions, yaw angles, different helmets, and the impact of body shape. The findings emphasised the significance of studying aerodynamics in a dynamic configuration, as the cyclist's movement directly affects aerodynamic forces.

The investigations into different yaw angles revealed substantial variations in forces along the y-axis, highlighting the importance of considering these angles in aerodynamic analyses. The choice of equipment also played a significant role, as evidenced by the observed reduction in drag area of up to 7.5% between different bikes and the variations in drag area among different helmets on different riders.

However, the most influential factor on drag area was found to be the cyclist's position. A well-optimised position effectively reduced the frontal area and, consequently, the drag area. This was demonstrated through the comparison of two different positions and the examination of various body shapes, as the body shape constrict the position.

Nevertheless, the evaluation of the cyclist's position encountered limitations. The implementation of the Mediapipe Pose algorithm aimed to replace the cyclist for accurate feedback, but several factors hindered its effectiveness. Challenges included poor light exposure, the suit, and bike colours, the helmet obscuring the cyclist's face, the shoulder obstructing the head at certain yaw angles, inaccurate joint coordinate projections, and the inability of the `2D_mediapipe_pose_detection.py` code to run without detecting the full body. Despite these limitations, it is important to note that the variation in positions on the cyclist should generally be minimal due to the constraints imposed by the bike's geometry.

Overall, the dynamic evaluation successfully examined aerodynamic parameters and their influences, highlighting the need to consider movement, yaw angles, equipment selection, and position optimisation in cyclist aerodynamics. But further improvements in position evaluation methods are necessary to enhance accuracy and provide comprehensive insights into optimising cyclist performance.

Chapter 6

Conclusion and further works

The primary objective of this research was to establish a comprehensive and dynamic evaluation framework within a wind tunnel setup, focusing on assessing the aerodynamics of time trial cyclists. By integrating motion tracking algorithms, the study aimed to develop a solution that enables precise replication of a cyclist's position, thereby facilitating more accurate measurements of aerodynamic performance. The ultimate goal was to deepen the understanding of the complex interplay between a cyclist's position, equipment choices, and aerodynamic efficiency, with the aim of driving advancements in time trial cycling.

To accomplish this objective, the study was structured into distinct phases. Firstly, a thorough evaluation of the aerodynamic impact of equipment, particularly helmets, was conducted to quantify variations in aerodynamic parameters resulting from different helmet designs. These findings contributed significantly to comprehending how equipment choices influence overall aerodynamic performance.

Subsequently, the study delved into investigating the influence of position variability on aerodynamic measurements. Cyclists often face challenges in maintaining consistent positions, making it difficult to accurately assess the true effects of positional changes on aerodynamics. By quantifying the magnitude of variations in repositioning without feedback, the study explored the effects of slight positional errors on aerodynamic measurements and compared them to equipment variations. The analysis highlighted the substantial influence of even minor angle adjustments on drag force. Notably, a difference in position could lead to drag force changes of up to 0.5 N, or variations in drag force between different helmets ranged from approximately 0.1 N to 1.8 N, underscoring the considerable impact of slight angle modifications, as both drag force values are of similar magnitude. These findings underscored the criticality of precise positioning to minimise drag and optimise overall performance.

To mitigate position variations, a feedback system based on motion tracking algorithms was developed. The system aimed to offer real-time information and support to cyclists, facilitating accurate replication of their positions during wind tunnel testing. The motion tracking

algorithm utilised was *Google*'s Mediapipe Pose, and various aspects of the algorithm were assessed. A comparison between 2D and 3D coordinates of Mediapipe Pose revealed that the 2D coordinates resulted in angles closer to the ones detected with the 3D cameras. Additionally, an attempt was made to apply a filter to reduce inaccuracy, but it was ultimately decided to exclude it to maintain a streamlined and lightweight code. Furthermore, the repeatability of the feedback system was examined, indicating that the results obtained from Mediapipe Pose provided position estimations with a margin of error of $\pm 5°$. Regrettably, this level of error proved to be too significant to reliably evaluate the specific effects of materials, such as helmets. Moreover, the study found that the accuracy of Mediapipe Pose was comparable to self-repositioning results, suggesting that it did not surpass self-repositioning in terms of accuracy. Nevertheless, Mediapipe Pose can still be valuable for other applications, such as assessing position replacements for simulations or evaluating cyclists' natural repositioning tendencies. An advantage of utilising Mediapipe Pose is its ability to provide position feedback with less cumbersome equipment compared to 3D cameras.

Lastly, the comprehensive analyses conducted in this study culminated in a final evaluation of the cyclist's aerodynamics within the wind tunnel, incorporating the combined effects of factors such as helmet design, cyclist positioning, yaw angle, and their interaction with airflow. By simulating real-world conditions and considering the dynamic nature of cycling, this evaluation offered valuable insights into the aerodynamic efficiency of time trial cyclists. The findings underscored the importance of investigating aerodynamics in a dynamic configuration, considering the direct impact of the cyclist's movement on aerodynamic forces.

The analysis of different yaw angles revealed significant variations in forces along the y-axis, highlighting the crucial role of considering these angles in aerodynamic studies. Equipment selection also emerged as a significant factor, with noticeable reductions in drag area of up to 7.5% observed between different bicycles and variations in drag area among different helmets worn by diverse riders.

But the most influential factor influencing drag area was identified as the cyclist's position. An optimally positioned cyclist achieved a notable reduction in frontal area and, consequently, drag area. This was exemplified through the comparison of two distinct positions and the examination of various body shapes, underscoring the impact of body shape on achieving an optimal position.

However, limitations were encountered in accurately assessing the cyclist's position. Challenges included factors like inadequate light exposure, variations in suit and bike colours, helmet obstructions, shoulder obstructions at specific yaw angles, imprecise joint coordinate projections, and the code's inability to detect the full body in `2D_mediapipe_pose_detection.py`. Despite these limitations, it is important to emphasise that variations in cyclist positions should generally be minimal due to the geometric constraints imposed by the bike and the fact that pro athletes were studied.

The identified limitations present numerous opportunities for improvement. The encountered challenges in the proper functioning of the Mediapipe Pose algorithm indicate several tracks for enhancing its performance and surpassing these limitations. Additionally, the aim would be to reduce the margin of error of 5° to enhance repeatability and achieve more precise cyclist repositioning, as well as increasing the 3D coordinates accuracy. By addressing these limitations and refining the measurement techniques, dynamic evaluations of cyclists' aerodynamics can unlock a vast array of possibilities for enhancing overall aerodynamic performance.

In addition to addressing the limitations specific to the Mediapipe Pose algorithm and improving cyclist repositioning, further works in the field of cycling aerodynamics offer a wide range of possibilities. One potential track is the exploration of advanced aerodynamic materials and technologies that can reduce drag and enhance performance. This could involve the development of innovative helmet designs, streamlined clothing, and aerodynamic bike components.

Another area of interest lies in optimising the interaction between the cyclist and their equipment. Fine-tuning the positioning of components such as handlebars, pedals, and wheels can have a significant impact on aerodynamic efficiency. Additionally, studying the aerodynamics of different riding positions, such as various body postures and hand placements, could provide valuable insights for cyclists to adopt more aerodynamically advantageous positions.

Furthermore, advancements in wearable sensor technology and real-time data analysis can enable cyclists to monitor their aerodynamic performance during training and races. This could involve the development of wearable devices that provide instant feedback on body position, drag forces, and aerodynamic efficiency, allowing cyclists to make adjustments in real-time and maximise their performance. Such technologies could allow evaluations of the aerodynamics outside a laboratory configuration, increasing the value of the data as they represent real-world conditions.

Overall, the field of cycling aerodynamics holds immense potential for further research and innovation. By continuously exploring new methodologies, technologies, and strategies, it is possible to unlock significant advancements in aerodynamic efficiency, ultimately leading to improved performance for cyclists at all levels. This opens up exciting prospects for further advancements in optimising cyclist aerodynamics.

Bibliography

[1] Helge Nørstrud, ed. *Sport aerodynamics*. CISM courses and lectures no. 506. OCLC: ocn297145523. Wien ; New York: Springer Verlag, 2008. 331 pp. ISBN: 978-3-211-89296-1.

[2] Fabio Malizia and Bert Blocken. "Cyclist aerodynamics through time: Better, faster, stronger". In: *Journal of Wind Engineering and Industrial Aerodynamics* 214 (July 2021), p. 104673. ISSN: 01676105. DOI: 10.1016/j.jweia.2021.104673. URL: https://linkinghub.elsevier.com/retrieve/pii/S0167610521001574 (visited on 05/28/2023).

[3] Luca Oggiano and Stig Leirdal. "Aerodynamic optimization and energy saving of cycling postures for international elite level cyclists." In: (2008).

[4] Daniel N Cassenti et al., eds. *Advances in Simulation and Digital Human Modeling: Proceedings of the AHFE 2020 Virtual Conferences on Human Factors and Simulation, and Digital Human Modeling and Applied Optimization, July 16-20, 2020, USA*. Vol. 1206. Advances in Intelligent Systems and Computing. Cham: Springer International Publishing, 2021. ISBN: 978-3-030-51063-3 978-3-030-51064-0. DOI: 10.1007/978-3-030-51064-0. URL: http://link.springer.com/10.1007/978-3-030-51064-0 (visited on 05/28/2023).

[5] Pierre Debraux et al. "Aerodynamic drag in cycling: methods of assessment". In: *Sports Biomechanics* 10.3 (Sept. 2011), pp. 197–218. ISSN: 1476-3141, 1752-6116. DOI: 10.1080/14763141.2011.592209. URL: http://www.tandfonline.com/doi/abs/10.1080/14763141.2011.592209 (visited on 05/28/2023).

[6] L. Underwood et al. "Aerodynamic drag and biomechanical power of a track cyclist as a function of shoulder and torso angles". In: *Sports Engineering* 14.2 (Dec. 2011), pp. 147–154. ISSN: 1369-7072, 1460-2687. DOI: 10.1007/s12283-011-0078-z. URL: http://link.springer.com/10.1007/s12283-011-0078-z (visited on 05/28/2023).

[7] R. A. Lukes, S. B. Chin, and S. J. Haake. "The understanding and development of cycling aerodynamics". In: *Sports Engineering* 8.2 (Dec. 2005), pp. 59–74. ISSN: 1369-7072, 1460-2687. DOI: 10.1007/BF02844004. URL: http://link.springer.com/10.1007/BF02844004 (visited on 05/28/2023).

[8] Thijs Defraeye et al. "Aerodynamic study of different cyclist positions: CFD analysis and full-scale wind-tunnel tests". In: *Journal of Biomechanics* 43.7 (May 2010), pp. 1262–1268. ISSN: 00219290. DOI: 10.1016/j.jbiomech.2010.01.025. URL: https://linkinghub.elsevier.com/retrieve/pii/S002192901000059X (visited on 06/01/2023).

[9] H Chowdhury, F Alam, and I Khan. "AN EXPERIMENTAL STUDY OF BICYCLE AERODYNAMICS". In: ().

[10] D.M. Fintelman et al. "Optimal cycling time trial position models: Aerodynamics versus power output and metabolic energy". In: *Journal of Biomechanics* 47.8 (June 2014), pp. 1894–1898. ISSN: 00219290. DOI: 10.1016/j.jbiomech.2014.02.029. URL: https://linkinghub.elsevier.com/retrieve/pii/S0021929014001407 (visited on 05/28/2023).

[11] Timothy N. Crouch et al. "Riding against the wind: a review of competition cycling aerodynamics". In: *Sports Engineering* 20.2 (June 2017), pp. 81–110. ISSN: 1369-7072, 1460-2687. DOI: 10.1007/s12283-017-0234-1. URL: http://link.springer.com/10.1007/s12283-017-0234-1 (visited on 05/28/2023).

[12] Juan García-López et al. "Reference values and improvement of aerodynamic drag in professional cyclists". In: *Journal of Sports Sciences* 26.3 (Feb. 2008), pp. 277–286. ISSN: 0264-0414, 1466-447X. DOI: 10.1080/02640410701501697. URL: http://www.tandfonline.com/doi/abs/10.1080/02640410701501697 (visited on 05/28/2023).

[13] Cheryl A. Wozniak Timmer. "Cycling Biomechanics: A Literature Review". In: *Journal of Orthopaedic & Sports Physical Therapy* 14.3 (Sept. 1991), pp. 106–113. ISSN: 0190-6011, 1938-1344. DOI: 10.2519/jospt.1991.14.3.106. URL: http://www.jospt.org/doi/10.2519/jospt.1991.14.3.106 (visited on 05/28/2023).

[14] Borut Fonda and Nejc Sarabon. "Biomechanics of Cycling". In: *Sport Science Review* 19.1 (Jan. 1, 2010). ISSN: 2069-7244, 2066-8732. DOI: 10.2478/v10237-011-0012-0. URL: http://archive.sciendo.com/SSR/ssr.2010.xix.issue-1-2/v10237-011-0012-0/v10237-011-0012-0.pdf (visited on 05/28/2023).

[15] Nicolas A. Turpin and Bruno Watier. "Cycling Biomechanics and Its Relationship to Performance". In: *Applied Sciences* 10.12 (June 15, 2020), p. 4112. ISSN: 2076-3417. DOI: 10.3390/app10124112. URL: https://www.mdpi.com/2076-3417/10/12/4112 (visited on 05/28/2023).

[16] D.M. Fintelman et al. "The effect of time trial cycling position on physiological and aerodynamic variables". In: *Journal of Sports Sciences* 33.16 (Oct. 2, 2015), pp. 1730–1737. ISSN: 0264-0414, 1466-447X. DOI: 10.1080/02640414.2015.1009936. URL: http://www.tandfonline.com/doi/full/10.1080/02640414.2015.1009936 (visited on 05/28/2023).

[17] Timothy Crouch et al. "A wind-tunnel case study: Increasing road cycling velocity by adopting an aerodynamically improved sprint position". In: *Proceedings of the Institution of Mechanical Engineers, Part P: Journal of Sports Engineering and Technology* 235.4 (Dec. 2021), pp. 301–309. ISSN: 1754-3371, 1754-338X. DOI: 10.1177/1754337119866962. URL: http://journals.sagepub.com/doi/10.1177/1754337119866962 (visited on 06/01/2023).

[18] Bert Blocken et al. "CFD analysis of an exceptional cyclist sprint position". In: *Sports Engineering* 22.1 (Mar. 2019), p. 10. ISSN: 1369-7072, 1460-2687. DOI: 10.1007/s12283-

019-0304-7. URL: http://link.springer.com/10.1007/s12283-019-0304-7 (visited on 06/01/2023).

[19] F. Grappe et al. "Effect of Cycling Position on Ventilatory and Metabolic Variables". In: *International Journal of Sports Medicine* 19.5 (July 1998), pp. 336–341. ISSN: 0172-4622, 1439-3964. DOI: 10.1055/s-2007-971927. URL: http://www.thieme-connect.de/DOI/DOI?10.1055/s-2007-971927 (visited on 06/01/2023).

[20] *The University of Liège Wind Tunnel Facility*. English. University of Liège. 27 pp.

[21] Greg Atkinson et al. "Distribution of Power Output During Cycling". In: *PubMed* (2007), pp. 647–667. DOI: 10.2165/00007256-200737080-00001.

[22] Kim B. Blair and Stephanie Sidelko. "Aerodynamic Performance of Cycling Time Trial Helmets (P76)". In: *The Engineering of Sport 7*. Paris: Springer Paris, 2008, pp. 371–377. ISBN: 978-2-287-09410-1 978-2-287-09411-8. DOI: 10.1007/978-2-287-09411-8_44. URL: http://link.springer.com/10.1007/978-2-287-09411-8_44 (visited on 06/01/2023).

[23] Firoz Alam et al. "Aerodynamics of Ribbed Bicycle Racing Helmets". In: *Procedia Engineering* 72 (2014), pp. 691–696. ISSN: 18777058. DOI: 10.1016/j.proeng.2014.06.117. URL: https://linkinghub.elsevier.com/retrieve/pii/S187770581400633X (visited on 06/01/2023).

[24] James Novak, David Burton, and Timothy Crouch. "Aerodynamic test results of bicycle helmets in different configurations: Towards a responsive design". In: *Proceedings of the Institution of Mechanical Engineers, Part P: Journal of Sports Engineering and Technology* 233.2 (June 2019), pp. 268–276. ISSN: 1754-3371, 1754-338X. DOI: 10.1177/1754337118822613. URL: http://journals.sagepub.com/doi/10.1177/1754337118822613 (visited on 06/01/2023).

[25] L. Underwood et al. "Helmet position, ventilation holes and drag in cycling". In: *Sports Engineering* 18.4 (Dec. 2015), pp. 241–248. ISSN: 1369-7072, 1460-2687. DOI: 10.1007/s12283-015-0181-7. URL: http://link.springer.com/10.1007/s12283-015-0181-7 (visited on 06/01/2023).

[26] Thomas Peeters et al. "The Correlation Between Frontal Area and Joint Angles During Cycling". In: (2021). DOI: https://doi.org/10.1007/978-3-030-51064-0_32. URL: http://link.springer.com/10.1007/978-3-030-51064-0 (visited on 05/28/2023).

[27] Rohit Josyula and Sarah Ostadabbas. *A Review on Human Pose Estimation*. Oct. 13, 2021. arXiv: 2110.06877[cs]. URL: http://arxiv.org/abs/2110.06877 (visited on 06/01/2023).

[28] Yiqiao Lin, Xueyan Jiao, and Lei Zhao. "Detection of 3D Human Posture Based on Improved Mediapipe". In: *Journal of Computer and Communications* 11.2 (2023), pp. 102–121. ISSN: 2327-5219, 2327-5227. DOI: 10.4236/jcc.2023.112008. URL: https://www.scirp.org/journal/doi.aspx?doi=10.4236/jcc.2023.112008 (visited on 06/01/2023).

[29] Naoto Ienaga et al. “Development and Verification of Postural Control Assessment Using Deep-Learning-Based Pose Estimators: Towards Clinical Applications”. In: *Occupational Therapy International* 2022 (Nov. 30, 2022). Ed. by Sheng Bin, pp. 1–9. ISSN: 1557-0703, 0966-7903. DOI: 10.1155/2022/6952999. URL: https://www.hindawi.com/journals/oti/2022/6952999/ (visited on 06/01/2023).

[30] Chang Soon Tony Hii et al. “Marker Free Gait Analysis using Pose Estimation Model”. In: *2022 IEEE 20th Student Conference on Research and Development (SCOReD)*. 2022 IEEE 20th Student Conference on Research and Development (SCOReD). Bangi, Malaysia: IEEE, Nov. 8, 2022, pp. 109–113. ISBN: 978-1-66547-488-7. DOI: 10.1109/SCOReD57082.2022.9974096. URL: https://ieeexplore.ieee.org/document/9974096/ (visited on 06/01/2023).

[31] Halimah Badioze Zaman et al., eds. *Advances in Visual Informatics: 7th International Visual Informatics Conference, IVIC 2021, Kajang, Malaysia, November 23–25, 2021, Proceedings*. Vol. 13051. Lecture Notes in Computer Science. Cham: Springer International Publishing, 2021. ISBN: 978-3-030-90234-6 978-3-030-90235-3. DOI: 10.1007/978-3-030-90235-3. URL: https://link.springer.com/10.1007/978-3-030-90235-3 (visited on 06/01/2023).

[32] Ce Zheng et al. *Deep Learning-Based Human Pose Estimation: A Survey*. Jan. 23, 2022. arXiv: 2012.13392[cs]. URL: http://arxiv.org/abs/2012.13392 (visited on 06/01/2023).

[33] Valentin Bazarevsky and Ivan Grishchenko. *On-device, Real-time Body Pose Tracking with MediaPipe BlazePose*. URL: https://ai.googleblog.com/2020/08/on-device-real-time-body-pose-tracking.html. (accessed: 05.05.2023).

[34] V. Sivakumar Reddy et al., eds. *Soft Computing and Signal Processing: Proceedings of 4th ICSCSP 2021*. Vol. 1413. Advances in Intelligent Systems and Computing. Singapore: Springer Nature Singapore, 2022. ISBN: 9789811670879 9789811670886. DOI: 10.1007/978-981-16-7088-6. URL: https://link.springer.com/10.1007/978-981-16-7088-6 (visited on 06/01/2023).

[35] Valentin Bazarevsky et al. *BlazePose: On-device Real-time Body Pose tracking*. June 17, 2020. arXiv: 2006.10204[cs]. URL: http://arxiv.org/abs/2006.10204 (visited on 06/01/2023).

[36] Camillo Lugaresi et al. “MediaPipe: A Framework for Perceiving and Processing Reality”. In: ().

[37] Hongyi Xu et al. “GHUM & GHUML: Generative 3D Human Shape and Articulated Pose Models”. In: *2020 IEEE/CVF Conference on Computer Vision and Pattern Recognition (CVPR)*. 2020 IEEE/CVF Conference on Computer Vision and Pattern Recognition (CVPR). Seattle, WA, USA: IEEE, June 2020, pp. 6183–6192. ISBN: 978-1-72817-168-5. DOI: 10.1109/CVPR42600.2020.00622. URL: https://ieeexplore.ieee.org/document/9157563/ (visited on 06/04/2023).

[38] *PART 1 GENERAL ORGANISATION OF CYCLING AS A SPORT*. English. GENERAL ORGANISATION OF CYCLING AS A SPORT. 94 pp.

[39] Nathan Barry et al. "Aerodynamic drag interactions between cyclists in a team pursuit". In: *Sports Engineering* 18 (2015), pp. 93–103.

Appendix A

Movement of the mannequin setup

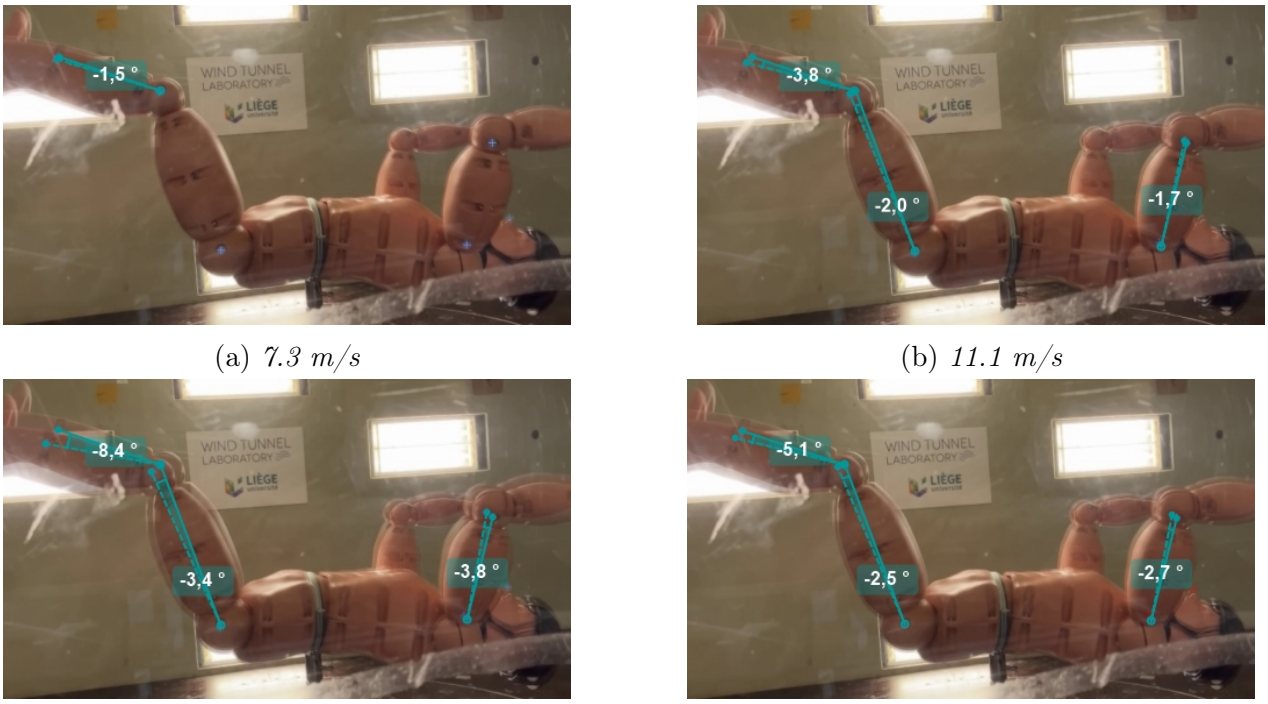

(a) *7.3 m/s*

(b) *11.1 m/s*

(c) *15 m/s*

(d) *18.9 m/s*

Figure A.1: *Difference in the position of the mannequin between the setup with no wind and with different wind speeds for the helmet 1.*

(a) *7.3 m/s*

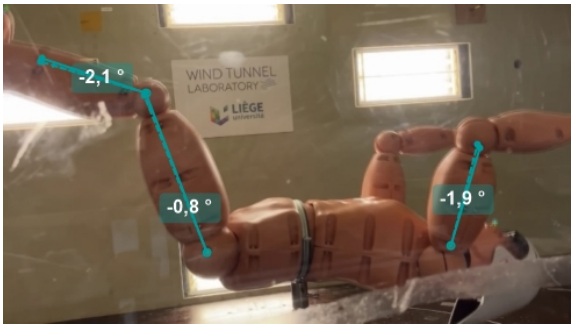

(b) *11.1*

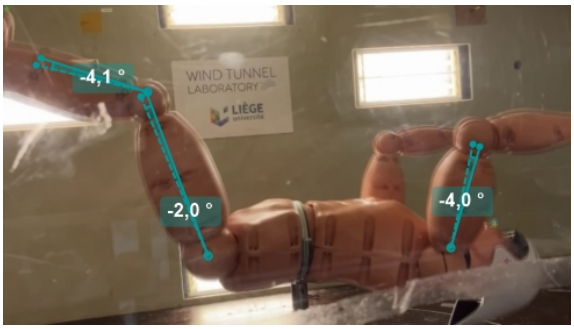

(c) *15 m/s*

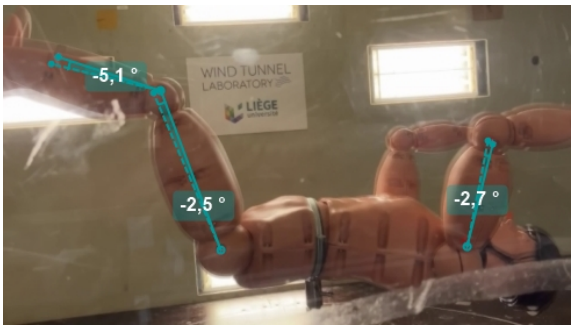

(d) *18.9 m/s*

Figure A.2: *Difference in the position of the mannequin between the setup with no wind and with different wind speeds for the helmet 2.*

Appendix B

Results of the helmets' aerodynamics for the mannequin setup

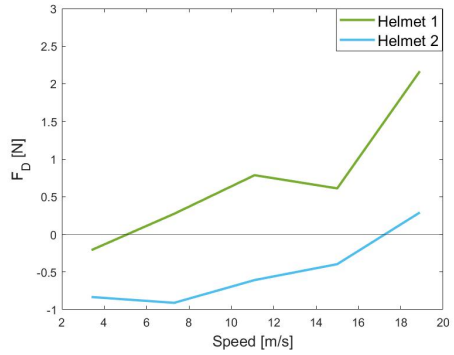

(a) *Drag force*

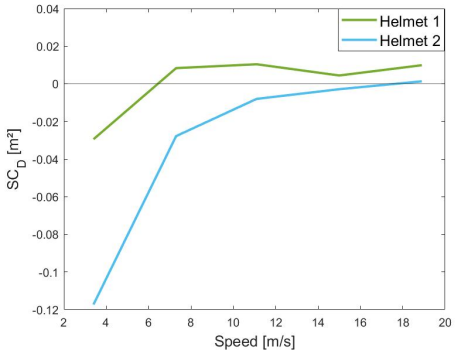

(b) *Drag area*

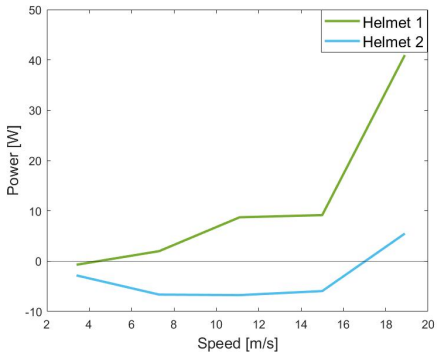

(c) *Power*

Figure B.1: *Drag force, drag area and power difference induced by the helmets compared to the mannequin without helmet.*

Appendix C

Codes

C.1 starting_position.py

```
import cv2
import mediapipe as mp
import numpy as np
from numpy import arctan, pi, signbit
from numpy.linalg import norm
import time

# Angle between two segments

def angle_btw(a,b,c,d):

    a = np.array(a) # start first vector
    b = np.array(b) # end first vector
    c = np.array(c) # start second vector
    d = np.array(d) # end second vector

    # Creation of the vectors and normalisation
    v1 = a-b
    v2 = d-c

    u1 = v1 / norm(v1)
    u2 = v2 / norm(v2)

    # Angle calculation
    y = u1 - u2
    x = u1 + u2

    a0 = 2 * arctan(norm(y) / norm(x))

    # Particular cases at 0 and 180
    if (not signbit(a0)) or signbit(pi - a0):
        radian = a0
    elif signbit(a0):
```

```
        radian = 0.0
    else:
        radian = pi

    angle = np.degrees(radian)

    return angle


# Function that detects and store the position

def starting_position():

    # Initialisation
    mp_drawing = mp.solutions.drawing_utils
    mp_drawing_styles = mp.solutions.drawing_styles
    mp_pose = mp.solutions.pose

    angle_min_elbow = 0
    angle_min_knee = 0
    angle_min_hip = 0
    angle_min_shoulder = 0
    angle_min_ankle = 0
    angle_min_neck = 0

    angle_elbow_list = []
    angle_shoulder_list = []
    angle_hip_list = []
    angle_knee_list = []
    angle_ankle_list = []
    angle_neck_list = []

    elbow = []
    shoulder = []
    hip = []
    knee = []
    ankle = []
    wrist = []
    ear = []

    # Image capture
    cap = cv2.VideoCapture(0) # (0) opens webcam, (1) opens another camera,
   ('path') opens a video or an image

    # Starting of the clock
    prev_frame_time = time.time()
    new_frame_time = 0.0
    total_time = []
    temp = 0.0
```

```
82      nb_frame = []
83      nb_frame_temp = 0
84
85      # Initiate the Mediapipe Pose algorithm and define the different
    parameters
86      with mp_pose.Pose(
87          min_detection_confidence=0.5,
88          min_tracking_confidence=0.5) as pose:
89          while cap.isOpened():
90              success, image = cap.read()
91              if not success:
92                  print("Ignoring empty camera frame.")
93                  # If loading a video, use 'break' instead of 'continue'.
94                  continue
95
96              # To improve performance, optionally mark the image as not
    writeable to
97              # pass by reference
98              image.flags.writeable = False
99              image = cv2.cvtColor(image, cv2.COLOR_BGR2RGB)
100             results = pose.process(image)
101
102             # Draw the pose annotation on the image.
103             image.flags.writeable = True
104             image = cv2.cvtColor(image, cv2.COLOR_RGB2BGR)
105
106             mp_drawing.draw_landmarks(
107                 image,
108                 results.pose_landmarks,
109                 mp_pose.POSE_CONNECTIONS,
110                 landmark_drawing_spec=mp_drawing_styles.
    get_default_pose_landmarks_style())
111             image = cv2.flip(image, 1)
112
113             # Extract landmarks
114             try:
115                 landmarks = results.pose_landmarks.landmark
116
117                 # Get coordinates of the different landmarks of interest
118                 shoulder = [landmarks[mp_pose.PoseLandmark.RIGHT_SHOULDER.
    value].x, landmarks[mp_pose.PoseLandmark.RIGHT_SHOULDER.value].y]
119                 elbow = [landmarks[mp_pose.PoseLandmark.RIGHT_ELBOW.value].x
    ,landmarks[mp_pose.PoseLandmark.RIGHT_ELBOW.value].y]
120                 wrist = [landmarks[mp_pose.PoseLandmark.RIGHT_WRIST.value].x
    ,landmarks[mp_pose.PoseLandmark.RIGHT_WRIST.value].y]
121                 hip = [landmarks[mp_pose.PoseLandmark.RIGHT_HIP.value].x,
    landmarks[mp_pose.PoseLandmark.RIGHT_HIP.value].y]
122                 knee = [landmarks[mp_pose.PoseLandmark.RIGHT_KNEE.value].x,
    landmarks[mp_pose.PoseLandmark.RIGHT_KNEE.value].y]
```

```
123                 ankle = [landmarks[mp_pose.PoseLandmark.RIGHT_ANKLE.value].x
    ,landmarks[mp_pose.PoseLandmark.RIGHT_ANKLE.value].y]
124                 heel = [landmarks[mp_pose.PoseLandmark.RIGHT_HEEL.value].x,
    landmarks[mp_pose.PoseLandmark.RIGHT_HEEL.value].y]
125                 ear = [landmarks[mp_pose.PoseLandmark.RIGHT_EAR.value].x,
    landmarks[mp_pose.PoseLandmark.RIGHT_EAR.value].y]
126                 foot = [landmarks[mp_pose.PoseLandmark.RIGHT_FOOT_INDEX.
    value].x,landmarks[mp_pose.PoseLandmark.RIGHT_FOOT_INDEX.value].y]
127
128
129
130                 # Calculate the angles of the neck, elbow, shoulder, hip,
    knee and ankle
131
132                 # Angle between one segment and the horizontal plane
133                 angle_neck_h = angle_btw(ear, shoulder, shoulder, [shoulder
    [0]+0.5, shoulder[1]])
134                 angle_elbow_h = angle_btw(wrist, elbow, elbow,  [elbow
    [0]-0.5, elbow[1]])
135                 angle_shoulder_h = angle_btw(elbow, shoulder, shoulder, [
    shoulder[0]-0.5, shoulder[1]])
136                 angle_hip_h = angle_btw(shoulder, hip, hip, [hip[0]+0.5, hip
    [1]])
137                 # Angle between two segments
138                 angle_knee = angle_btw(hip, knee, knee, ankle)
139                 angle_ankle = angle_btw(knee, ankle, heel, foot)
140
141                 # Keep only 2 decimals
142                 angle_elbow = round(angle_elbow_h,2)
143                 angle_hip = 180-angle_hip_h
144                 angle_hip = round(angle_hip,2)
145                 angle_knee = round(angle_knee,2)
146                 angle_shoulder = round(angle_shoulder_h,2)
147                 angle_ankle = round(angle_ankle,2)
148                 angle_neck = 180-angle_neck_h
149                 angle_neck = round(angle_neck,2)
150
151                 angle_min_elbow = float(round(angle_elbow,2))
152                 angle_min_knee = float(round(angle_knee,2))
153                 angle_min_hip = float(round(angle_hip,2))
154                 angle_min_shoulder = float(round(angle_shoulder,2))
155                 angle_min_ankle = float(round(angle_ankle,2))
156                 angle_min_neck = float(round(angle_neck,2))
157
158                 # Store the angles
159                 angle_elbow_list.append(angle_min_elbow)
160                 angle_shoulder_list.append(angle_min_shoulder)
161                 angle_hip_list.append(angle_min_hip)
162                 angle_knee_list.append(angle_min_knee)
```

```
                angle_ankle_list.append(angle_min_ankle)
                angle_neck_list.append(angle_min_neck)

            except:
                pass

            # Write the values of the angles on the image
            #Elbow angle:
            cv2.putText(image, "Elbow-joint angle : " + str(angle_min_elbow)
    ,
                (30,140),
                cv2.FONT_HERSHEY_SIMPLEX, 0.8, (255,255,255), 2, cv2.LINE_AA
    )
            #Shoulder angle:
            cv2.putText(image, "Shoulder-joint angle : " + str(
    angle_min_shoulder),
                (30,100),
                cv2.FONT_HERSHEY_SIMPLEX, 0.8, (255,255,255), 2, cv2.LINE_AA
    )

             #Hip angle:
            cv2.putText(image, "Hip-joint angle : " + str(angle_min_hip),
                (30,180),
                cv2.FONT_HERSHEY_SIMPLEX, 0.8, (255,255,255), 2, cv2.LINE_AA
    )

            #Knee angle:
            cv2.putText(image, "Knee-joint angle : " + str(angle_min_knee),
                (30,220),
                cv2.FONT_HERSHEY_SIMPLEX, 0.8, (255,255,255), 2, cv2.LINE_AA
    )

            #Ankle angle:
            cv2.putText(image, "Ankle-joint angle : " + str(angle_min_ankle)
    ,
                (30,260),
                cv2.FONT_HERSHEY_SIMPLEX, 0.8, (255,255,255), 2, cv2.LINE_AA
    )

            #Neck angle:
            cv2.putText(image, "Neck-joint angle : " + str(angle_min_neck),
                (30,60),
                cv2.FONT_HERSHEY_SIMPLEX, 0.8, (255,255,255), 2, cv2.LINE_AA
    )

            # Compute the time since the starting of the clock in order to
    have the fps
            new_frame_time = time.time()
            temp += (new_frame_time-prev_frame_time)
```

```
202
203             total_time.append(temp)
204
205             fps = 1/(new_frame_time-prev_frame_time)
206             prev_frame_time = new_frame_time
207
208             nb_frame_temp += 1
209             nb_frame.append(nb_frame_temp)
210
211
212             # Display the image
213             cv2.namedWindow('MediaPipe Pose', cv2.WINDOW_KEEPRATIO)
214             cv2.setWindowProperty('MediaPipe Pose', cv2.WND_PROP_FULLSCREEN,
    cv2.WINDOW_FULLSCREEN)
215             cv2.imshow('MediaPipe Pose', image)
216             cv2.resizeWindow('MediaPipe Pose', 800, 800)
217
218             if cv2.waitKey(1) == ord('q'):
219                 break
220
221         # Store the angles
222         newarray = [angle_neck_list, angle_elbow_list, angle_shoulder_list,
    angle_hip_list, angle_knee_list, angle_ankle_list]
223         cap.release()
224
225         # Take the mean of the last few seconds as the good position
226         position = [round(np.mean(newarray[0][-10:-1]),2), round(np.mean(
    newarray[1][-10:-1]),2), round(np.mean(newarray[2][-10:-1]),2), round(np.
    mean(newarray[3][-10:-1]),2), round(np.mean(newarray[4][-10:-1]),2)]
227
228
229     return(position)
230
231 # Run the function
232
233 position = starting_position()
234
235 # Save the results
236 file = open("path" + '.txt', "w")
237 file.write('\n '.join([str(i) for i in position]))
238 file.close()
239 print(position)
```

C.2 2D_mediapipe_pose_detection.py

```
import cv2
import mediapipe as mp
import numpy as np
import math
from numpy import arctan, pi, signbit
from numpy.linalg import norm
import time
import os


# Angle between two segments

def angle_btw(a,b,c,d):

    a = np.array(a) # start first vector
    b = np.array(b) # end first vector
    c = np.array(c) # start second vector
    d = np.array(d) # end second vector

    # Creation of the vectors and normalisation
    v1 = a-b
    v2 = d-c

    u1 = v1 / norm(v1)
    u2 = v2 / norm(v2)

    # Angle calculation
    y = u1 - u2
    x = u1 + u2

    a0 = 2 * arctan(norm(y) / norm(x))

    # Particular cases at 0 and 180
    if (not signbit(a0)) or signbit(pi - a0):
        radian = a0
    elif signbit(a0):
        radian = 0.0
    else:
        radian = pi

    angle = np.degrees(radian)

    return angle

# Draw colored lines on image

def posture(good, ok_min, ok_max, angle, pt1, pt2, image):
```

```
48
49      # Define the colours
50      red = (50, 50, 255)
51      green = (127, 255, 0)
52      yellow = (0, 255, 255)
53      orange = (0, 140, 255)
54
55      # Draw the lines in the right colour at the right place depending on the
        angle values,
56      # it also define the indication to display on the screen
57      height, width, depth = image.shape
58      if  good[0] <= angle <= good[1] :
59          cv2.line(image, (int(width-pt1[0]*width),int(pt1[1]*height)), (int(
        width-pt2[0]*width),int(pt2[1]*height)), green, 10)
60          indication = 'ok'
61
62      elif ok_min[0] <= angle <= ok_min[1]:
63          cv2.line(image, (int(width-pt1[0]*width),int(pt1[1]*height)), (int(
        width-pt2[0]*width),int(pt2[1]*height)), yellow, 10)# yellow when smaller
        angles
64          indication = 'increase'
65
66      elif ok_max[0] < angle < ok_max[1]:
67          cv2.line(image, (int(width-pt1[0]*width),int(pt1[1]*height)), (int(
        width-pt2[0]*width),int(pt2[1]*height)), orange, 10)#orange when bigger
        angles
68          indication = 'decrease'
69
70      elif ok_max[1] < angle:
71          cv2.line(image,(int(width-pt1[0]*width),int(pt1[1]*height)),  (int(
        width-pt2[0]*width),int(pt2[1]*height)), red, 10)
72          indication = 'decrease'
73
74      else:
75          cv2.line(image,(int(width-pt1[0]*width),int(pt1[1]*height)),  (int(
        width-pt2[0]*width),int(pt2[1]*height)), red, 10)
76          indication = 'increase'
77
78      return indication
79
80  # Read .txt file with the reference position
81
82  def read_position(file):
83    good_position = []
84    file = open(file, "r")
85    good_position_temp = file.read()
86    file.close()
87    good_position_temp = good_position_temp.split("\n")
88    for word in good_position_temp:
```

```
    good_position.append(float(word))
  print(good_position)
  return(good_position)

# Read the reference position
good_position = read_position("path/good_position" + '.txt')

# Detect, display and store the position

# Initialisation
mp_drawing = mp.solutions.drawing_utils
mp_drawing_styles = mp.solutions.drawing_styles
mp_pose = mp.solutions.pose

angle_min_elbow = 0
angle_min_knee = 0
angle_min_hip = 0
angle_min_shoulder = 0
angle_min_ankle = 0
angle_min_neck = 0

angle_elbow_list = []
angle_shoulder_list = []
angle_hip_list = []
angle_knee_list = []
angle_ankle_list = []
angle_neck_list = []

elbow = []
shoulder = []
hip = []
knee = []
ankle = []
wrist = []
ear = []

# Image capture
cap = cv2.VideoCapture(0) # (0) opens webcam, (1) opens another camera, ('
    path') opens a video or an image

# Starting of the clock
prev_frame_time = time.time()
new_frame_time = 0.0
total_time = []
temp = 0
nb_frame = []
nb_frame_temp = 0

# Initiate the Mediapipe Pose algorithm and define the different parameters
```

```
with mp_pose.Pose(
    min_detection_confidence=0.5,
    min_tracking_confidence=0.5) as pose:
  while cap.isOpened():
    success, image = cap.read()
    if not success:
      print("Ignoring empty camera frame.")
      # If loading a video, use 'break' instead of 'continue'.
      continue

    # To improve performance, optionally mark the image as not writeable to
    # pass by reference
    image.flags.writeable = False
    image = cv2.cvtColor(image, cv2.COLOR_BGR2RGB)
    results = pose.process(image)

    # Draw the pose annotation on the image.
    image.flags.writeable = True
    image = cv2.cvtColor(image, cv2.COLOR_RGB2BGR)

    mp_drawing.draw_landmarks(
        image,
        results.pose_landmarks,
        mp_pose.POSE_CONNECTIONS,
        landmark_drawing_spec=mp_drawing_styles.
    get_default_pose_landmarks_style())
    image = cv2.flip(image, 1)

    # Extract landmarks
    try:
        landmarks = results.pose_landmarks.landmark

         # Get coordinates of the different landmarks of interest
        shoulder = [landmarks[mp_pose.PoseLandmark.RIGHT_SHOULDER.value].x,
    landmarks[mp_pose.PoseLandmark.RIGHT_SHOULDER.value].y]
        elbow = [landmarks[mp_pose.PoseLandmark.RIGHT_ELBOW.value].x,
    landmarks[mp_pose.PoseLandmark.RIGHT_ELBOW.value].y]
        wrist = [landmarks[mp_pose.PoseLandmark.RIGHT_WRIST.value].x,
    landmarks[mp_pose.PoseLandmark.RIGHT_WRIST.value].y]
        hip = [landmarks[mp_pose.PoseLandmark.RIGHT_HIP.value].x,landmarks[
    mp_pose.PoseLandmark.RIGHT_HIP.value].y]
        knee = [landmarks[mp_pose.PoseLandmark.RIGHT_KNEE.value].x,landmarks
    [mp_pose.PoseLandmark.RIGHT_KNEE.value].y]
        ankle = [landmarks[mp_pose.PoseLandmark.RIGHT_ANKLE.value].x,
    landmarks[mp_pose.PoseLandmark.RIGHT_ANKLE.value].y]
        heel = [landmarks[mp_pose.PoseLandmark.RIGHT_HEEL.value].x,landmarks
    [mp_pose.PoseLandmark.RIGHT_HEEL.value].y]
        ear = [landmarks[mp_pose.PoseLandmark.RIGHT_EAR.value].x,landmarks[
    mp_pose.PoseLandmark.RIGHT_EAR.value].y]
```

```
177         foot = [landmarks[mp_pose.PoseLandmark.RIGHT_FOOT_INDEX.value].x,
    landmarks[mp_pose.PoseLandmark.RIGHT_FOOT_INDEX.value].y]
178 
179         # Calculate the angles of the neck, elbow, shoulder, hip, knee and
    ankle
180 
181         # Angle between one segment and the horizontal plane
182         angle_neck_h = angle_btw(ear, shoulder, shoulder, [shoulder[0]+0.5,
    shoulder[1]])
183         angle_elbow_h = angle_btw(wrist, elbow, elbow,  [elbow[0]-0.5, elbow
    [1]])
184         angle_shoulder_h = angle_btw(elbow, shoulder, shoulder, [shoulder
    [0]-0.5, shoulder[1]])
185         angle_hip_h = angle_btw(shoulder, hip, hip, [hip[0]+0.5, hip[1]])
186         # Angle between two segments
187         angle_knee = angle_btw(hip, knee, knee, ankle)
188         angle_ankle = angle_btw(knee, ankle, heel, foot)
189 
190         # Keep only 2 decimals
191         angle_elbow = round(angle_elbow_h,2)
192         angle_hip = 180-angle_hip_h
193         angle_hip = round(angle_hip,2)
194         angle_knee = round(angle_knee,2)
195         angle_shoulder = round(angle_shoulder_h,2)
196         angle_ankle = round(angle_ankle,2)
197         angle_neck = 180-angle_neck_h
198         angle_neck = round(angle_neck,2)
199 
200         angle_min_elbow = float(round(angle_elbow,2))
201         angle_min_knee = float(round(angle_knee,2))
202         angle_min_hip = float(round(angle_hip,2))
203         angle_min_shoulder = float(round(angle_shoulder,2))
204         angle_min_ankle = float(round(angle_ankle,2))
205         angle_min_neck = float(round(angle_neck,2))
206 
207         # Store the angles
208         angle_elbow_list.append(angle_min_elbow)
209         angle_shoulder_list.append(angle_min_shoulder)
210         angle_hip_list.append(angle_min_hip)
211         angle_knee_list.append(angle_min_knee)
212         angle_ankle_list.append(angle_min_ankle)
213         angle_neck_list.append(angle_min_neck)
214 
215     except:
216             pass
217 
218     # Determine whether the current position is a good posture or bad
    posture.
219     ind_neck = posture([good_position[0]-2.5,good_position[0]+2.5], [
```

```
    good_position[0]-5,good_position[0]-2.5], [good_position[0]+2.5,
    good_position[0]+5], angle_min_neck, shoulder, ear, image) # position of
    the neck
220  ind_elbow = posture([good_position[1]-2.5,good_position[1]+2.5], [
    good_position[1]-5,good_position[1]-2.5], [good_position[1]+2.5,
    good_position[1]+5], angle_min_elbow, elbow, wrist, image) # position of
    the elbow
221  ind_shoulder = posture([good_position[2]-2.5,good_position[2]+2.5], [
    good_position[2]-5,good_position[2]-2.5], [good_position[2]+2.5,
    good_position[2]+5], angle_min_shoulder, shoulder, elbow, image) #
    position of the shoulder
222  ind_torso = posture([good_position[3]-2.5,good_position[3]+2.5], [
    good_position[3]-5,good_position[3]-2.5], [good_position[3]+2.5,
    good_position[3]+5], angle_min_hip, shoulder, hip, image) # position of
    the torso (hip)
223
224  # Write the indications on the image
225  #Elbow angle:
226  cv2.putText(image, "Elbow-joint angle : " + str(ind_elbow),  #
    angle_min_elbow
227              (30,120),
228              cv2.FONT_HERSHEY_SIMPLEX, 0.8, (255,255,255), 2, cv2.LINE_AA
    )
229  #Shoulder angle:
230  cv2.putText(image, "Shoulder-joint angle : " + str(ind_shoulder),
231              (30,80),
232              cv2.FONT_HERSHEY_SIMPLEX, 0.8, (255,255,255), 2, cv2.LINE_AA
    )
233
234  #Hip angle:
235  cv2.putText(image, "Hip-joint angle : " + str(ind_torso),
236              (30,160),
237              cv2.FONT_HERSHEY_SIMPLEX, 0.8, (255,255,255), 2, cv2.LINE_AA
    )
238
239  #Neck angle:
240  cv2.putText(image, "Neck-joint angle : " + str(ind_neck),
241              (30,40),
242              cv2.FONT_HERSHEY_SIMPLEX, 0.8, (255,255,255), 2, cv2.LINE_AA
    )
243
244  # Compute the time since the starting of the clock in order to have the
    fps
245  new_frame_time = time.time()
246  temp += (new_frame_time-prev_frame_time)
247
248  total_time.append(temp)
249
250  fps = 1/(new_frame_time-prev_frame_time)
```

```
    prev_frame_time = new_frame_time

    nb_frame_temp += 1
    nb_frame.append(nb_frame_temp)

    # Display the image
    cv2.namedWindow('MediaPipe Pose', cv2.WINDOW_KEEPRATIO)
    cv2.setWindowProperty('MediaPipe Pose', cv2.WND_PROP_FULLSCREEN, cv2.
    WINDOW_FULLSCREEN)
    cv2.imshow('MediaPipe Pose', image)
    cv2.resizeWindow('MediaPipe Pose', 1000, 1000)

    if cv2.waitKey(1) == ord('q'):
      break

# Store the angles
newarray = [angle_elbow_list, angle_shoulder_list, angle_hip_list,
    angle_knee_list, angle_ankle_list, total_time, nb_frame]

# Save the results
file = open("path" + '.txt', "w")
file.write('\n '.join([str(i) for i in newarray]))
file.close()

# Check that the results are correctly saved
size_txt = os.path.getsize("path" + '.txt')
isempty = size_txt == 0
print(".txt file is empty :", isempty)

cap.release()
```